19950103 061

CHARACTERIZATION OF FATIGUE BEHAVIOR
OF 2-D WOVEN FABRIC REINFORCED
CERAMIC MATRIX COMPOSITE
AT ELEVATED TEMPERATURE

THESIS

Daniel J. Groner, Captain, USAF

AFIT/GAE/ENY/94D-15

DEPARTMENT OF THE AIR FORCE

AIR UNIVERSITY

AIR FORCE INSTITUTE OF TECHNOLOGY

Wright-Patterson Air Force Base, Ohio

AFIT/GAE/ENY/94D-15

CHARACTERIZATION OF FATIGUE BEHAVIOR
OF 2-D WOVEN FABRIC REINFORCED
CERAMIC MATRIX COMPOSITE
AT ELEVATED TEMPERATURE

THESIS

Daniel J. Groner, Captain, USAF

AFIT/GAE/ENY/94D-15

A-1

AFIT/GAE/ENY/94D-15

CHARACTERIZATION OF FATIGUE BEHAVIOR OF 2-D WOVEN

FABRIC REINFORCED CERAMIC MATRIX COMPOSITE

AT ELEVATED TEMPERATURE

THESIS

Presented to the Faculty of the School of Engineering

of the Air Force Institute of Technology

Air University

In Partial Fulfillment of the

Requirements for the Degree of

Master of Science in Aeronautical Engineering

Daniel J. Groner

Captain, USAF

December 1994

Preface

The purpose of this study was to investigate the fatigue response of a woven fabric reinforced ceramic matrix composite(CMC). In addition the failure mechanisms and monotonic tensile test behavior were investigated. The ceramic matrix composite studied was enhanced SiC/SiC CMC formed by a chemical vapor infiltration (CVI) process. The specimens were provided by DuPont Lanxide Composites Inc. Tension-tension fatigue tests were performed to develop the S-N relationship of the material. All fatigue tests were performed at a temperature of 1100°C while with a triangular waveform load of 1.0 Hz frequency. Two geometries of specimens were investigated; unnotched and notched.

I wish to thank my wife, Carol and children, John and Amy for their invaluable assistance and support during the work for this thesis. Thanks to Mark Derriso and Dan Rioux for their assistance and instruction with the test and investigation hardware. Also, of course, thanks to Dr. Mall for his guiding questions and subtle support as I explored the intricacies of woven fabric ceramics. Lastly, I wish to thank Captain Bill Moschelle of the Aero-Propulsion and Power Directorate, Wright Laboratory for sponsoring this work.

<div align="right">Daniel J. Groner</div>

Table of Contents

List of Figures

List of Tables

Abstract

The purpose of this study was to investigate the high temperature performance of a woven fabric reinforced ceramic matrix composite under fatigue loading conditions. Specifically, the test had three objectives: (1) To determine the relationship between maximum stress level and the number of cycles to failure of specimens with and without hole, (2) To document the behavior of specimens with and without hole under monotonic tensile loading, and (3) To investigate the initiation and progression of damage during fatigue and monotonic loading conditions.

The composite used was a woven fabric reinforced ceramic matrix. The fibers were Nicalon formed into continuous multifilament yarns with the elemental composition Si-C-O, silicon carbide(SiC); and the matrix was silicon carbide deposited by chemical vapor infiltration(CVI).

Fatigue tensile tests were performed on seven notched specimens and five unnotched specimens to develop a stress versus number of cycles to failure (S-N) relationship for the material. The notch was in the form of a central hole of 3.06 mm diameter in the specimen of 9.31 mm width for a D/W ratio of 0.33. The S-N curves for the with and without hole cases were compared to evaluate the effects of notch or stress raiser in the enhanced SiC/SiC ceramic composite. After testing, the

specimens were sectioned and examined. Damage mechanisms, both initiation and progression, were evaluated based on this microscopic examination along with modulus and stiffness degradation during cycling, and observations of previous studies.

During monotonic tensile testing, the unnotched specimen had an ultimate stress(σ_{ult}) of 230 MPa and a proportional limit(PL) of 85 MPa. The notched specimen displayed σ_{ult} of 228 MPa and no clearly defined PL. This indicates a negligible stress concentration factor under monotonic tensile loading. Likewise, the fatigue strength was only diminished by 10% in the presence of the central notch; this is considered a negligible notch sensitivity.

In all cases, the failure of the notched specimens initiated adjacent to the hole while failure of the unnotched specimens initiated at the edges and inherent pores. The damage progression in monotonic loading and high stress fatigue tests was inter-yarn cracking originating at the pores between the 0° and 90° yarns. This was followed by transverse matrix cracking of the 90° yarns leading to matrix cracking, fiber pullout, and yarn splitting of the 0° yarns. This damage progression was characteristic of both notched and unnotched specimens.

In contrast, the initial portion of damage regions in the high cycle regime were characterized by a smooth surface as the

crack penetrated with little regard to fiber/matrix interface regions. After crack propagation progressed to the final failure region of specimen life, the damage mechanisms reverted to those previously described for low cycle fatigue prior to final failure.

CHARACTERIZATION OF FATIGUE BEHAVIOR OF 2-D WOVEN FABRIC REINFORCED CERAMIC MATRIX COMPOSITE AT ELEVATED TEMPERATURE

I. Introduction

A. Background

Composites consist of one or more discontinuous phases embedded in a continuous phase. The discontinuous phase is normally called the reinforcement or reinforcing material. This is the fiber in fiber reinforced composites. The continuous phase is called the matrix. Fiber reinforced composite materials are an important class of composites to which the ceramic matrix composites belong. Fiber reinforcement may be either non-woven such as in unidirectional(UD) composite or woven fabric(WF). UD composites have laminates of fibers each oriented in one given direction while WF composites consist of fabric reinforcement layers.

Ceramics hold a tremendous potential for such applications as internal combustion engines, gas turbines, electronics, and

surgical implants. They can withstand higher temperatures than metals or polymers and have a high level of hardness. Their weaknesses are low failure strain and low fracture toughness. Monolithic ceramics have a high notch sensitivity and extreme brittleness. The general focus, in the development of ceramic matrix composites, is to minimize the aforementioned weaknesses while maximizing the strength and stiffness .

The extreme brittle nature of ceramics promotes the tendency of any crack or flaw leading to catastrophic failure due to stress concentration at the crack tip. The focus of the development of ceramic matrix composites is to inhibit this tendency to catastrophic failure through the use of fiber reinforcing. If the fibers are strong, and the fiber-matrix interfacial bonds are relatively weak, the fiber debond in close proximity to the crack tip permits the fibers to carry loads through the crack. This prevents a matrix crack from resulting in catastrophic failure, and permits a composite ultimate stress well beyond the matrix failure strain[16].

One of the most promising applications of ceramic matrix composite technology is in the fabrication of high temperature engine components. Since internal engine parts are subjected to cyclic variations in load, it is important to characterize the effects of stress fatigue cycling at high temperature. Holes are often necessary for the attachment of components

during assembly for rivets or bolts. Holes are also necessary for cutouts required for several other applications. For these reasons, high temperature fatigue characteristics and the effects of geometric discontinuities, such as holes, are two important aspects of the investigation in ceramic matrix composite materials.

The composite investigated in the present study was a woven fabric ceramic matrix, enhanced SiC/SiC. The fibers were Nicalon formed into continuous multifilament yarns with the elemental composition Si-C-O, silicon carbide(SiC); and the matrix was silicon carbide(SiC) deposited by chemical vapor infiltration(CVI). The reinforcement yarns were in the form of a woven configuration. The enhanced SiC/SiC CMC differs in microstructure and material from the CMCs of previous investigations involving hole effect studies. This need about high temperature fatigue behavior in centrally notched woven fabric CMCs provides the motivation for the present work.

B.   Purpose

The purpose of this study was to investigate the high temperature performance of a woven fabric reinforced ceramic matrix composite under fatigue tension-tension loading conditions. Specifically, the test had three objectives: (1)

to determine the relationship between maximum stress level and the number of cycles to failure with and without a centrally located hole, (2) to document the behavior of notched and un-notched specimens subjected to monotonic tensile loading, and (3) to investigate the damage mechanisms, both initiation and progression, during fatigue and monotonic loading conditions.

C.   Approach

The composite investigated in the present study was a 2-D woven fabric reinforced enhanced SiC/SiC ceramic matrix composite.   The reinforcement fibers consisted of Nicalon formed into continuous multifilament yarns and woven to form a fabric with the elemental composition Si-C-O, silicon carbide (SiC); and the matrix was silicon carbide (SiC) deposited by chemical vapor infiltration (CVI).   Enhanced SiC/SiC CMC has been the subject of previous studies which focused on monotonic tensile testing at room temperature and elevated temperature and un-notched room temperature versus high temperature fatigue testing.   This thesis will present elevated temperature notched versus un-notched fatigue research.

Tests, in the present study, were conducted at 1100°C in laboratory atmospheric conditions.   The tension-tension fatigue tests were accomplished using a minimum to maximum stress ratio

of 0.1. Maximum stress versus number of cycles to failure curves will be presented to graphically illustrate the fatigue life diagram of notched and un-notched configurations.

The specimens, used in this work (see Figure 1-1), were produced by DuPont Lanxide Composites Inc. The un-notched specimens had a dog-bone geometry to ensure the failure in the center portion away from the grips. The notched specimens had a centrally located circular hole with a diameter to specimen width ratio (D/W) of 0.331 ± 0.003.
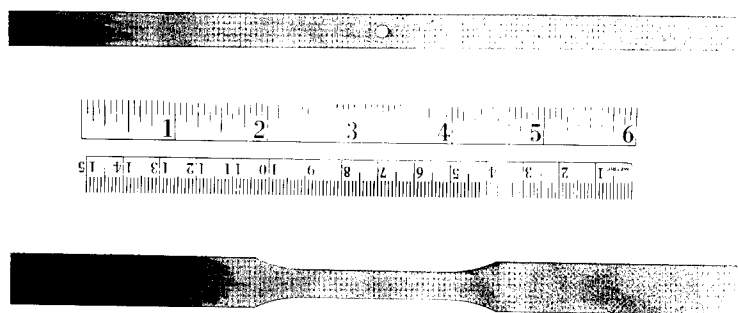
Figure 1-1 SiC/SiC specimens Prior to Testing.

To evaluate the fatigue behavior, several techniques are utilized on both the macroscopic and microscopic level. These techniques include modulus behavior during fatigue testing,

1.5

stress-strain behavior during both monotonic tensile testing and fatigue testing, optical microscopy, and scanning electron microscopy.

Chapter II describes the motivation behind CMC development in general and the experimental background leading up to this work. Chapter III describes the material and specimen details, including the techniques used in their manufacture and test preparation. It also presents the experimental method including the test equipment and test procedure. Chapter IV presents and discusses the test results. It includes presentation and discussion of the S-N curves and degradation of elastic modulus during fatigue. Chapter IV also presents and discusses stress strain curves, fracture surfaces, and damage mechanisms. Chapter V presents the conclusions and Chapter VI the presents the recommendations.

II Background

The motivation behind the development of CMCs is the possibility of reducing the notch sensitivity and increasing the fracture toughness of ceramics alone. Brennan and Prewo [2] were the initial researchers who quantified this increase in toughness due to the presence of high strength, high stiffness fibers. Marshall and Evans [17] isolated this increase in toughness to the ability of the fiber to carry loads through the crack. Unlike linear elastic fracture mechanics, where one crack propagates through the material, crack initiation in CMCs is characterized by many small matrix cracks. In CMCs, they found that once a crack reached an unbroken fiber, the energy required to extend the crack was independent of crack size. Fiber to matrix interface failure is therefore important in developing high fracture toughness.

Two failure modes are possible in CMC materials. First the fibers may be relatively weak and the interfacial bond relatively strong. This combination allows the matrix crack to penetrate through the fibers resulting in catastrophic failure of the material. The second failure mode arises from a material comprised of strong fibers and weak interfacial bonds. Here the matrix crack grows around the fiber as the fiber/matrix interface debonds both in front of and behind the

2.1

Fiber

Matrix

Crack Wake Debond   Crack Front Debond
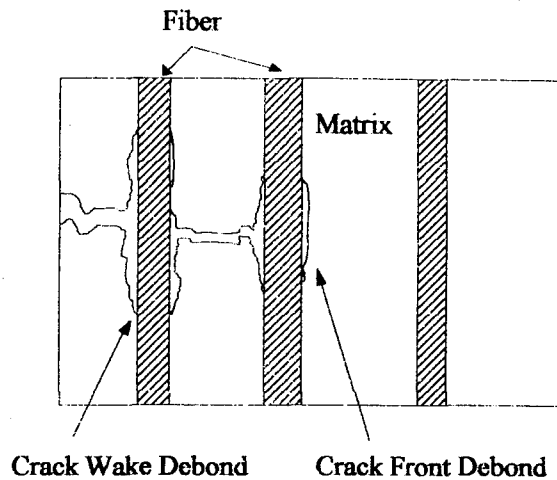
Figure 2-1 Fiber Debonding

crack tip as shown in Figure 2-1. This is the desired failure
mode because a matrix crack does not result in catastrophic
failure making this the chosen path in CMC development[16].

Three major mechanisms of toughness and strengthening are
present in CMC materials. The first is multiple matrix
cracking which is illustrated schematically in Figure 2-2.
Multiple fracture analysis was proposed by Aveston, Cooper, and
Kelley (ACK theory)[1]. They used energy balance to relate
strength of the microstructure to fiber reinforcement. The
second toughening mechanism is crack impediment. Crack bowing
originates from the second phase particles in the path of a
propagating crack[9]. The crack tends to bow between the
second phase particles until the fracture toughness of the
particles is reached. This bowing causes the stress intensity

2.2
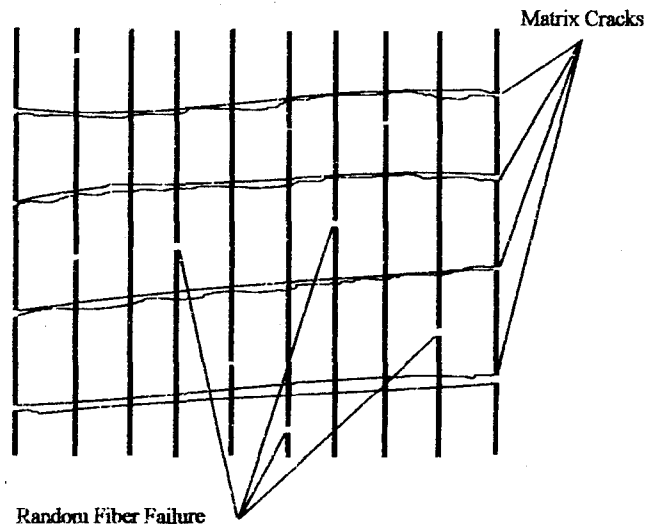
Figure 2-2   Multiple Matrix Cracking

along the deflected crack to decrease thus increasing fracture
toughness.   The matrix cracks are deflected and sometimes
completely arrested as they approach and bypass fiber strands
which are equivalent to second phase particles in the CMC
system.

The third type of toughening mechanism is fiber pull-out.
Fibers that bridge over the matrix crack contain breaks away
from the matrix crack proximity.   The broken fibers dissipate
energy by frictional sliding, which occurs as the broken ends
of the fibers pull out of the matrix.   Long pullout lengths are
desirable and this is controlled by the interfacial shear
stress (ISS).   This debonding before failure and fiber pullout
are essential in improving the resistance to catastrophic

2.3

failure or toughness of the CMC. Many have studied fracture toughness and damage development in CMCs[18, 13, 23, 7, 8, 22, 14, 5, 6]. These studies did not investigate notched CMCs.

Bullock [3] and Moschelle [20] investigated the notched CMCs. Bullock studied the SiC/1723, composed of continuous silicon titanium carbide fibers in an aluminosilicate glass ceramic matrix under monotonic tensile loading condition. He varied the ratio of hole diameter to specimen width and found that for both the $[0]_8$ and $[0/90]_{2s}$ layups, the specimens were relatively notch insensitive. Moschelle performed fatigue tests on the same material and found the $[0/90]_{2s}$ to be notch insensitive to fatigue. He did, however, find the $[0]_8$ layup to be notch sensitive. These studies concentrated on composites with fiber reinforcement rather than ceramic composites with fabric reinforcement. One would suspect the 0 degree yarns to interact with the 90 degree yarns in a different fashion when employed in woven layups than with cross ply layups.

Several studies have been conducted with woven fabric reinforced epoxy matrix, composites (eg. Fujii, Naik)[10, 21]. The performance of the SiC/SiC specimen may be somewhat analogous to polymeric composites, however the materials are far too different to draw a strong analogy. The epoxy matrix, in the carbon/glass composites, has a modulus (E_m) much lower

2.4

than the modulus of the fibers (E_f), thus the fibers carry the majority of the load and behavior is dominated by fiber properties. SiC/SiC on the other hand is a matrix dominated composite where E_f/E_m is about unity or less.

The SiC matrix has a higher level of hardness than epoxy matrix. To prevent catastrophic crack propagation in CMCs, it is desired to have low fiber to matrix bond strength. The cross-ply layup CMC loaded in tension has an initial linear stress-strain relationship. After reaching the end of the linear range, known as the proportional limit (PL), matrix cracks develop in the 90 degree plies. These cracks produce a reduction in slope of the stress strain curve. Crack extension energy is dissipated by fiber pullout, crack bending around fibers, and multiple matrix cracking. This simplistic look at "fracture mechanics" of CMCs immediately highlights the strengths and weaknesses of this approach to toughening ceramics. While the 0° fibers behave in very much the desired manner, the 90° fibers readily debond transferring the load to the 0° plies. A 0/90 crossply layup, thus, gives the reduced area strength of the notched specimen as reported by Mall et al[15]. The woven fabric layup, however, promotes an interaction not present in the fiber reinforced composites.

In the 2-D woven fabric composite the "0" and "90" yarns are interlaced in each ply as shown in Figure 2-3. Composites
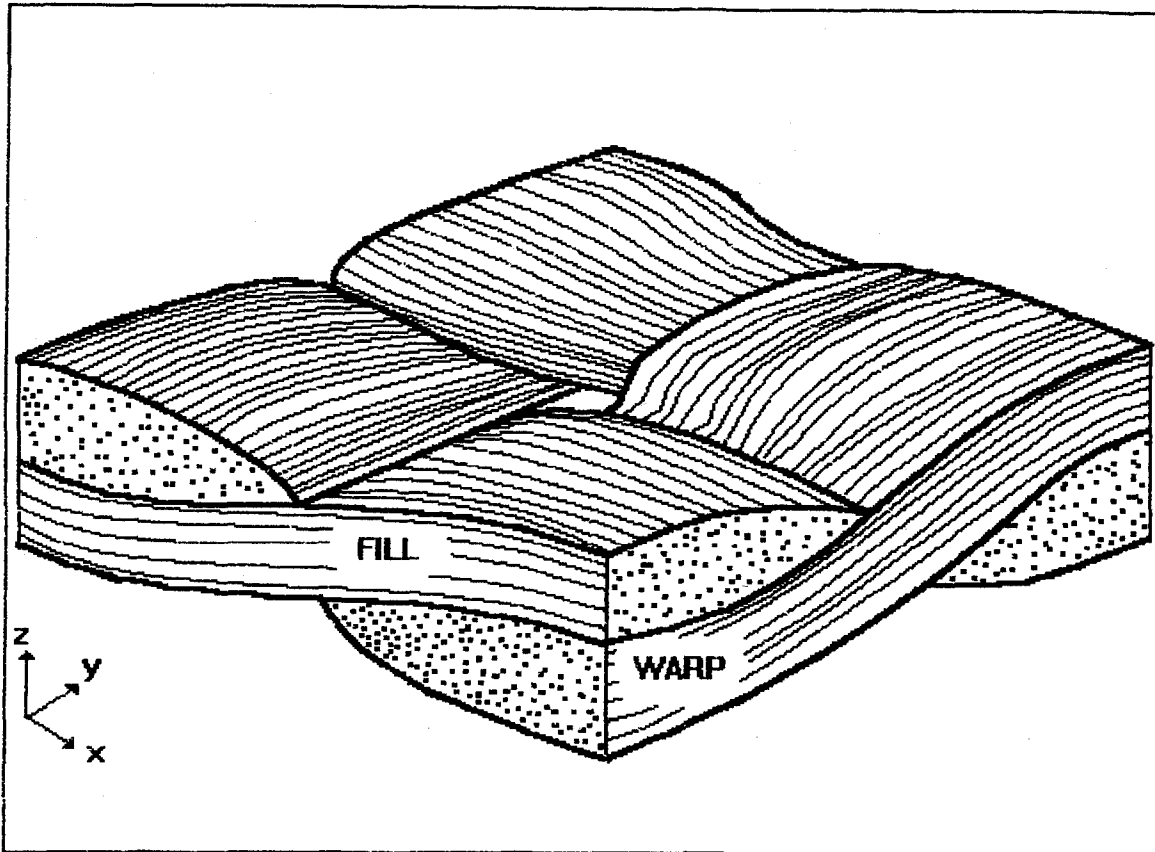
Figure 2-3   Woven Fabric Composite Reinforcement Structure

with this type of reinforcement structure are known as textile composites.   Chen has studied the enhanced SiC/SiC CMC under room and elevated temperature monotonic tensile conditions and reports damage progression as follows[4].   When stressed in tension initial damage takes place in the inter-yarn region; that is, the porous matrix between the warp (90°) and fill (0° or weft) yarns, Figure 2-4.   This damage initiates at the 84 MPa load level during 1200°C tests.   Stress strain behavior beyond this point is not linear; therefore, this 84 MPa stress level denotes the proportional limit.   As the stress level

2.6

approaches 150 MPa, the matrix of the 90° yarns begins to crack. These cracks propagate and some penetrate into the 0° yarn region. At this stress level interface debonding takes
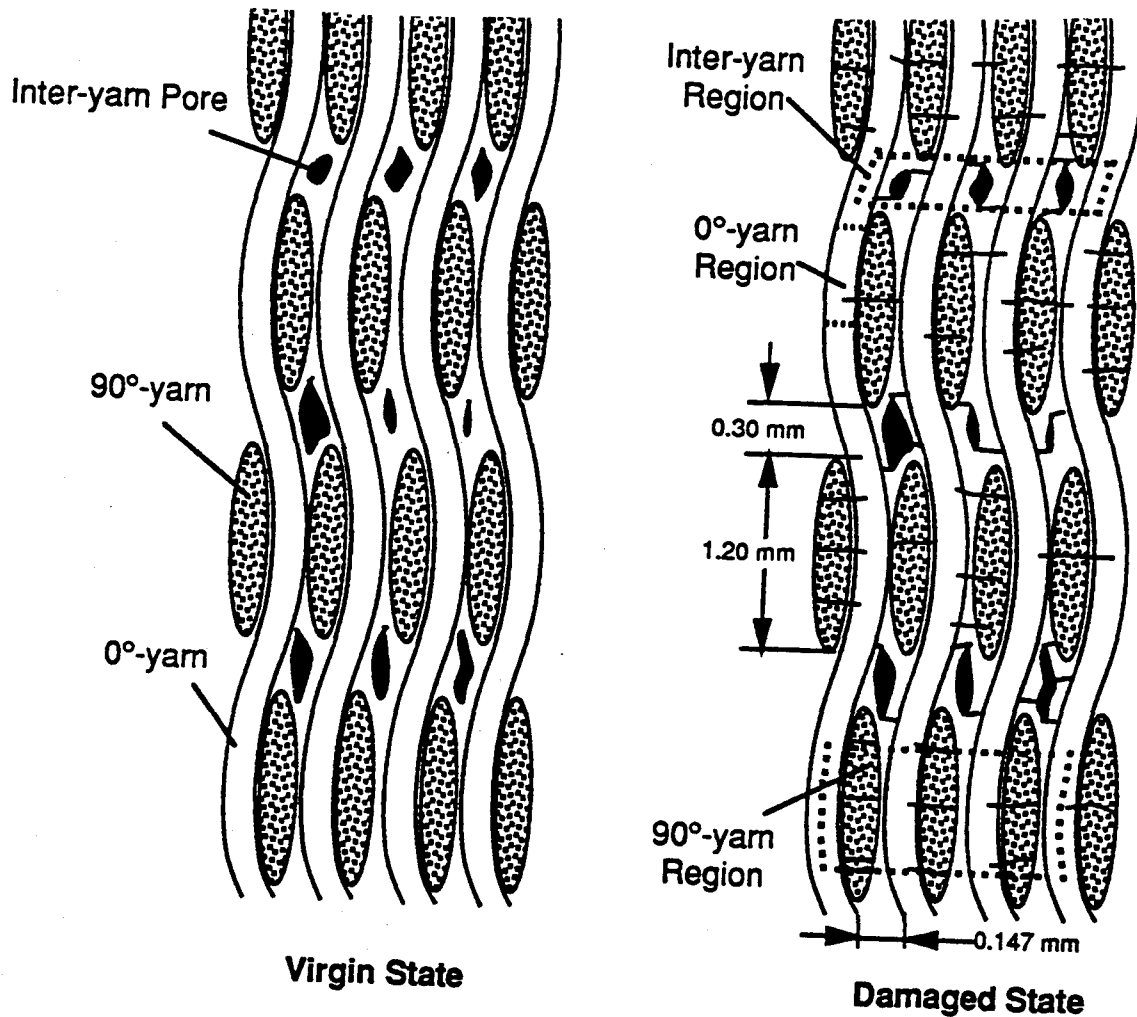
Figure 2-4 Schematic of Virgin and Damaged States in Woven Composite

place and the accompanying fiber pullout acts as an arrest mechanism. As the cracks propagate into the 0° yarns, matrix cracking occurs within the yarns. This is followed by fiber breakage and yarn splitting. Figure 2-4 schematically

illustrates undamaged versus damaged SiC/SiC woven fabric. Final failure occurs when 0° fracture takes place in the wake of final linkup of the 90° yarn cracks.

Fatigue life is a function of many parameters; among them are maximum stress level, minimum to maximum load ratio, load wave shape, cycle frequency, test section temperature and, specimen geometry. An example of specimen geometry is the presence or lack of a hole in the test specimen. Fatigue tests at room temperature and elevated temperature have been performed by Mehran et al [19] on enhanced SiC/SiC. They tested with a sine wave with a load ratio of 0.1 and a frequency of 10 Hz. They found this material would run out (endure beyond 1,000,000 cycles) at load levels significantly above the proportional limit. They also reported a significantly reduced fatigue life at elevated temperatures.

Characterization of 2-D woven ceramic matrix composites in general and enhanced SiC/SiC in particular has, thus, progressed to the level that elevated temperature notched tests are necessary. The present work investigated the effect of a centrally located circular hole on fatigue life, damage initiation, and damage progression. The tests were conducted at elevated temperature (1100°C), with a 1.0 Hz triangular wave, and a fixed hole diameter to width ratio, D/W, in the notched specimens of 0.33. The parameters of interest were

presence of a hole and stress level in the specimen. All other previously described variables were held constant thereby isolating the test results to stress level or specimen geometry.

III Experimental Procedure

This chapter provides the details of the experimental work. Part A describes the composite material and how it was manufactured. Part B describes how the specimens were prepared for tensile fatigue testing. Part C describes the test equipment, and how the test was conducted. Part D describes the test procedure.

A. *Material and Specimen Details*

The material tested was the enhanced SiC/SiC ceramic matrix composite (CMC). The fibers were Nicalon formed into continuous multifilament yarns with the elemental composition Si-C-O, silicon carbide (SiC); and the matrix was silicon carbide deposited by chemical vapor infiltration (CVI). Nicalon has the favorable characteristics of flexibility (low resistance to bending and a high bend radius before breaking) and small diameter (about 15 μm). Other advantages are its ability to form complex shapes and its consistent properties. The process for forming Nicalon starts with a polymeric precursor, Dichlorodimethysilane and through several manufacturing process steps, the high strength SiC fiber is formed[27]. Figure 3-1 presents a schematic of the Nicalon

3.1

fiber manufacturing process. The SiC fibers are spun into yarns and woven to form the fabric used in making the preform for the CVI process.

```
            ┌─────────────────────────────────┐
            │ Dichlorodimethylsilane          │
            └─────────────────────────────────┘
         ( Dechlorination with  Na            )
            ┌─────────────────────────────────┐
            │ Polydimethylsilane              │
            └─────────────────────────────────┘
      ( Polymerization at 470  °C in autoclave      )
            ┌─────────────────────────────────┐
            │ Polycarbosilane                 │
            └─────────────────────────────────┘
        ( Melt spinning at 350 °C                 )
            ┌─────────────────────────────────┐
            │ Polycarbosilane fiber           │
            └─────────────────────────────────┘
      ( Curing at 190 °C in air or room temperat  ure in ozone )
            ┌─────────────────────────────────┐
            │ Polycarbosilane fibers with molecular │
            │ cross-linking by oxygen         │
            └─────────────────────────────────┘
      ( Pyrolysis: heating to 1300 °C in vacuum         )
            ┌─────────────────────────────────┐
            │ SiC fiber                       │
            │ Amorphous or micro crystalline  │
            │ Beta-SiC                        │
            └─────────────────────────────────┘
```

Figure 3-1   Schematic of Nicalon Manufacturing

The CVI process is an extension of chemical vapor deposition(CVD) technology which is used for forming refractory coatings, electronic materials, and ceramic fibers[11]. The CVI process for making SiC/SiC CMC begins with the preform. The precursor gas infiltrates the preform, dissociates, and deposits the matrix on the fiber surface. Matrix accumulates

radially around each fiber. Figure 3-2 schematically illustrates the CVI process used in the production of SiC/SiC.
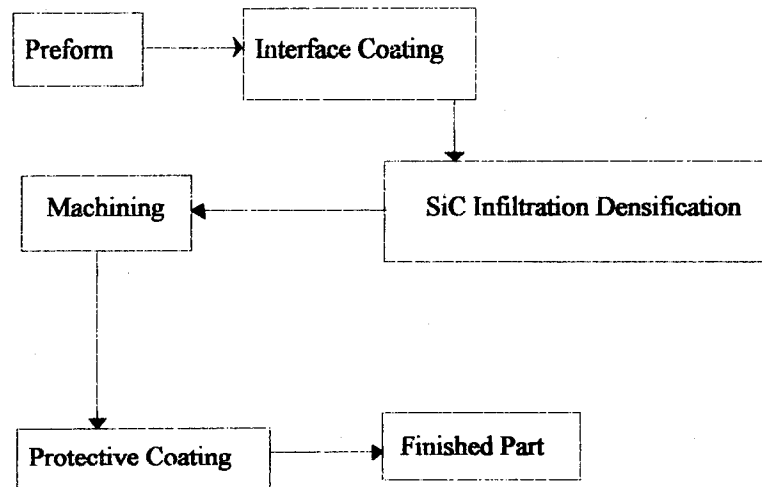
Figure 3-2 Production of CMC Component Using the CVI Process

These specimens (see Figure 1-1) were produced by DuPont Lanxide Composites Inc. All specimens had a thickness of 3.33 ± 0.03 mm. The un-notched specimens had a width in the gauge section of 8.12 ± 0.08 mm and the notched specimens were 9.60 ± 0.09 mm wide. The notch was in the form of a center hole, 3.18 mm in diameter. Other dimensions, as well as overall specimen geometry are shown in the schematic view of Figure 3.3. DuPont also provided some fatigue results on un-notched specimens[12]. They subjected the material used in their corresponding elevated temperature fatigue tests to a triangular wave load with a frequency of 0.5 Hz. Their test

3.3

results indicated a fatigue life of 1,500 cycles with a maximum
stress loading of 180 MPa and a fatigue life of 15,000 cycles
when the specimens were subjected to 120 MPa maximum stress
loading. The present work differs in that it used a 1 Hz
triangular wave.
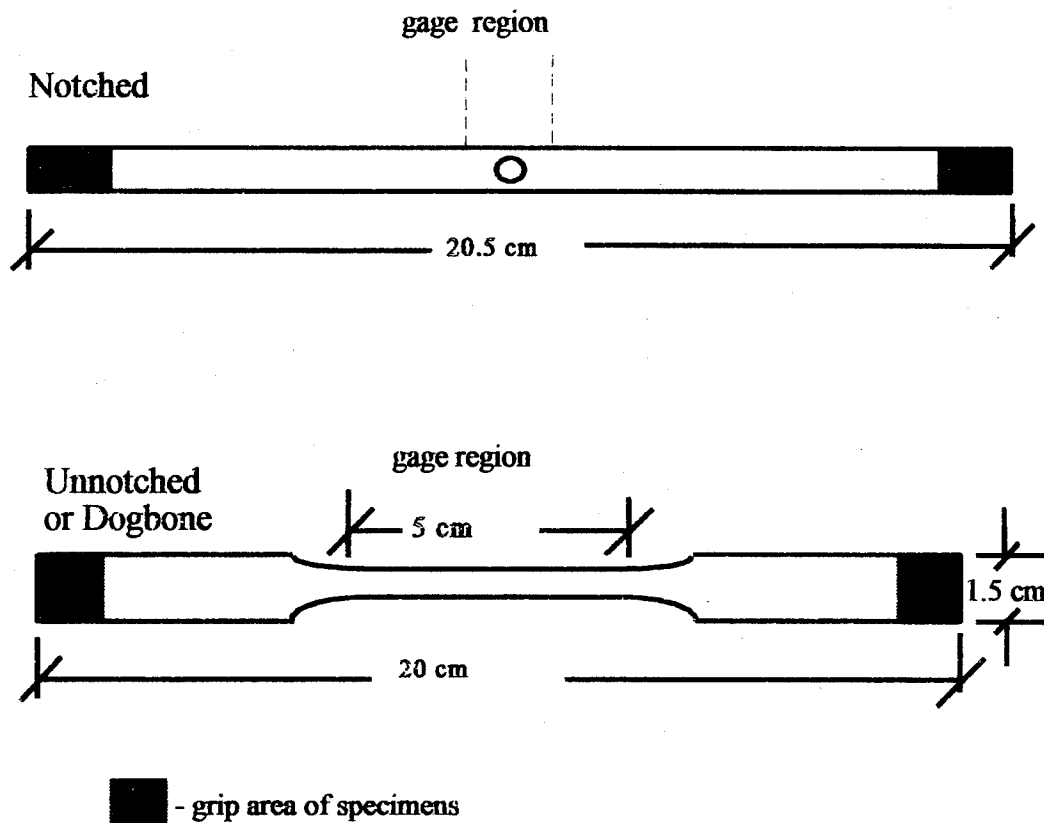
Figure 3-3 Test Specimen Geometry

B.   *Specimen Preparation*

The notched specimens could be polished on one edge to enable microscopic viewing during testing using the Questar measurement system, edge replication, and optical microscopic photography. A polished edge is shown in Figure 3-4 with clearly exposed yarns, matrix, and pores. The polishing was performed by using successively finer diamond suspension polishing liquid on Texmet cloth covered wheels. The first

——— Pore

——— 90° Yarn

——— 0° Yarn

Load Direction ◄————————►
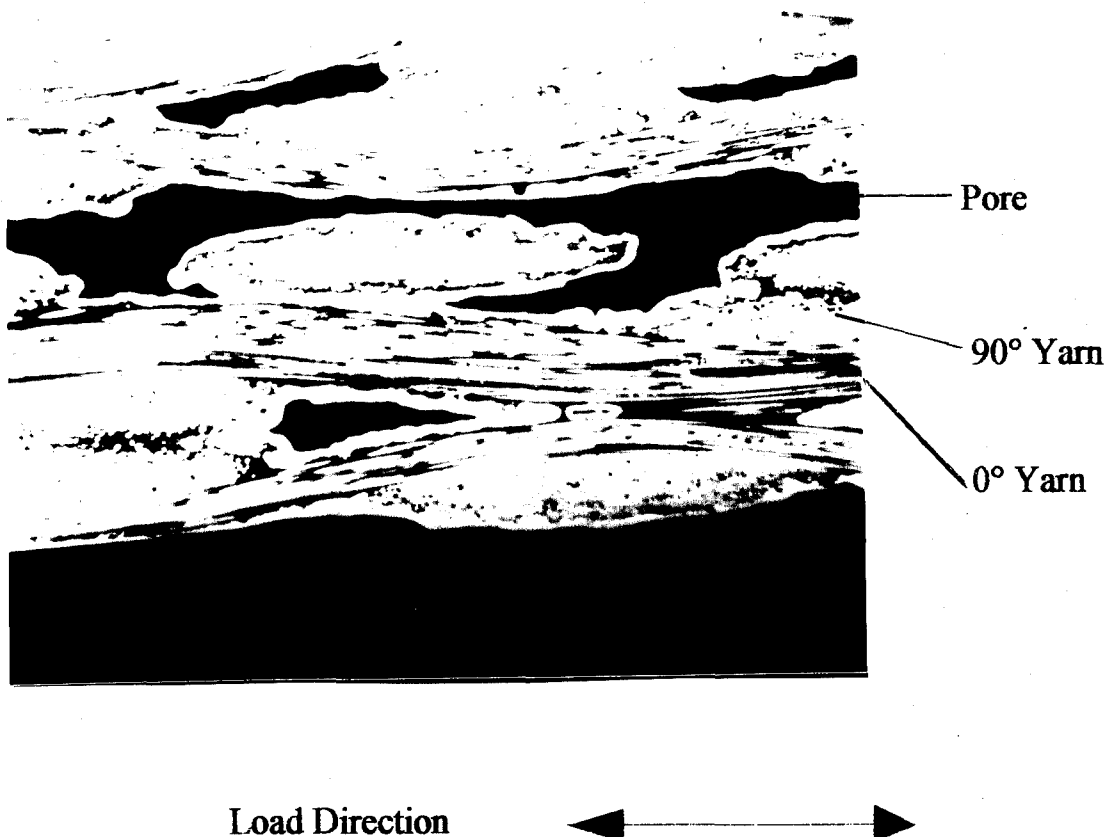
Figure 3-4   Undamaged Polished Edge of Specimen 100X

3.5

suspension was 45 micron diamond dust, and the final suspension was 1 micron. Five notched specimens were polished in this manner.

The above described polishing process removed the matrix and protective coatings from the polished edge. While permitting viewing of the fibers, the polishing process may have the possible negative side effects of introducing additional free edge effects and environmental degradation. The polished specimens were the 190 MPa, 175 MPa, 150 MPa, 125 MPa, and 100 MPa test specimens. The 110 MPa test specimen, which was not polished, fell on the lower end of the scatter band of cyclic fatigue life interpolated from the fatigue cycles endured by the polished specimens. Polishing, thus, appears to have had no detrimental effect on the outcome of the present fatigue testing.

No tabs were applied to the grip area of the notched or unnotched specimens because the narrow region of the dogbone, in the unnotched case, and hole, in the notched case, confined the failure region of the specimen in the gage area. The specimens were clamped by two sets of hydraulic wedge grip assemblies with a clamping pressure of 5 MPa. This value was chosen because of Chen's success with a clamping pressure of 5.52 MPa[4]. Wedge grips with a smooth grip surface, rather than serrated, were used to minimize damage to the specimens.

The above described grip configuration held the specimens without damage or slippage during fatigue and monotonic tensile testing.

C. *Test Equipment*

A 22.4 KN Material Test System (MTS) horizontal tensile tester (see Figure 3-5) was used for the present study. Cooling water was provided by a Neslab model HX 75 cooler.
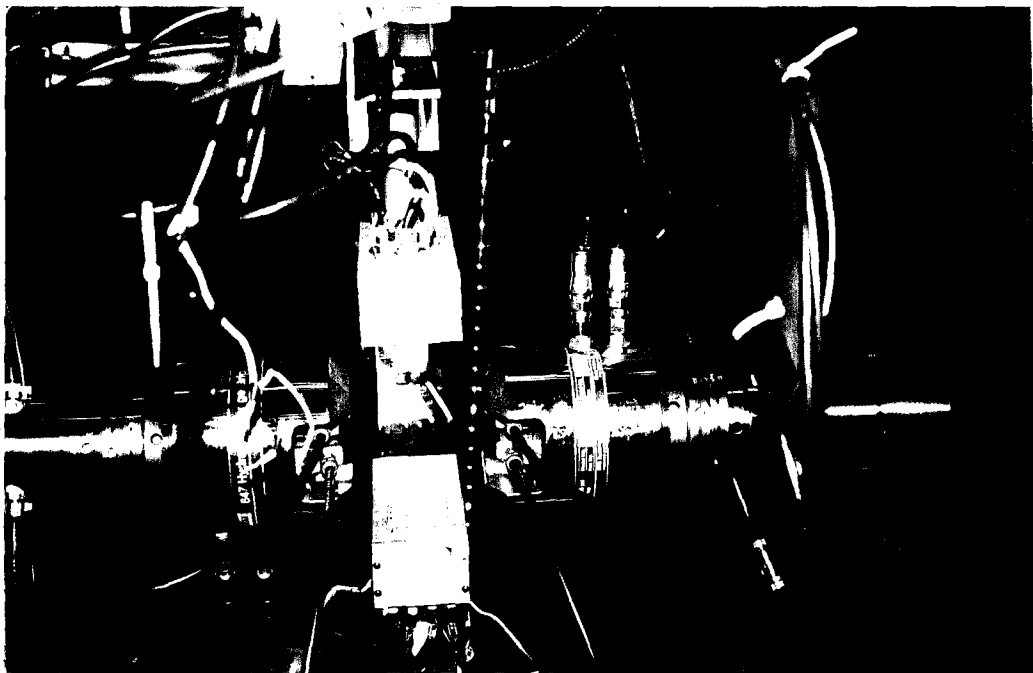
Figure 3-5 Horizontal Test Section with lamps

Cooling water was circulated through the grip wedges in the MTS 647 series grip wedge assembly. The water also cooled the heat

lamps and the isolation block between the grip wedge assemblies and the model 661.2 load cell. The heating lamp assemblies were manufactured locally by the Air Force Institute of Technology (AFIT) machine shop. Besides being water cooled, they had an internal airflow to improve heat dissipation.

The hydraulic grip wedge assemblies were operated by means of an MTS 685 Hydraulic Grip supply. Tensile pressure was applied to the specimen through the use of a Model 244 hydraulic actuator. Test specimen displacement was measured by means of an MTS model 632.53 E-14 extensometer. The extensometer gage length was 1.27 mm and it was calibrated to display 0.0127 mm full scale displacement for a maximum one percent strain. Monitoring and control functions were provided through an MTS model 458.2 microconsole with appropriate displacement, force, and strain plug-ins. Some feedback signals had to be filtered, and this was done through a Rockland model 852 filter. Barber-Colman 560 temperature controllers regulated the heat lamp assemblies to maintain the specimen in the test section at a constant 1100°C. The temperature controllers used feedback (temperature control) thermocouples mounted directly on the specimen. Fatigue testing was accomplished using MATE software developed by University of Dayton.

D.   Test Procedure

The major difficulties encountered while preparing for this series of fatigue tests were alignment of the grips and temperature control of the specimen. To perform the alignment an adjustment control, MTS model 609 was mounted on the test station between the load cell and the head block. An aluminum bar with eight strain gages was mounted in the grips of the test section. Deformation of the aluminum block could be monitored using alignment software and a micro-computer. The top (left in the photograph of Figure 3-5) grip alignment and rotation were adjusted until all strain gages displayed less than 100 μstrain variation.

Using the lamps in the standard perpendicular configuration shown in Figure 3-5 and Figure 3-6(a), the notched specimens were easily heated to the test temperature of 1100°C in the gage length for elevated temperature testing. The quartz extensometer probes were positioned 1.27 cm apart with the notch centered evenly between them. This lamp configuration proved inadequate for heating the unnotched specimens.

The first attempt to test an unnotched specimen used a perpendicular lamp configuration as used for the notched specimens.   The lamp housing width was 5 cm and the

3.9

Notched Test
Lamp Configuration
Side View

(a)

lamp assembly

lamps

display thermocouple

feedback
thermocouples

extensometer
probes

5 cm

display
thermocouple

feedback
thermocouples

(b)

Un-notched Test
Lamp Configuration
Top View

(Top lamp assembly omitted for clarity)

lamps
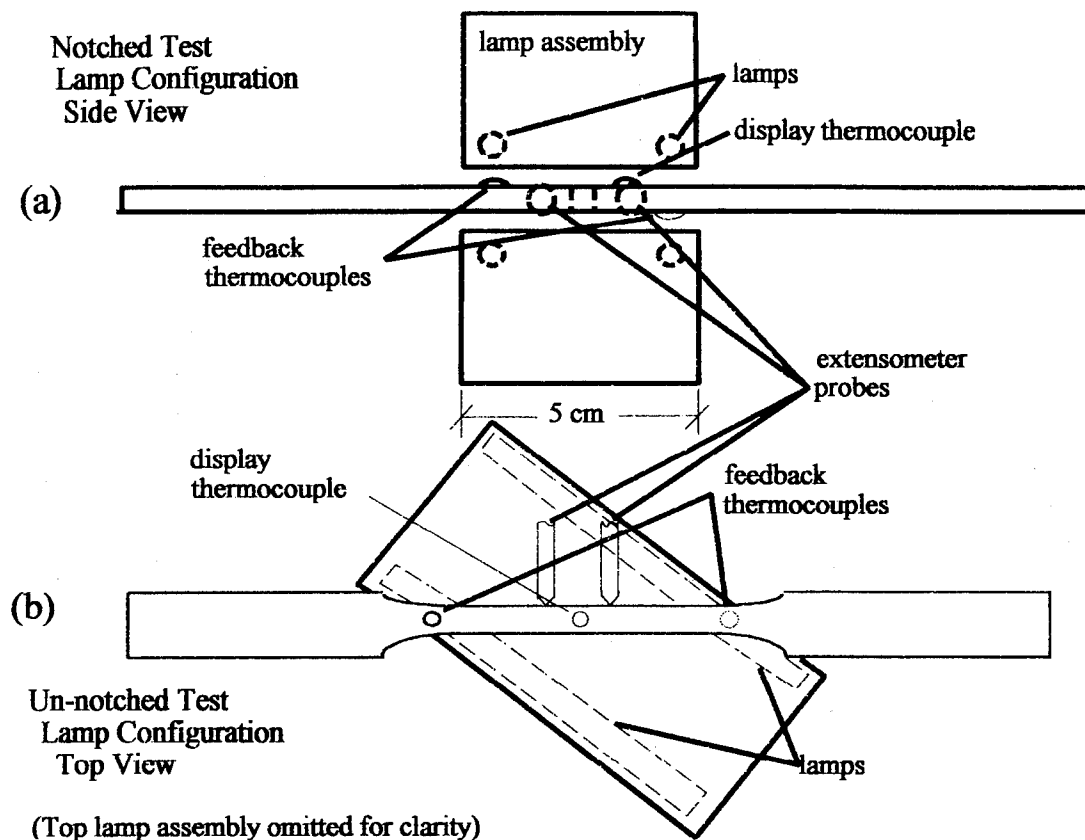
Figure 3-6   Heat Lamp Assembly Configuration

width of the dogbone (shoulder to shoulder) was 7.5 cm.   For
the   unnotched   test   the   extensometer   probes   were   again
positioned 1.27 cm apart, near the center of the narrow gage
region of the specimen.   Despite stringent temperature control
in the gage length (between extensometer probes), the specimen
failed at the edge of the shoulder.   With the heat lamp
assemblies oriented in the perpendicular configuration, the
temperature at the shoulder of the dogbone specimen was far

3.10

below the 1100°C test temperature. Inspection of the stress strain data revealed no modulus degradation had taken place during the cyclic fatigue testing. The absence of modulus degradation indicated the extensometer did not monitor deformation behavior typical of the failure zone. Since SiC/SiC has significantly different fatigue properties at room temperature than at elevated temperature [19], it is necessary to heat the entire narrow region of the unnotched specimen. In this way, the stress-strain behavior monitored by means of the extensometer and load cell is assuredly typical of the behavior preceding failure of the specimen.

After extensive temperature instrumentation of a "dummy" specimen the lamp assembly configuration of Figure 3-6(b) was found to give the required 1100°C temperature in the gage length and a temperature gradient of 75°C to the base of the shoulder. This temperature distribution was sufficient to produce behavior in the gage length typical of fracture area behavior in the specimen and provided legitimate fatigue life data points for the S-N curve.

The complete lay-out of the test procedure is shown in Figure 3-7. Seven notched specimens and five unnotched specimens were tested in tension-tension fatigue. These tests provided sufficient data points to establish the notched and unnotched S-N curves.
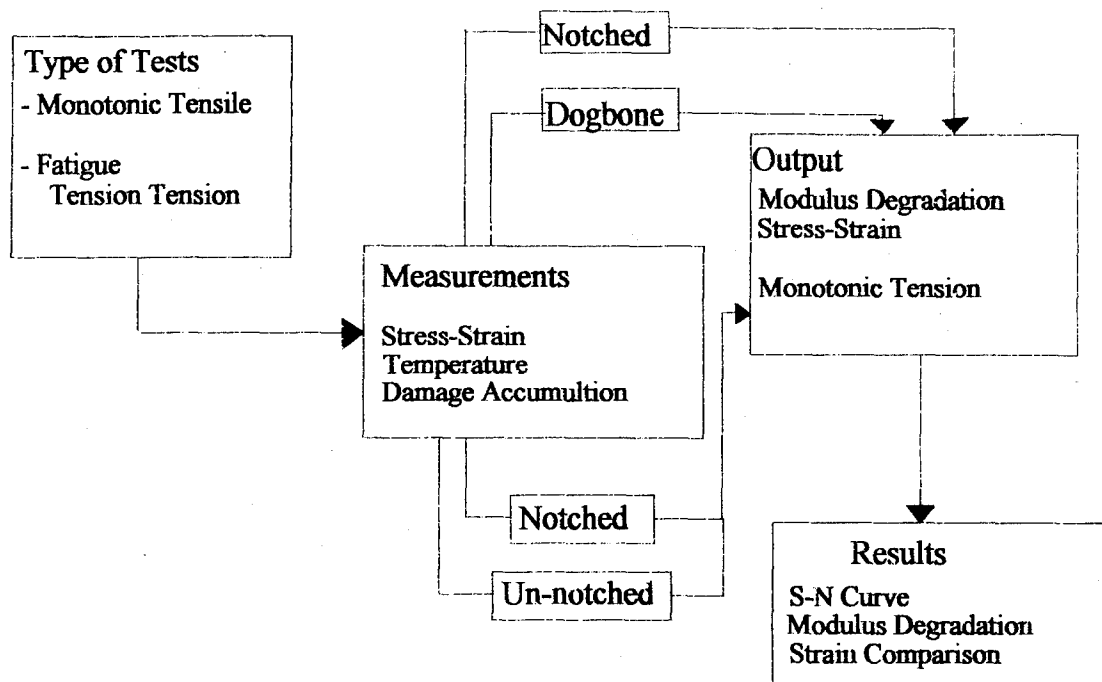
Figure 3-7   Schematic of Experimental Approach

During each fatigue test, force and displacement data were gathered periodically. Typically, at the beginning of a test, data was gathered every 20 cycles and the period of data collection was increased as the number of cycles increased. Approximately 1000 force-displacement data points were saved during each data acquasition cycle (DAC). This data was later used computing modulus and evaluating stress-strain relationships. During data reduction, force-displacement data was converted to stress strain data in the following manner:

$$F/A = \sigma \tag{1}$$

where F is the force applied through the hydraulic actuator and A is the area of the gage section. For the unnotched specimens the area is merely the cross-sectional area at the center of the gage region; however for the notched specimens:

$$A = (W-D)\,T \tag{2}$$

where W is the width of the notched specimen, D is the diameter of the hole and T is the thickness of the specimen. This is referred to as the reduced area.

IV RESULTS AND DISCUSSION

This chapter provides details of all tests conducted. All fatigue tests were conducted in the tension-tension mode at 1100°C. The loading spectrum corresponded to a triangular wave with a frequency of 1.0 Hz. The ratio of minimum to maximum load in all cases was 0.1. The tests are referenced by maximum applied stress level where the stress is defined as the applied tensile load per unit area. The area used in determining the stress level is the cross sectional area at the gauge length in the unnotched specimens and in the case of the notched specimens, it is further reduced by the area of the hole as described in section III D. The notched specimens had a centrally located circular hole with a hole diameter to specimen width ratio (D/W) of 0.331 ± 0.003. Results from these tests involving notched and unnotched configurations will be presented and comparisons will be made with the previous work.

Section A discusses monotonic tensile tests of the uunnotchedand notched specimens. Section B discusses the fatigue tests of the unnotched specimens. Section C discusses the fatigue tests of the notched specimens. The tests in sections B and C are presented in the order of applied maximum stress from the highest to lowest values. Section D presents

4.1

the S-N curves and discusses the fatigue life of the notched
and uunnotchedspecimens. Section E presents and discusses the
comparative stiffness behavior of the notched and unnotched
specimens. Section F discusses the deformation behavior of
uunnotchedand notched specimens during fatigue testing.
Section G discusses damage mechanisms related to low and high
levels of fatigue stress in both notched and unnotched
specimens.

A.   *Monotonic Tensile Tests*

Previous fatigue studies have shown that fatigue testing
at stresses below the proportional limit, σ_{PL}, of a material
results in run-out[24, 25]. Run-out was defined as survival of
the specimen when subjected to the loading of one million
cycles. The proportional limit is the end of the initial
linear region of the stress-strain curve. A monotonic tensile
test identifies the proportional limit and provides substantial
insight into the behavior of the material. Monotonic tensile
tests have been completed on this material by Chen [4] and
DuPont [12]. They found that beyond the proportional limit, the
stress-strain curve becomes non-linear as damage takes place
progressively in the inter yarn region, 90° matrix, 0° matrix,
0° fibers, and 0° yarns as described in section II. Table 4-1
compares the results of the present test with previous work.

4.2

Table 4-1

RESULTS OF UNNOTCHED, MONOTONIC TENSION TESTS

Value	DuPont [12]	Chen [4]	Present
Temperature	1000°C	1200°C	1100°C
Environment	Air	Argon gas	Air
σ_{ult} (MPa)	250	228	230+
e_f (%)	0.61	.7	.42+
E (GPa)	145	186	145
σ_{PL} (MPa)	87	84	60

+ These values are lower than would have been achieved had the specimen broken in the gage length
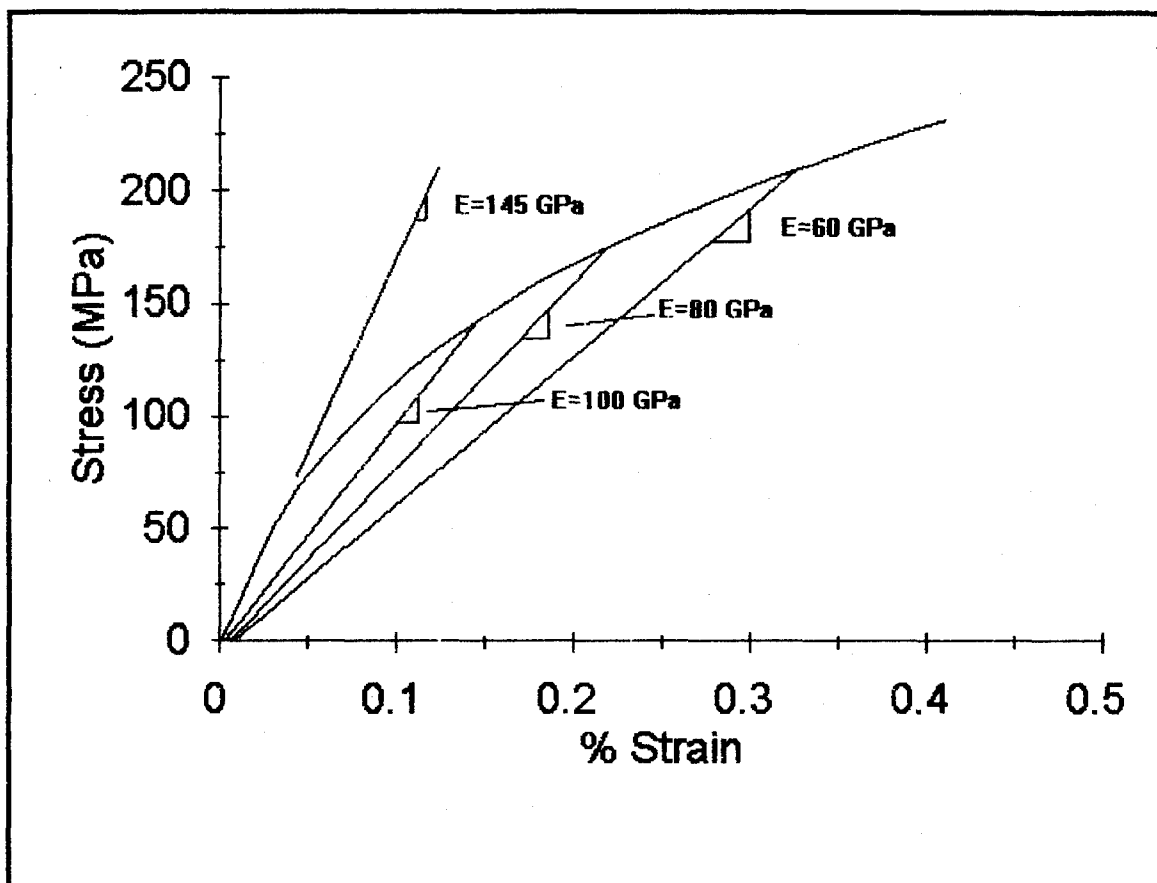

Figure 4-1   Unnotched Static Stress-Strain Curve

Figure 4-1 shows the unnotched stress strain curve of the present study with predicted unload paths for three successive stress levels. The Young's modulus is the slope of the initial linear region of the stress-strain curve and is found to be 145 GPa. The static test specimen failed at the grips, rather than in the gauge length. As a result, the values of ultimate tensile strength, σ_{ult} and fracture strain, ϵ_f may be slightly higher than those indicated in Table 4-1. In previous work [4], when the plain weave, enhanced SiC/SiC material was loaded beyond the proportional limit, σ_{PL}, and unloaded (before failure), the stress-strain plots were found to be extremely linear. The monotonic tensile test stress strain curve, Figure 4-1, shows the predicted unloading and loading paths for stress levels of 140, 170, and 210 MPa.

The notched specimen stress levels were calculated using the reduced area of the hole region:

$$\sigma = F/(W-D)T \qquad (3)$$

where F is the force applied, W and T are the specimen width and thickness respectively, and D is the diameter of the hole. Therefore, the displacement and strain data of notched specimens do not correlate directly to the data for unnotched specimens. In this case, deformation is not uniform throughout the entire gauge length, but is concentrated in the narrow region near the hole. The stress-strain plot for the notched

specimen does not represent a true material property; therefore, the slope of the linear portion of the stress strain curve is referred to as stiffness, S, instead of modulus. The stress-strain curve for the notched specimen tested under monotonic loading is shown in Figure 4-2 with three predicted
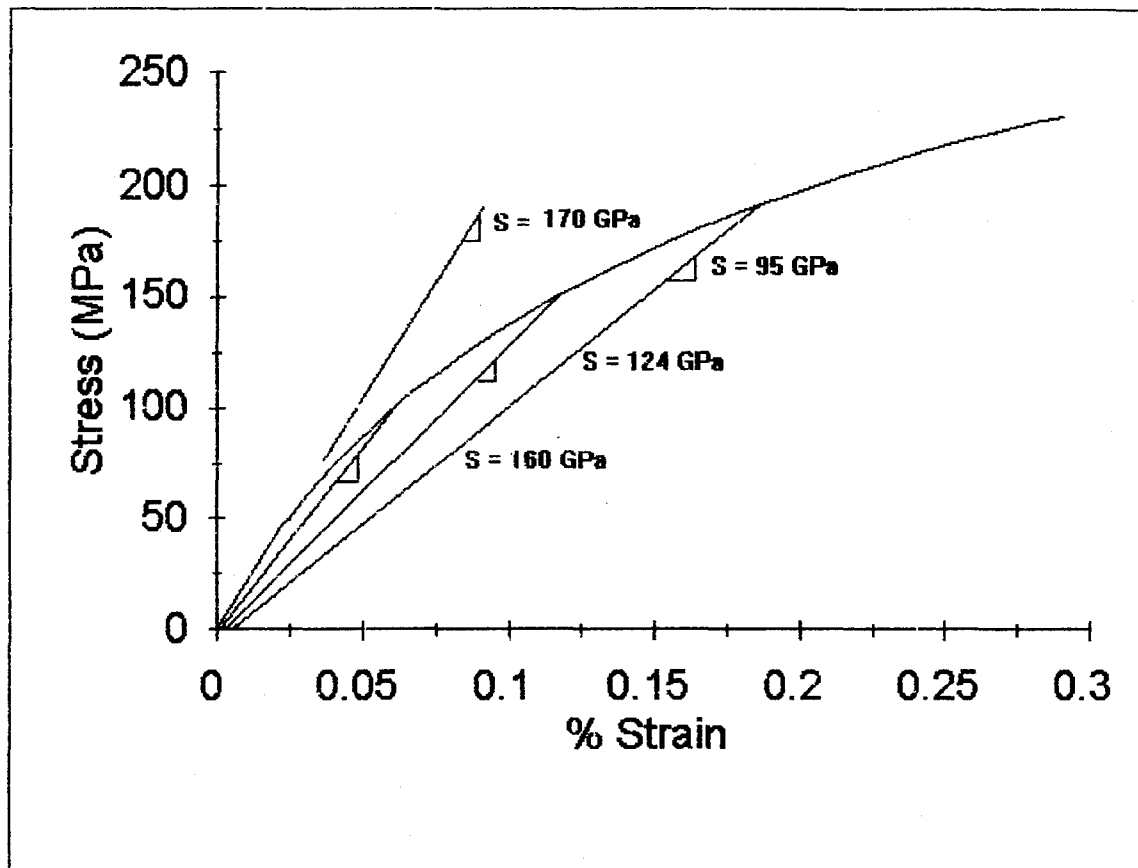

Figure 4-2 Monotonic Tensile Stress-Strain Curve of the Notched Specimen

unload paths for increasing levels of stress. A proportional limit does not appear to exist in the case of notched specimens except at a very low stress level (about 40 MPa). Non-linear

4.5

stress strain response is observed from the beginning through the end of the loading portion of the first cycle of the fatigue tests. For purposes of comparison, slope of the curve below 60 MPa is taken as the initial stiffness of the first cycle during fatigue testing. Due to the somewhat linear nature of the load-displacement plot at such a low load level, this slope may be treated equivalent to the unnotched modulus. These differences in the slope and curvature of the initial portion of the stress-strain curves may be attributed to stress concentration effects near the hole.

Failure (ultimate tensile strength) of the notched specimen occurred at 228 MPa, a value slightly lower than that of the unnotched specimen. During fatigue testing of the notched specimen, the most significant change in stress strain behavior occured in the first cycle, as it did in the uunnotchedspecimen. The loading portion of the first fatigue cycle always followed a stress-strain curve similar to that exhibited during monotonic tensile testing until the maximum load was reached for the given test. The unloading portion of the first cycle, and subsequent recycling followed a linear path during fatigue testing. The predicted unloading paths at stress levels of 100, 150, and 190 MPa are shown in Figure 4-2.

The results of notched and unnotched monotonic tensile tests are compared in Table 4-2. Notice the apparent lack of

Table 4-2

COMPARISON OF NOTCHED VS. UNNOTCHED MONOTONIC TENSILE TESTS

		Notched	Unnotched
σ_{ult}	(MPa)	228	230+
ϵ_f	(%)	0.29	0.42+
Stiffness	(GPa)	170	145

+ These values are lower than would have been achieved
had the specimen broken in the gage length

stress concentration effect in ultimate tensile strength, σ_{ult},
but stress concentration near the hole causes a reduction in
failure strain, ϵ_f, and an increase in stiffness.

The magnified fracture surface is shown in Figure 4-3 and
a scanning electron micrograph of the fracture surface is
presented in Figure 4-4. Note the jagged fracture surface and
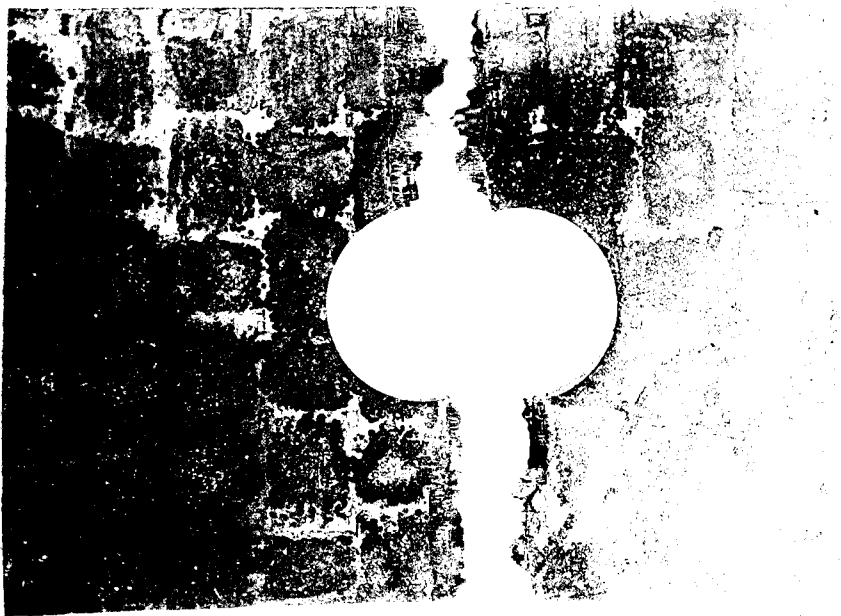
Figure 4-3 Static Notched Test, Fracture Surface 8X Mag.
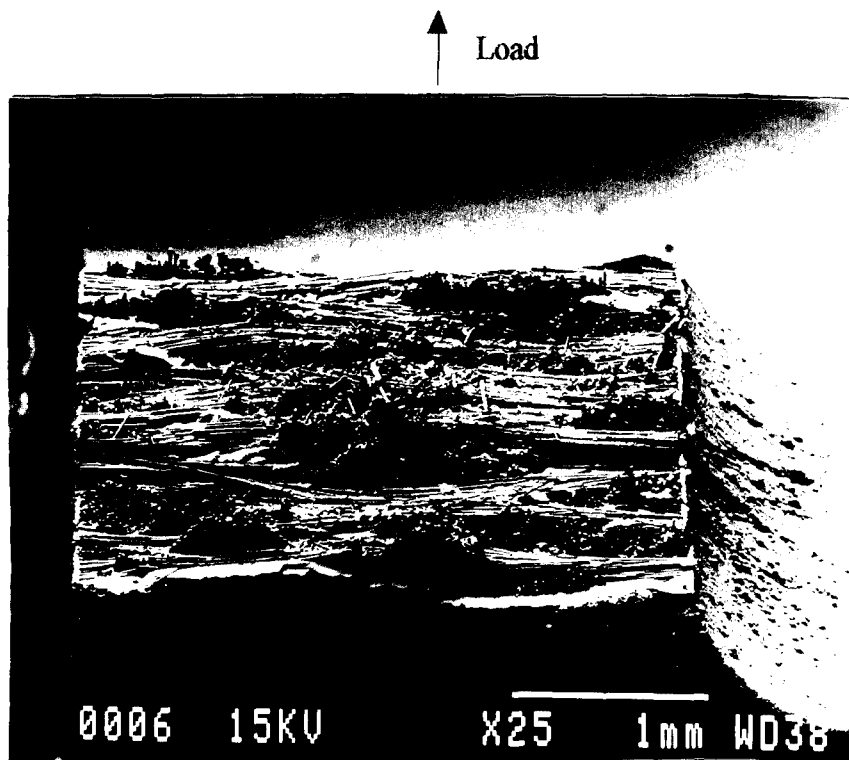
4.7

Load ↑

Figure 4-4 Notched Monotonic Tensile Fracture Surface, Scanning Electron Micrograph, 25X

high degree of fiber pullout displayed in the photograph. The long standing fiber bunches are the remains of 0° yarns. The fibers of the 90° yarns are visible between the 0° yarns on the fracture surface. Note also that the fracture extends perpendicular to the uniaxial load.

B.   Unnotched Fatigue results

The unnotched fatigue test with the highest tensile stress level was the 210 MPa test.   It cycled 977 times before failure.   A view of the fracture is presented in Figure 4-5. The 210 MPa test stress-strain curves at four specific cycles of the test are shown in Figure 4-6.   The stress-strain behavior during the first cycle exhibited the same nonlinearity above the proportional limit as previously described for monotonic tensile testing; however, the stress strain curves of

Loading
Direction
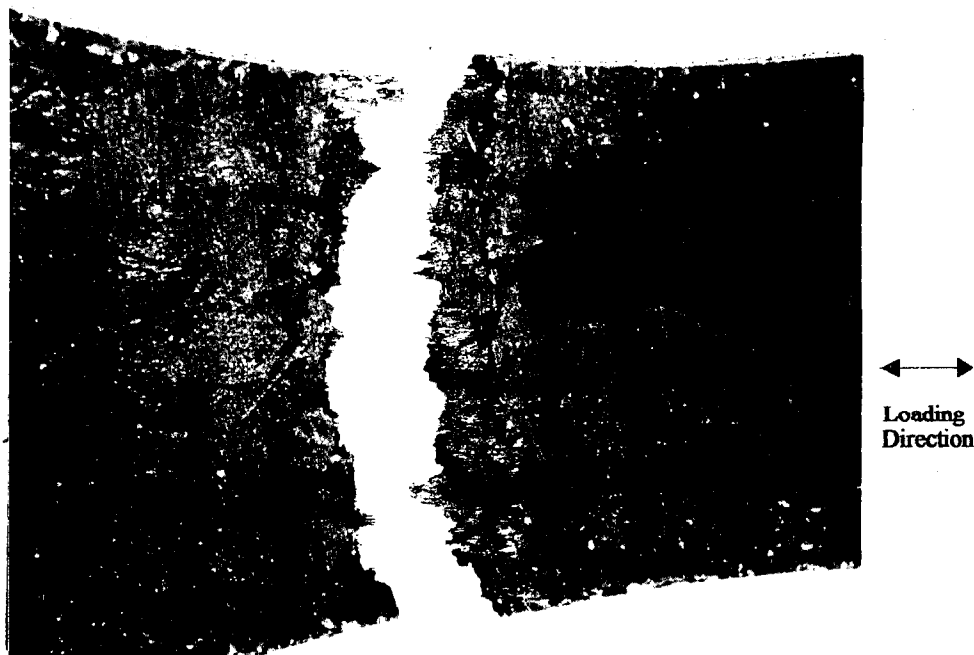
Figure 4-5   Fracture Surface, Top View,
210 MPa Unnotched Test, 8X
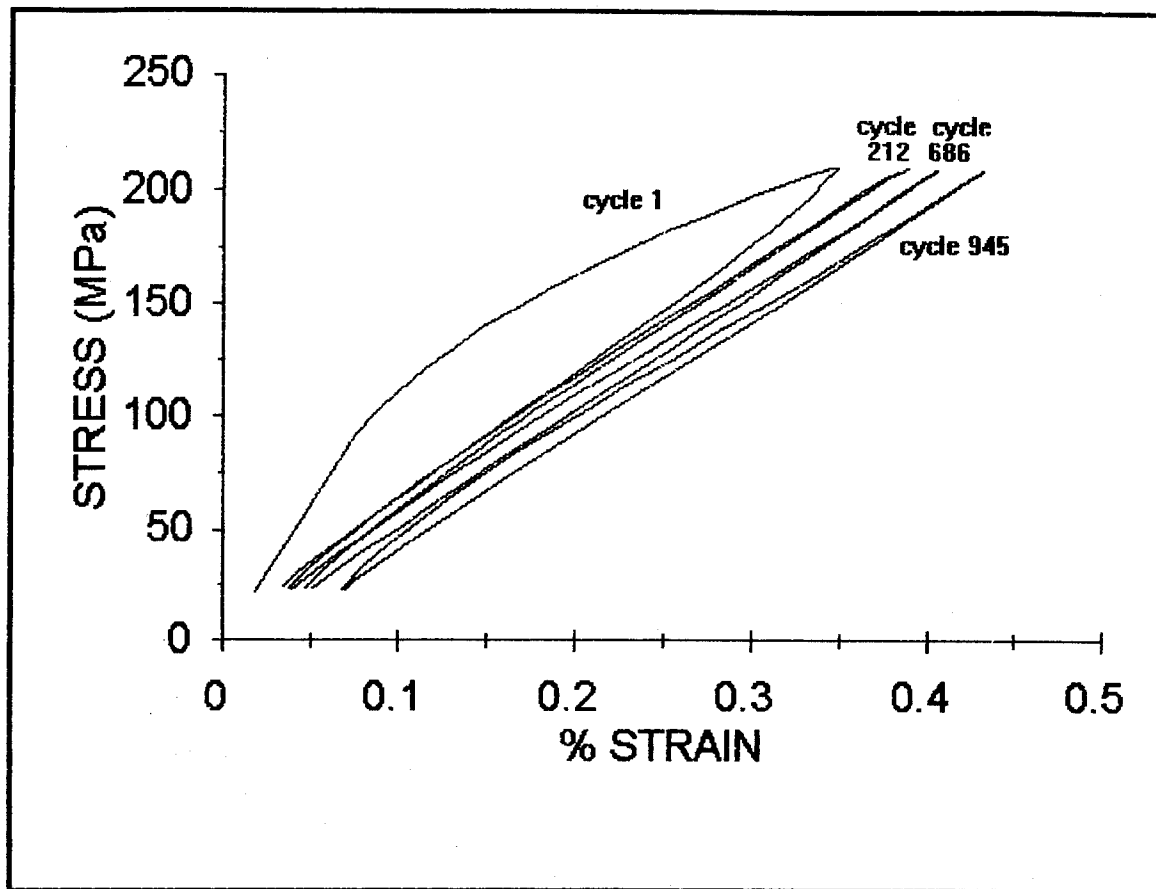
Figure 4-6 210 MPa Unnotched Stress-Strain Curves

subsequent cycles are relatively linear. Since the 210 MPa
load level was well above the proportional limit, significant
damage occurred on the first cycle. After this first cycle
damage, there is a slight residual strain accumulation
indicating permanent deformation as a result of the cyclic
loading.

The damage accrued and the modulus degraded slightly with
further cycling as plotted in Figure 4-7. The first cycle

4.10
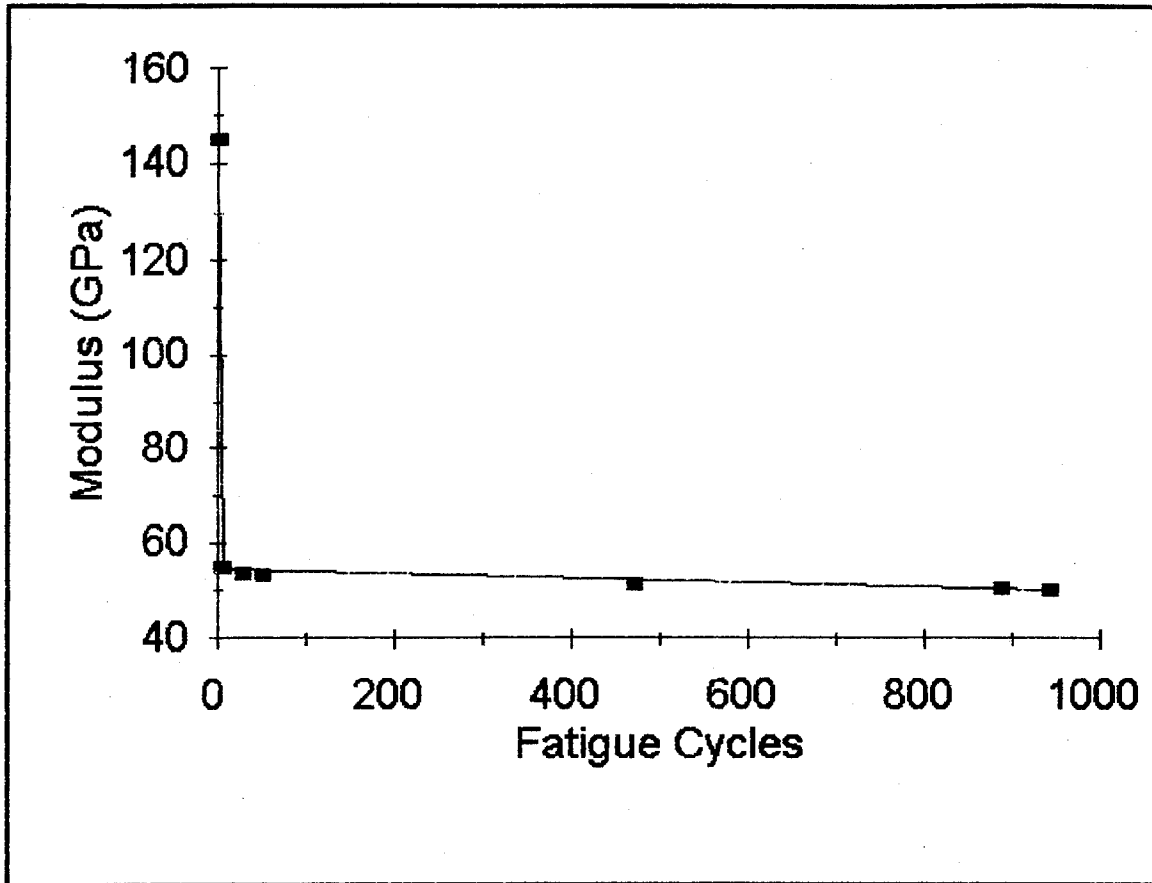
Figure 4-7 210 MPa Unnotched Modulus Reduction

modulus is the Young's modulus obtained in the monotonic
tensile test. Subsequent modulus values are those provided by
the MATE test software. MATE uses the differential (difference
between maximum and minimum) stress and strain in this
calculation as follows:

$$E = \frac{\sigma_{max} - \sigma_{min}}{\epsilon_{max} - \epsilon_{min}}$$ (4)

Due to the linear nature of the stress strain behavior of the
fatigue cycles this method gives satisfactory results. The

4.11

variation in the modulus during cycling, in many cases, is a good indication of what is taking place in the material when subjected to fatigue. The first cycle damage may be quantified in the form of initial modulus reduction. Note the 62% decrease in modulus from 145 GPa in the linear loading region of the first cycle to average value of 55 GPa exhibited during the cycling of the test. It is important to note the excellent correlation of this cyclic fatigue modulus of 55 GPa with the 60 GPa modulus predicted via the monotonic tensile test up to a stress of 210 MPa. After this initial modulus reduction (denoting microstructural damage), the modulus remained essentially constant for the entire life of the test.

To investigate the microstructural damage, scanning electron microscopy (SEM) was used in this study. A low power (X12) SEM view of the fractured surface is shown in Figure 4-8. This SEM micrograph is obtained by tilting the specimen at an angle of 45° to the electron beam in order to highlight fiber pullout lengths along with the overall contour of the fracture surface. The surface exhibits a jagged appearance with evidence of matrix/fiber interface debonding in the form of fiber pullout. This morphology of surface and damage are very similar to that exhibited during high temperature monotonic testing[4]. The surface of Figure 4-8 displays a high degree of matrix/fiber interface debond in the 0° yarns.

4.12
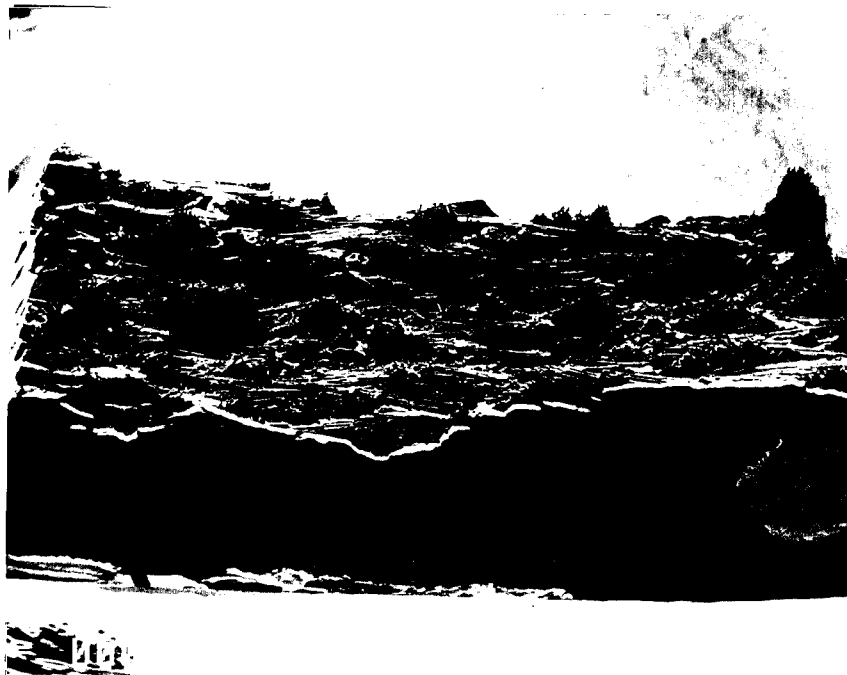
Figure 4-8   SEM Micrograph of Failure Surface at 45°
Angle, 210 MPa Test, 12X

It is important to note the standing fiber bunches, evidence of
fiber matrix interface debonding and fiber pullout in the 0°
yarns.   The clearly visible fibers in the 90° yarns are
evidence of the 90° matrix micro-cracking and crack deflection
along interface regions.   Initial load level was sufficient to
bring all these damage mechanisms into play.

The first unnotched fatigue test at intermediate stress
level was the 170 MPa test.   It cycled 6,881 times before
failure.   A magnified view of the fractured specimen is shown
in Figure 4-9.   Note the slightly smoother fracture surface as
opposed to the 210 MPa test (Figure 4-5).

4.13

Figure 4-9   170 MPa Fracture Surface 8X

The stress vs. strain curves for four specific cycles of the 170 MPa test are shown in Figure 4-10.   The response was again nonlinear because the load level was, of course, above the proportional limit.   A slight residual strain accumulation indicates permanent deformation as a result of the fatigue. The increased hysteresis and decreased slope over the life of the test may be attributed to cumulative microstructural damage.

Figure 4-11 shows the modulus reduction over the life of the 170 MPa unnotched fatigue test.   This is further evidence of the microstructural damage taking place during the test.

Figure 4-10   Stress-strain 170 MPa Unnotched Test

Overall a modulus reduction of 52% is observed from the Young's
modulus of the loading portion of the first cycle to the
modulus of the third cycle in this test.   The 80 GPa Young's
modulus predicted by plotting a line to the 170 MPa stress
level of the unnotched monotonic tensile test shows the good
correlation with the 70 GPa displayed in this 170 MPa fatigue
test.   After the first cycle damage, indicated by the large
initial reduction of modulus, further damage effects a constant
rate modulus reduction over the life of the test until the
specimen fails at a modulus of 60 GPa.
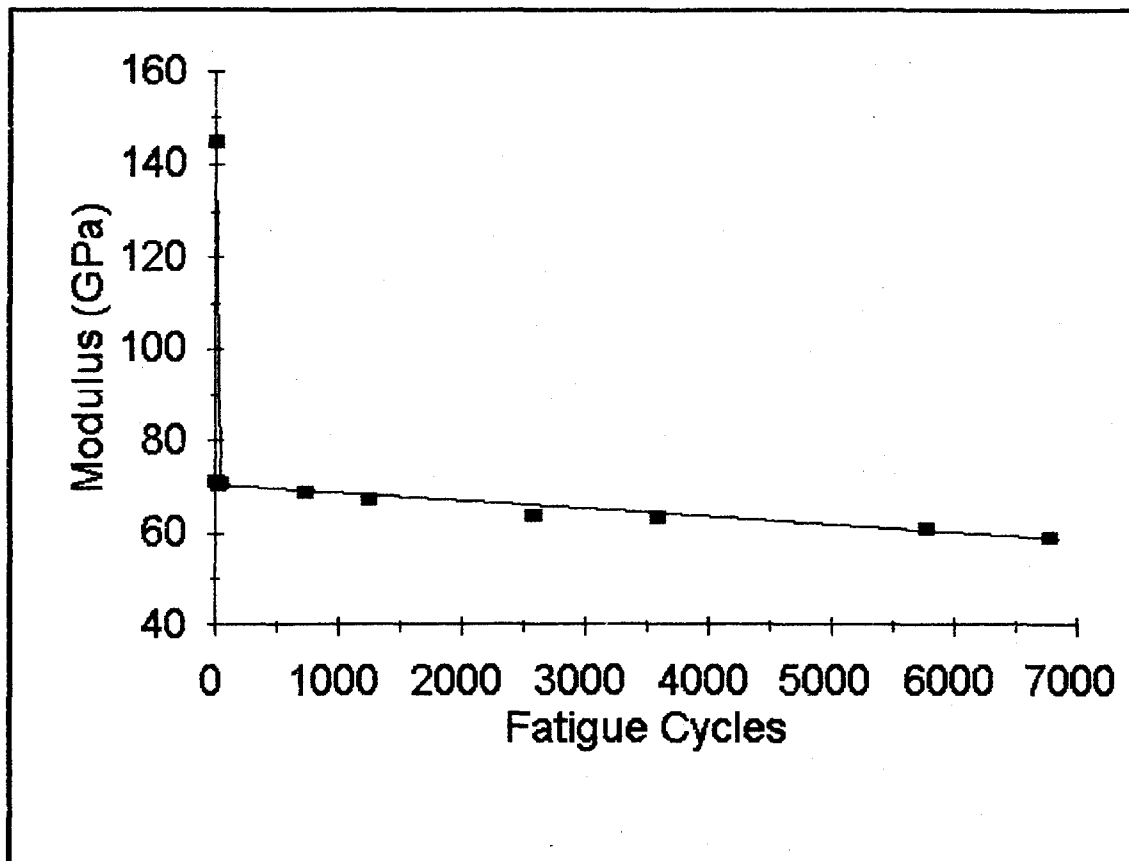
Figure 4-11   170 MPa Unnotched Modulus Reduction

The next fatigue stress level of unnotched test was the 140 MPa test. This specimen cycled 25,343 times before failure. A magnified view of the fracture is shown in Figure 4-12. Four stress-strain curves of the 140 MPa test are shown in Figure 4-13. The specimen's stress-strain response showed a slight progressive increase in nonlinearity which is most likely attributable to the progression of multiple matrix micro-cracking and fiber pullout. Residual strain increased in magnitude over the life of the test indicating some micro-structural damage accumulation.

4.16

Figure 4-12   140 MPa Unnotched Failure Surface, 8X
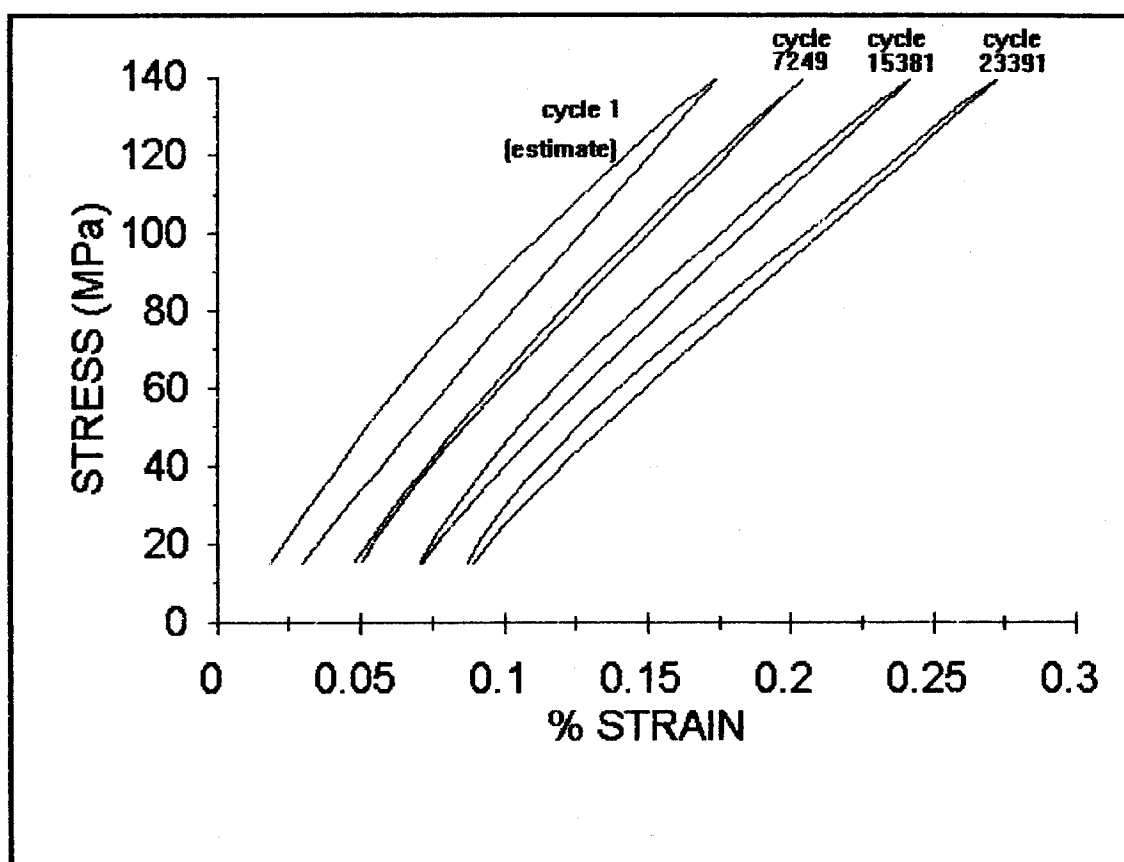
Figure 4-13   140 MPa Unnotched Stress Strain Curves

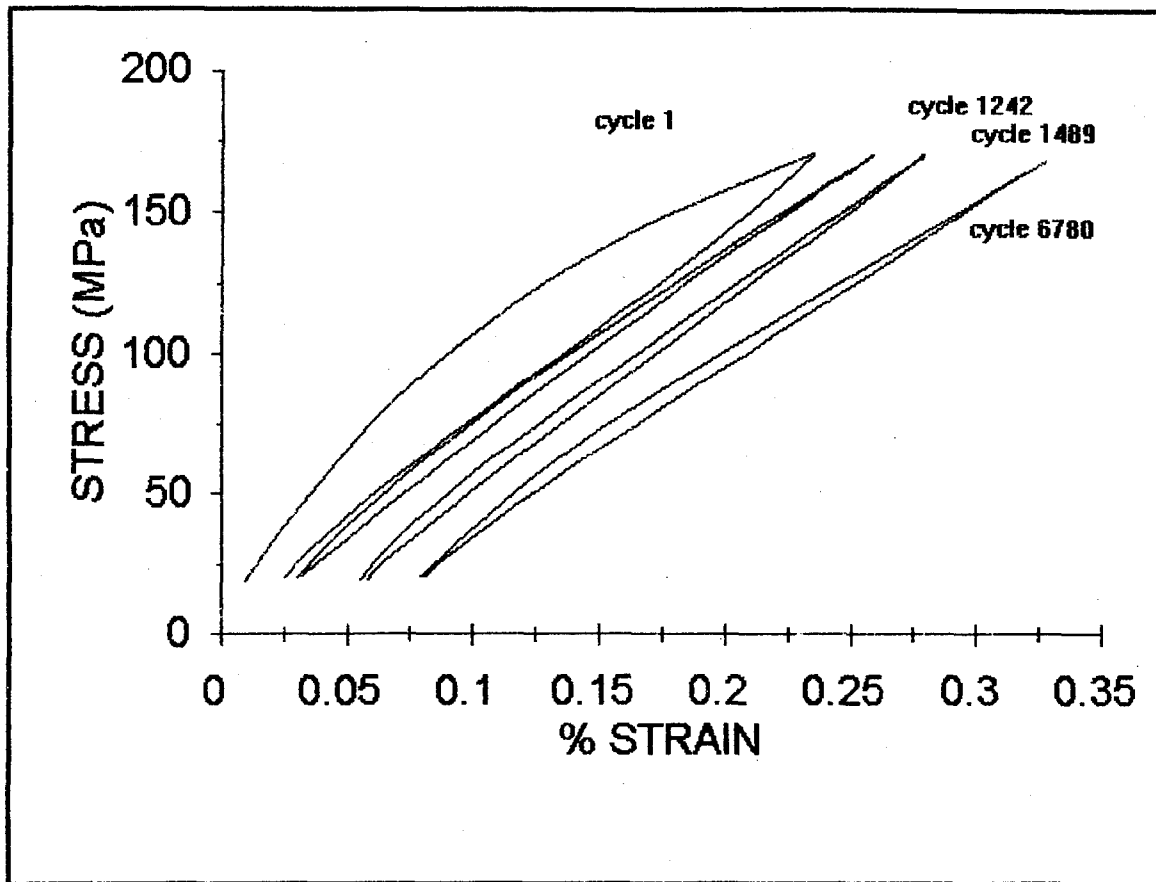Figure 4-14 shows the modulus reduction over the life of the test. This is further evidence of the microstructural damage taking place during the test. An initial modulus reduction of 31% was observed. This 31% first cycle modulus degradation to 100 GPa correlated exactly with the Young's modulus predicted by projecting a line from the origin to the 140 MPa stress level of the monotonic tensile test stress-strain curve. At this stress level, as opposed to higher fatigue stress levels, the modulus behavior assumed a slightly different nature. The initial cycle again produced modulus
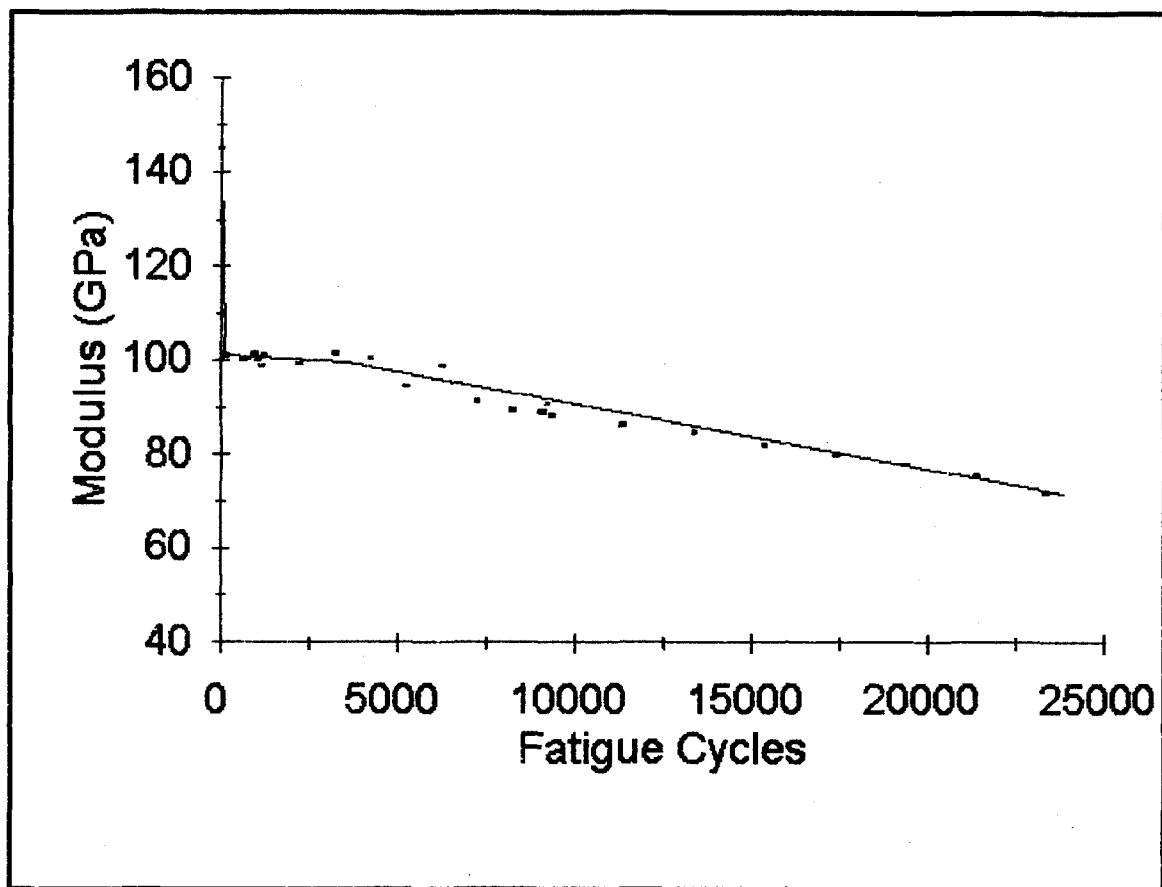
Figure 4-14   140 MPa Unnotched Modulus Reduction

degradation symptomatic of first cycle micro-structural damage; however, in this test the modulus remained near the 100 GPa level for a short time after which it degraded steadily until the specimen failure. It may be postulated that the first cycle failed to activate all damage mechanisms, but the fatigue promoted the development of multiple matrix micro-cracking and fiber pullout causing the modulus to decrease at a constant rate until eventual failure.

A scanning electon micrograph of the fracture surface of this test is presented in Figure 4-15. This surface displays the same damage mechanisms as noted in previous tests; however, reduced fiber pull-out is also evident.
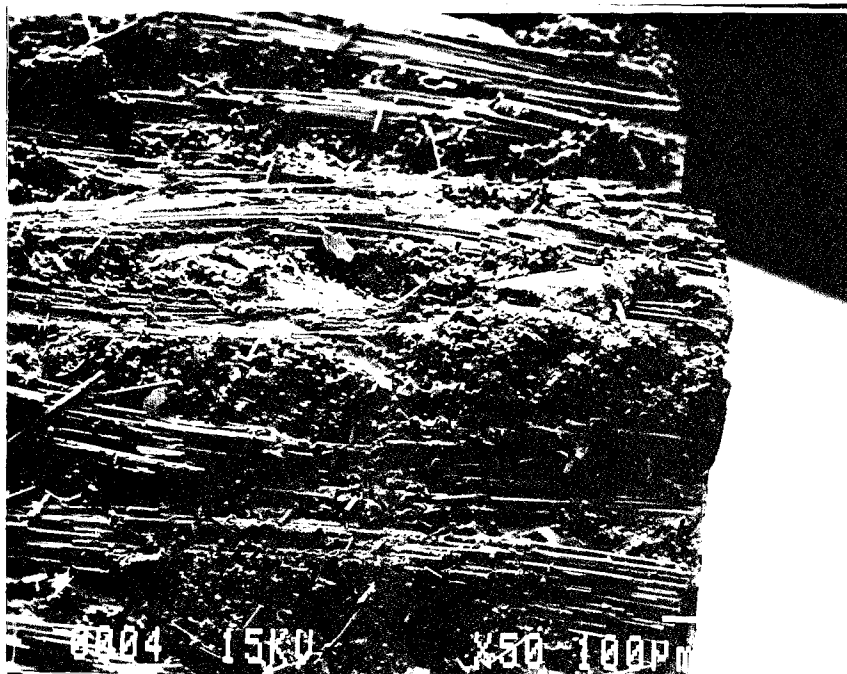
Figure 4-15 SEM Photomicrograph of Failure Surface at 45° Angle, 140 MPa Unnotched Test, 50X

4.19

The next lowest stress level of unnotched fatigue test was the 120 MPa test. It cycled 44,041 times before failure. A magnified view of the fracture is shown in Figure 4-16. The stress-strain curves of this test are plotted in Figure 4-17. This figure shows stress-strain response at four specific cycles of the test. This test had the most linear stress strain curves with the least hysteresis during the early cycles. The specimen showed almost completely linear response at cycle two with very little hysteresis and very slight nonlinearity. As the test progressed, however, hysteresis and
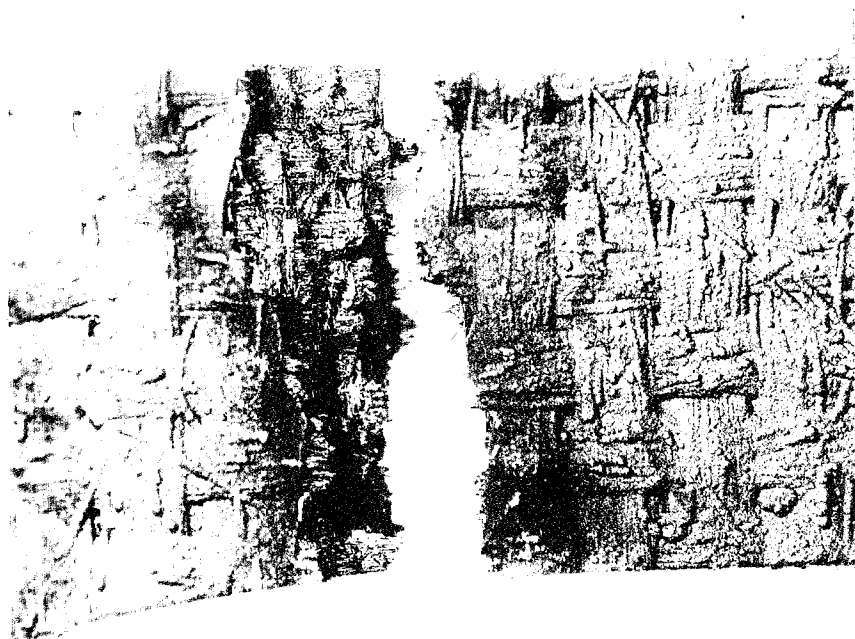
Figure 4-16   Fracture Surface, 120 MPa Unnotched Test, 8X
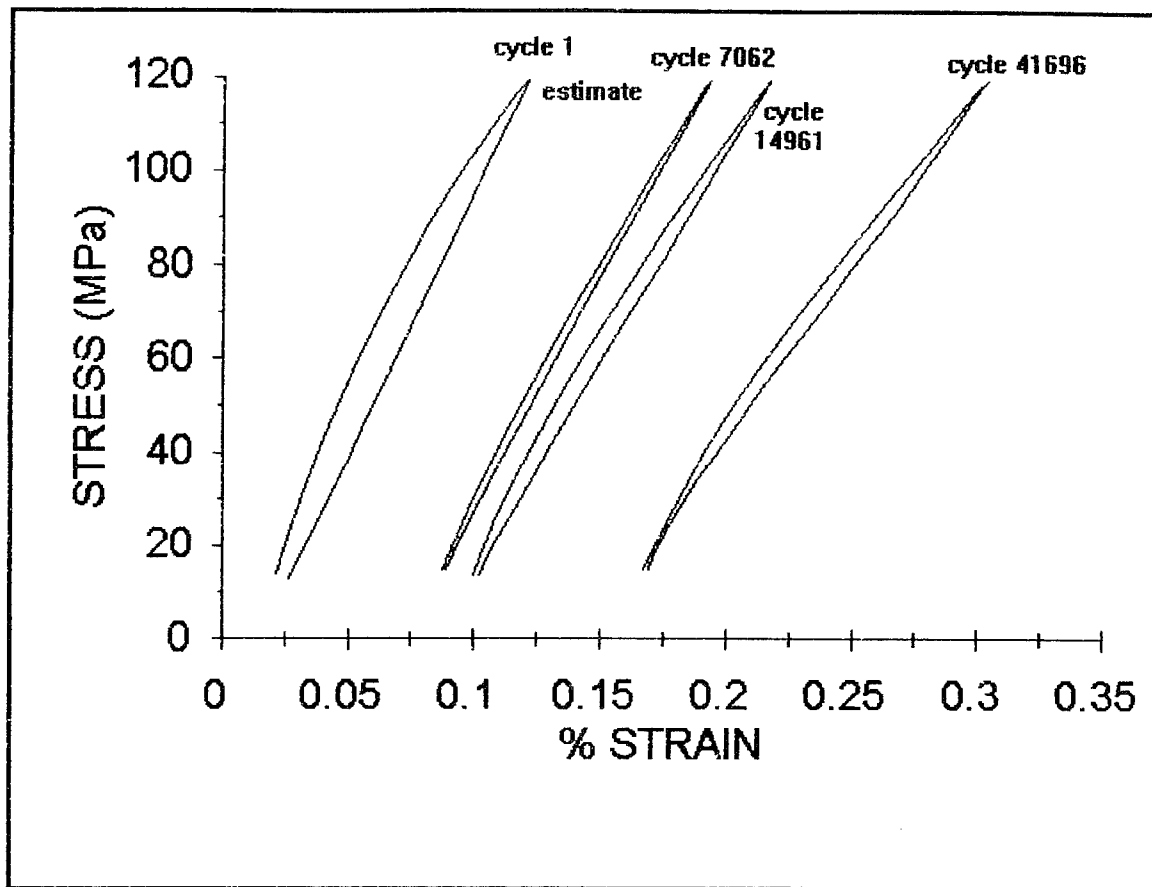
Figure 4-17   120 MPa Unnotched Stress-strain Results

non-linearity increased.   Near the end of specimen fatigue life, the stress-strain curves exhibited again a good amount of hysteresis and non-linearity.

Figure 4-18 shows the modulus reduction over the life of the test.   Note the 21% loss of modulus from 145 GPa in the linear region of the first cycle to an average value of 115 GPa exhibited during the cycling of the test.   A low magnification micrograph of the fracture surface is shown in Figure 4-19.

4.21
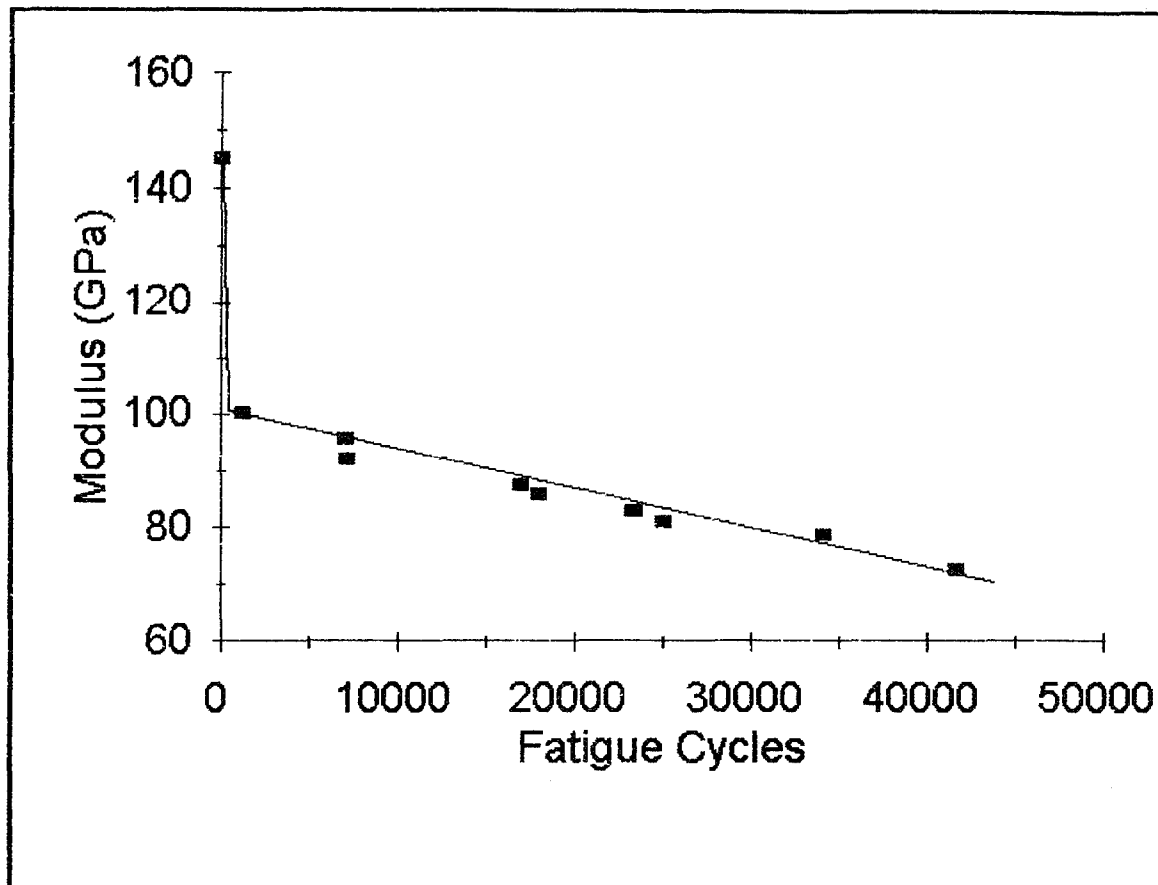
Figure 4-18   120 MPa Unnotched Modulus Reduction
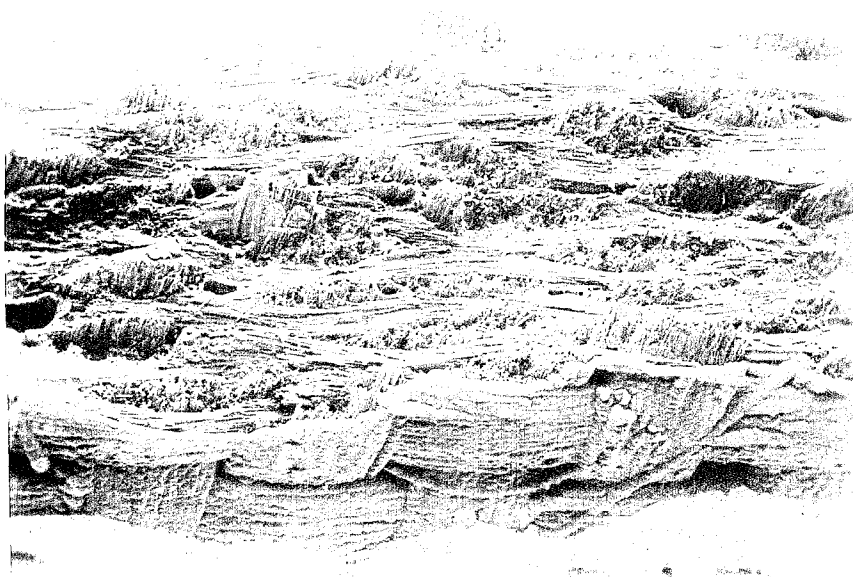
Figure 4-19   Scanning Electron Micrograph of Fracture
Surface, 120 MPa Unnotched Test, 15X

Closer inspection revealed the smooth fracture appearance was due to crack propagation through the fibers of the 0° yarns rather than fiber pullout which predominated the fracture surface of the higher fatigue stress level tests. As discussed in Chapter II, fiber pullout is desired to promote multiple matrix micro-cracking and composite toughness. One can see a significantly different type of damage than was evident in the 210 MPa test. Here failure, especially at the corners, exhibits far less fiber pullout.

The lowest stress level of unnotched fatigue test was the 110 MPa test. It cycled 259,249 times before failure. A magnified optical micrograph of the fracture surface is presented in Figure 4-20. This specimen was the only unnotched specimen which had the failure in the center of the gage length.
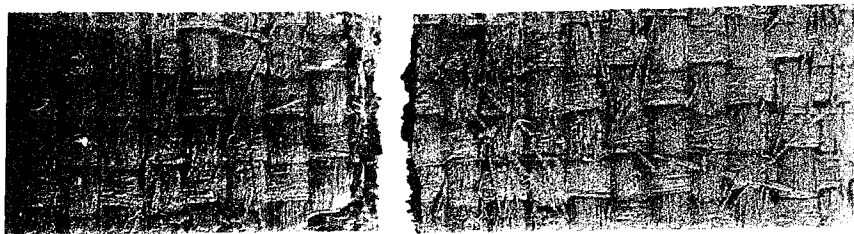
Figure 4-20   Fracture Surface, 110 MPa Unnotched Test, 7X

Figure 4-21 plots the modulus reduction over the life of the specimen. Notice the modulus reduction of this test has a somewhat different character than previous unnotched tests. In the 110 MPa test, the modulus did not degrade below 110 GPa
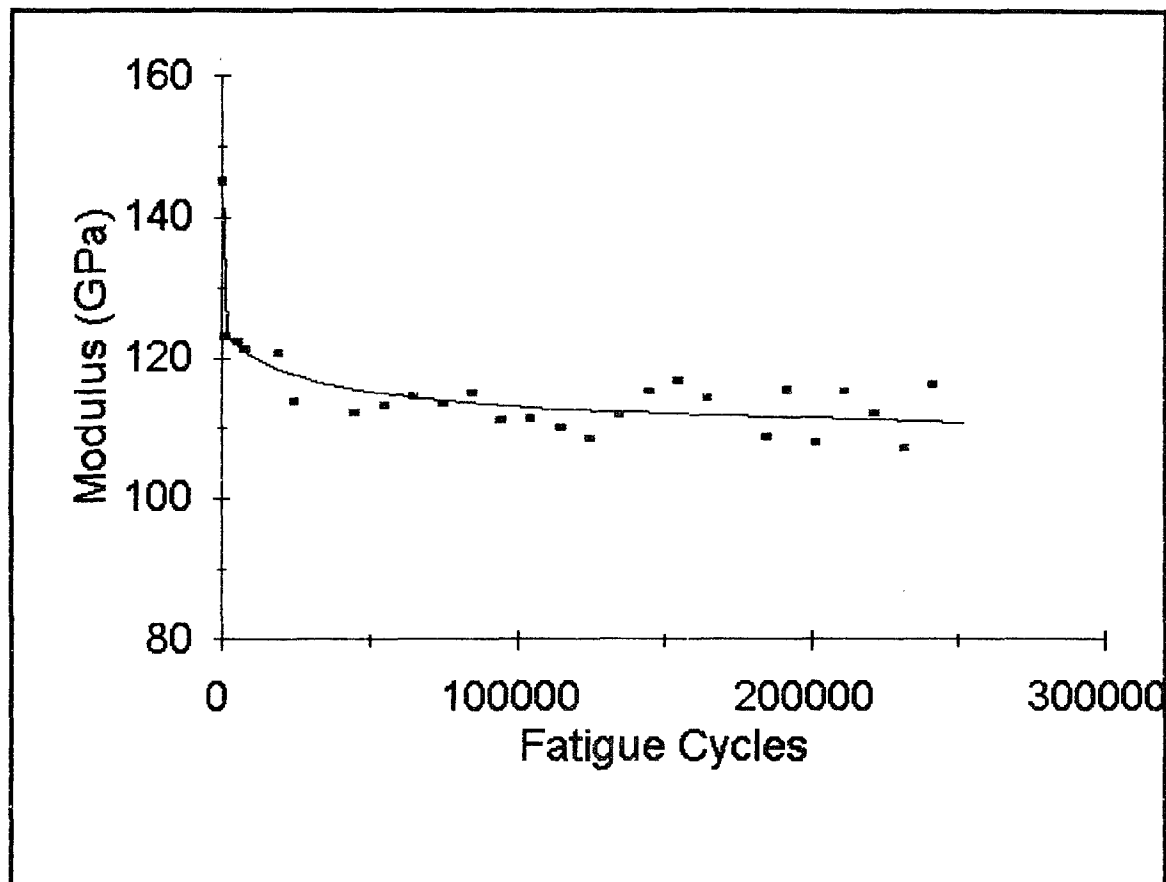
Figure 4-21   110 MPa Unnotched Modulus Reduction

before its failure. This behavior implies that the low stress fatigue damage mode has changed substantially from that of high stress fatigue. Figure 4-22 provides a 45° angular perspective view of this specimen's fracture surface and shows a marked contrast to the 210 MPa surface (Figure 4-8). The smoother
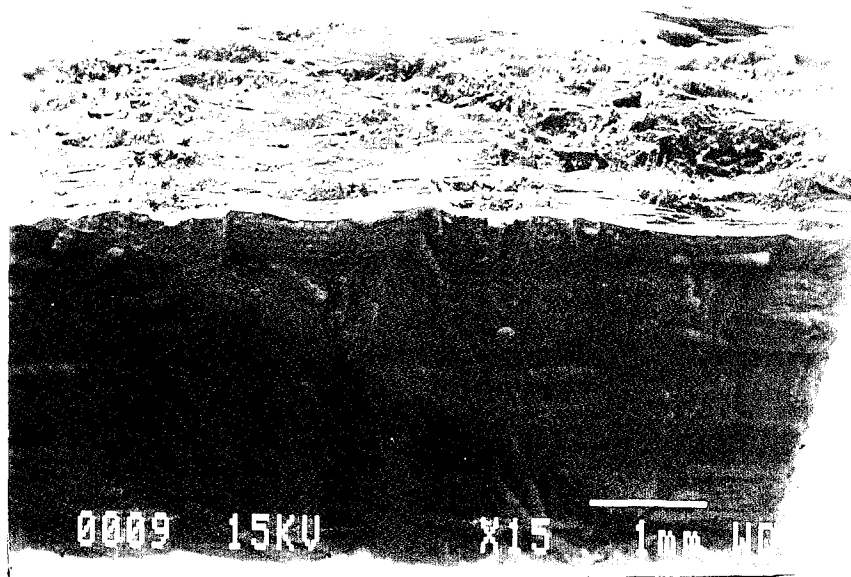
Figure 4-22   Scanning Electron Micrograph of Fracture
Surface, 110 MPa Unnotched Test, 15X

surface of the 110 MPa test indicates a lack of fiber pullout

similar to that discussed for the 120 MPa test.

B.   *Notched Fatigue Results*

This section provides the results of the notched specimen

tests.   Damage in these specimens, especially at the higher

stress levels, occurred in the region adjacent to the hole and

perpendicular to the load.   The notched specimen stress levels

were calculated using the reduced area of the hole region.

Therefore, the displacement and strain data do not correlate

4.25

directly to that of the unnotched specimens. In this case, deformation is not uniform throughout the entire gauge length, but is concentrated in the narrow region near the hole. The stress-strain plot for the notched specimen does not represent a true material property; therefore, the slope of the linear portion of the stress strain curve is referred to as stiffness, instead of modulus. The elevated stiffness observed during these tests, then, is not an indication that the hole makes the material stiffer but is rather a byproduct of the measurement technique.

First cycle stiffness is calculated from the initial, somewhat linear region of the stress strain curve below 70 MPa load. Subsequent cycle stiffness values are taken directly from MATE output. MATE uses the difference between maximum and minimum stress divided by the difference between maximum and minimum strain to calculate modulus. That modulus output is the stiffness for these notched specimens and in most cases this technique is very accurate due to the extreme linearity of the stress strain curve after first cycle damage.

The highest fatigue stress level notched test was the 190 MPa test. It cycled 95 times before failure. A view of the fractured specimen is shown in Figure 4-23. Figure 4-24 provides a 45° angular perspective view of the fractured surface and hole. The stress-strain curves at three specific

4.26

Figure 4-23   190 MPa Notched Fracture Surface, 8X Mag.
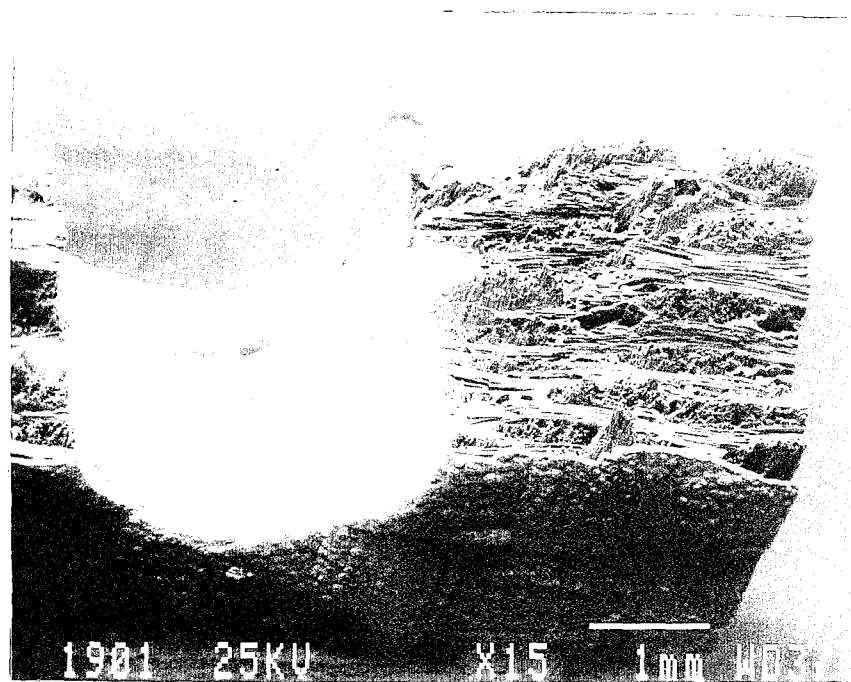
Figure 4-24   Scanning Electron Micrograph of Fracture
Surface, 190 MPa Notched Test, 15X

cycles of the 190 MPa test are presented in Figure 4-25. Here

non-linearity of the stress-strain curve is much less

pronounced than that exhibited in the unnotched tests due to
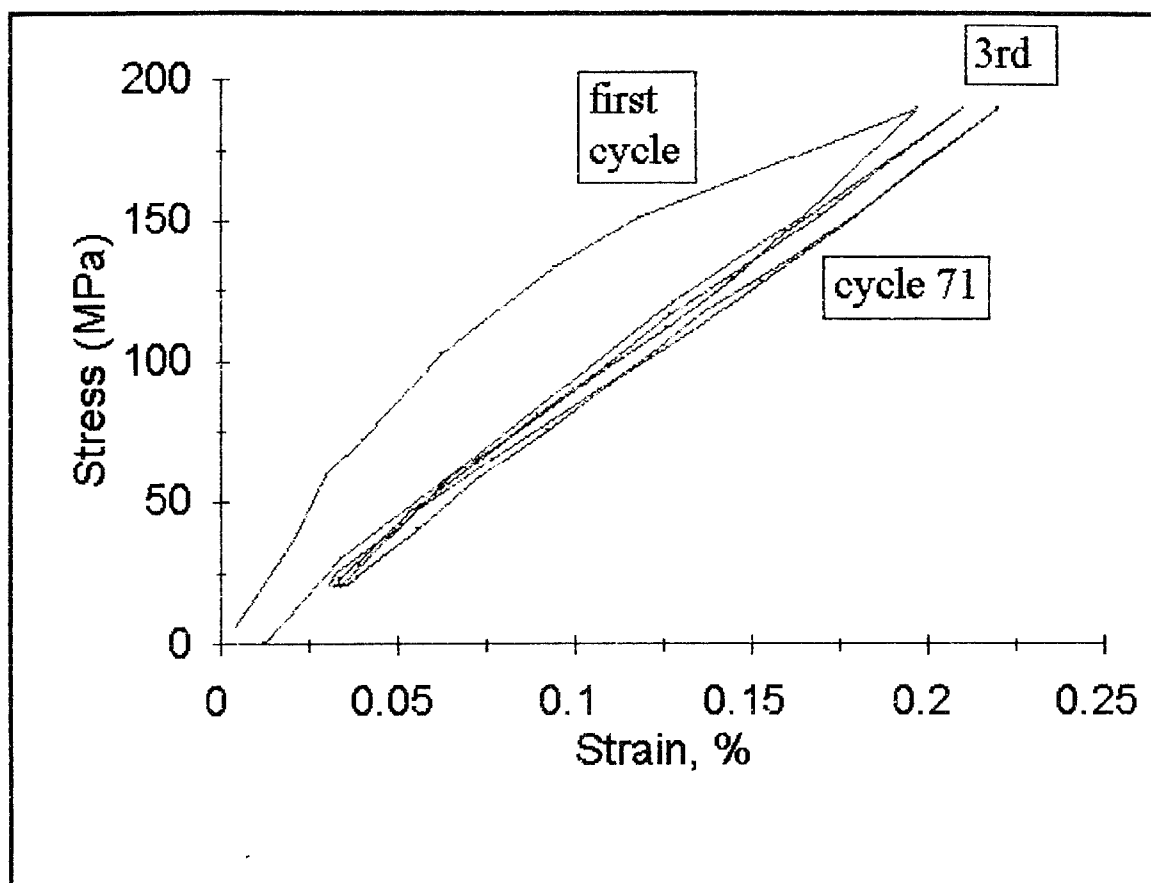
Figure 4-25 190 MPa Notched Stress-strain Curves

the aforementioned stress concentration effects. The slight

residual strain accumulation indicates little additional

deformation resulting from the fatigue loading. Figure 4-26

shows the stiffness reduction over the life of the test as

further evidence of the damage taking place during the test.

First cycle modulus is the Young's modulus obtained in the

monotonic tensile test. Third cycle stiffness had fallen to 97 GPa showing a 45% degradation. The third cycle stiffness of 97 GPa also shows excellent correlation with the stiffness value of 95 GPa predicted by the monotonic tensile test discussion. Stiffness after this first cycle, diminishes slightly until failure.
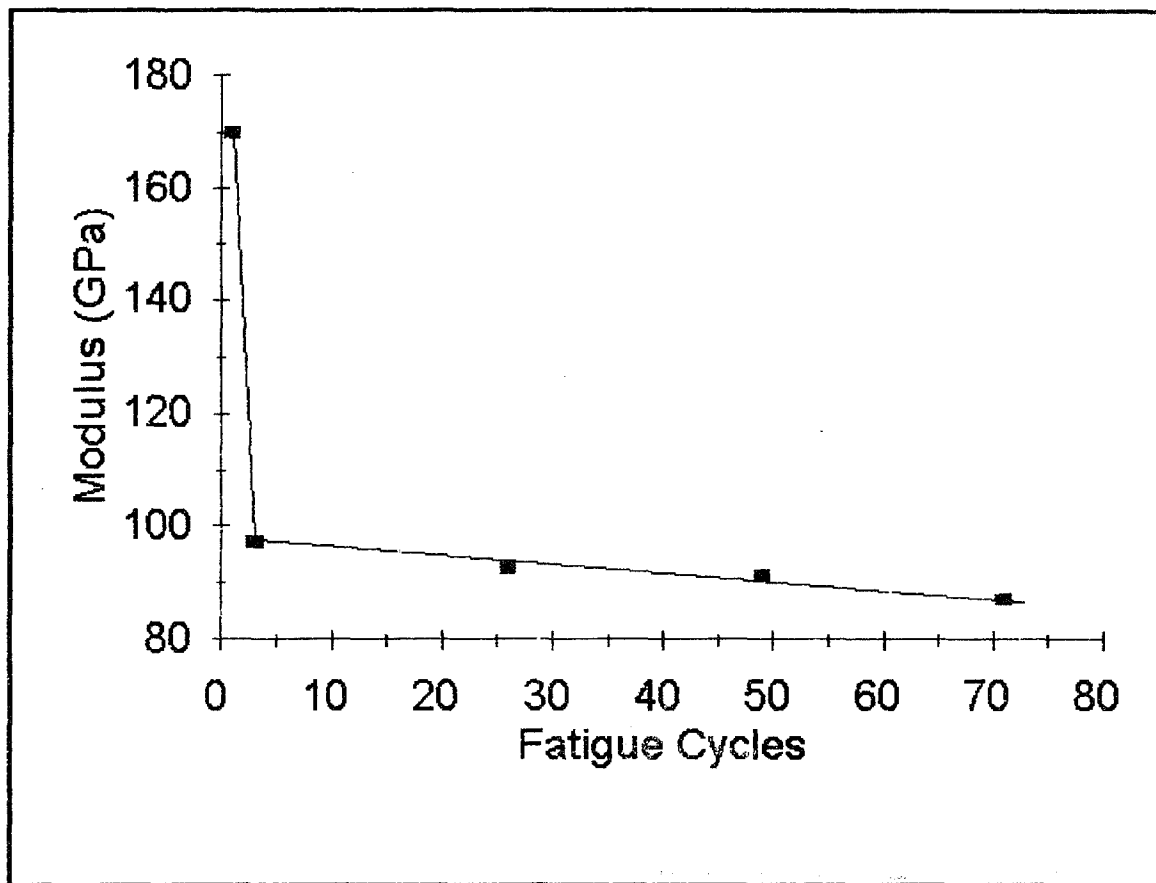
Figure 4-26   190 MPa Notched Test Stiffness Reduction

The next stress level notched fatigue test was the 175 MPa test. It cycled 1,676 times before failure. A view of the fractured specimen is shown in Figure 4-27. Figure 4-28 shows

4.29

the stiffness reduction over the life of the test. This can be taken as evidence of the damage taking place during the test. Initial stiffness reduction of 34% is observed from 170 GPa in the static test to 112 GPa of the second cycle stiffness of this test. A further stiffness reduction, prior to failure, up to 90 GPa takes place over the life of the test. This stiffness magnitude at failure correlates with the 190 MPa notched test which also had a stiffness of approximately 90 GPa at failure. The 175 MPa notched specimen stress-strain curves are presented in Appendix B along with all other notched test stress-strain curves not included in this section.
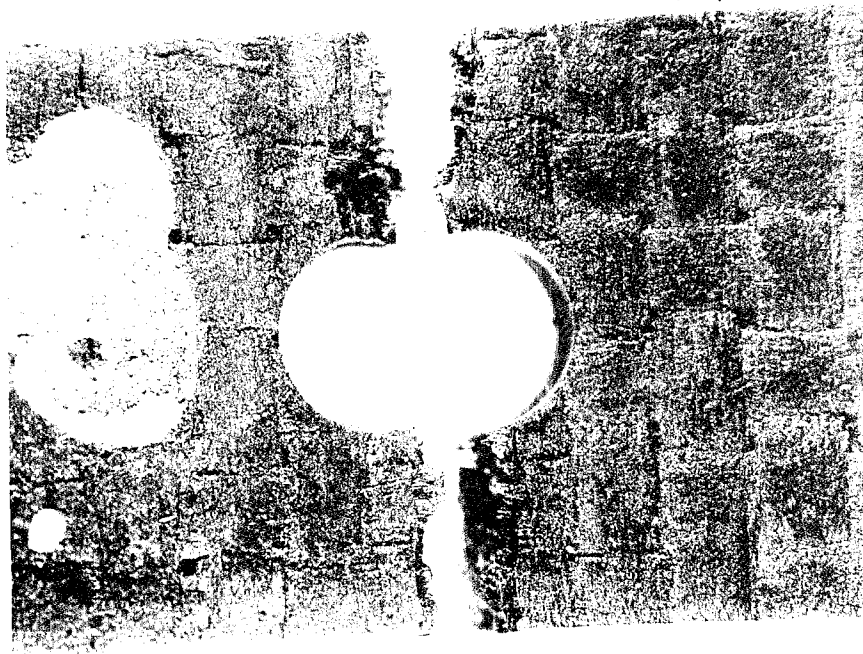
Figure 4-27   175 MPa Notched Fracture Surface, 8X Mag.
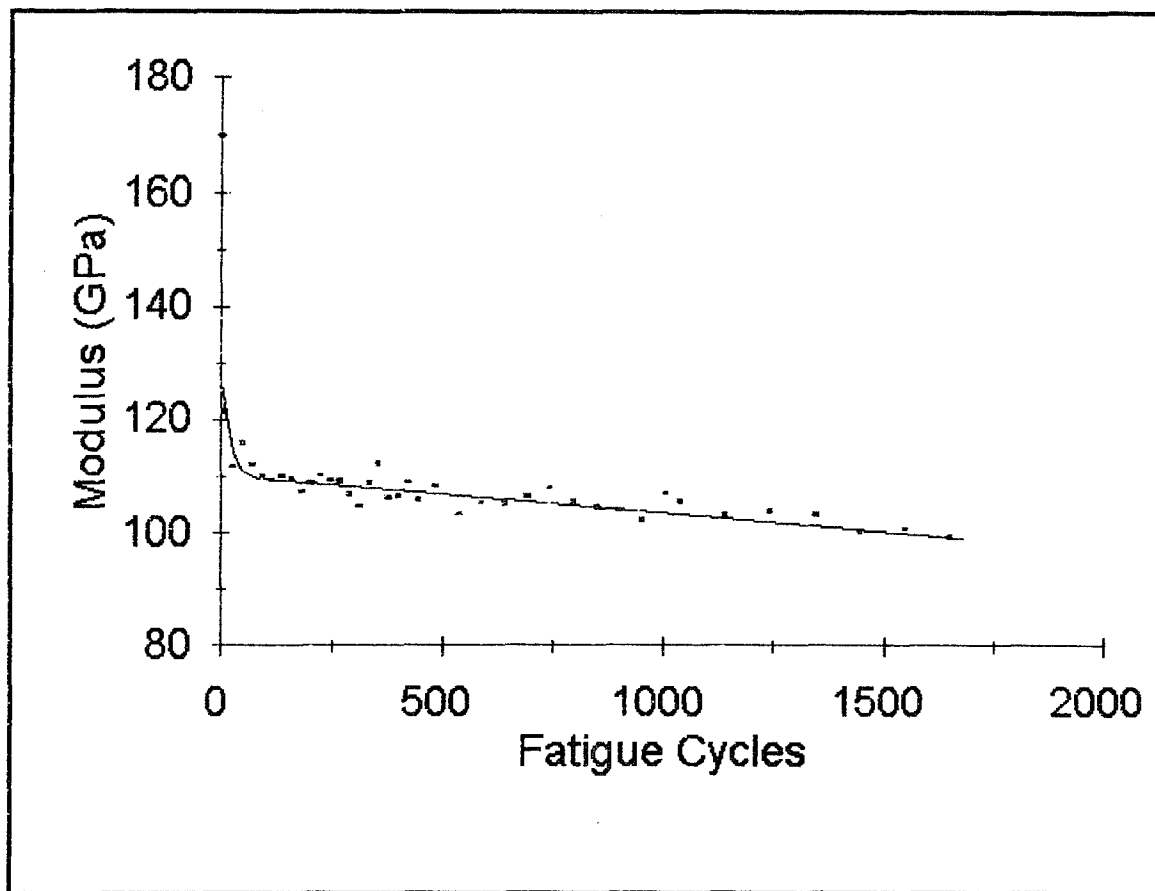
Figure 4-28 175 MPa Notched Stiffness Reduction

The results of the 150 MPa stress notched fatigue test are presented next. This test cycled 9,687 times before specimen failure. A view of the fractured specimen is shown in Figure 4-29. Figure 4-30 shows the stiffness reduction over the life of the test. This stiffness reduction is evidence of the damage taking place during the test. Initial stiffness reduction of 29% is observed from 170 GPa of the static test to 120 GPa which is the stiffness after the first fatigue cycle of this test. After the pronounced loss of stiffness in the first

4.31
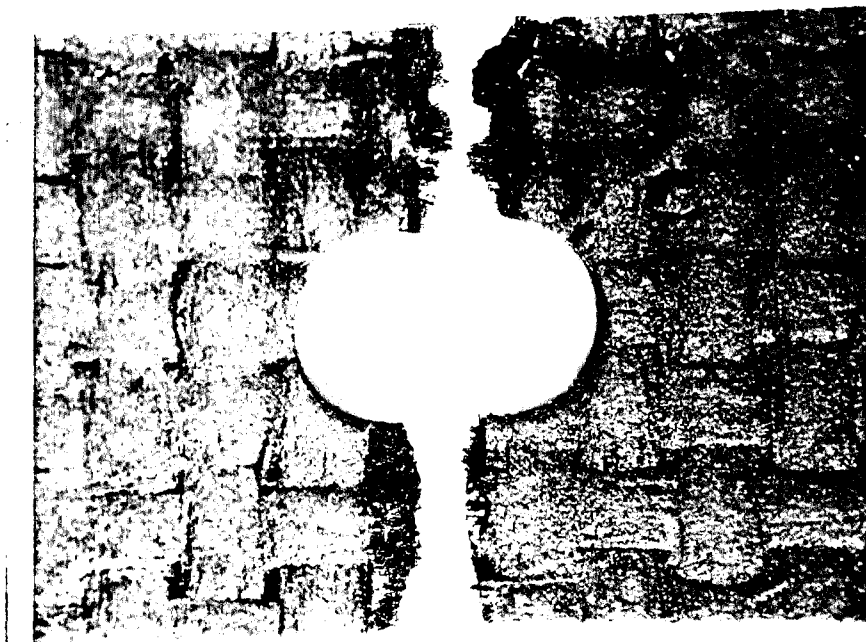
Figure 4-29   150 MPa Notched Test, Fracture Surface
8X Magnification
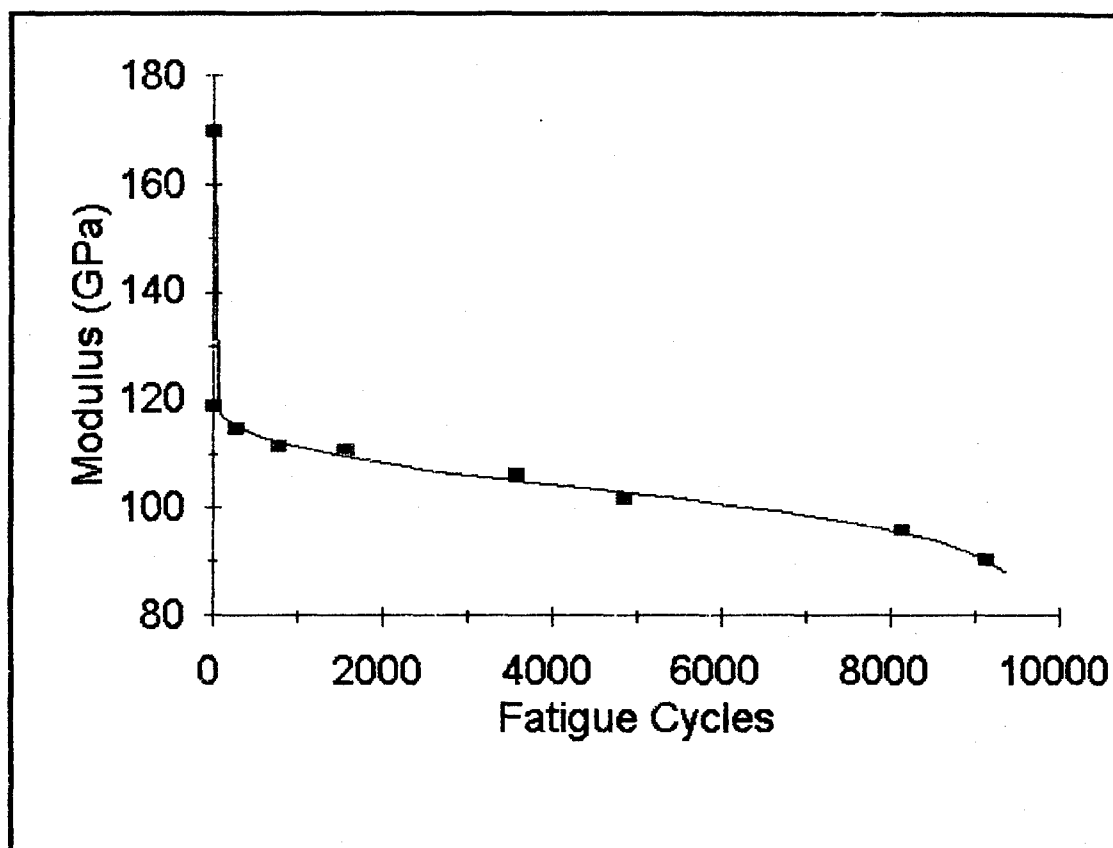
Figure 4-30   150 MPa Notched Stiffness Reduction

cycle, the stiffness diminished at a linear rate until final
fracture of the test specimen occured. The early fatigue cycle
stiffness of 120 GPa of this test is in excellent agreement
with the 124 GPa stiffness predicted by plotting a line to the
150 MPa stress level of the notched monotonic tensile stress-
strain curve in section 4 A. As in the two previously
discussed tests, the modulus had decreased to approximately 90
GPa at the time of specimen failure.

The next stress level notched fatigue test was the 125 MPa
test. It cycled 19,544 times before failure. A magnified view
of the fractured specimen is shown in Figure 4-31. Figure 4-32
plots the stiffness reduction over the life of this test. This
stiffness degradation is evidence of the microstructural damage

Figure 4-31   125 MPa Notched Fracture Surface, 8X
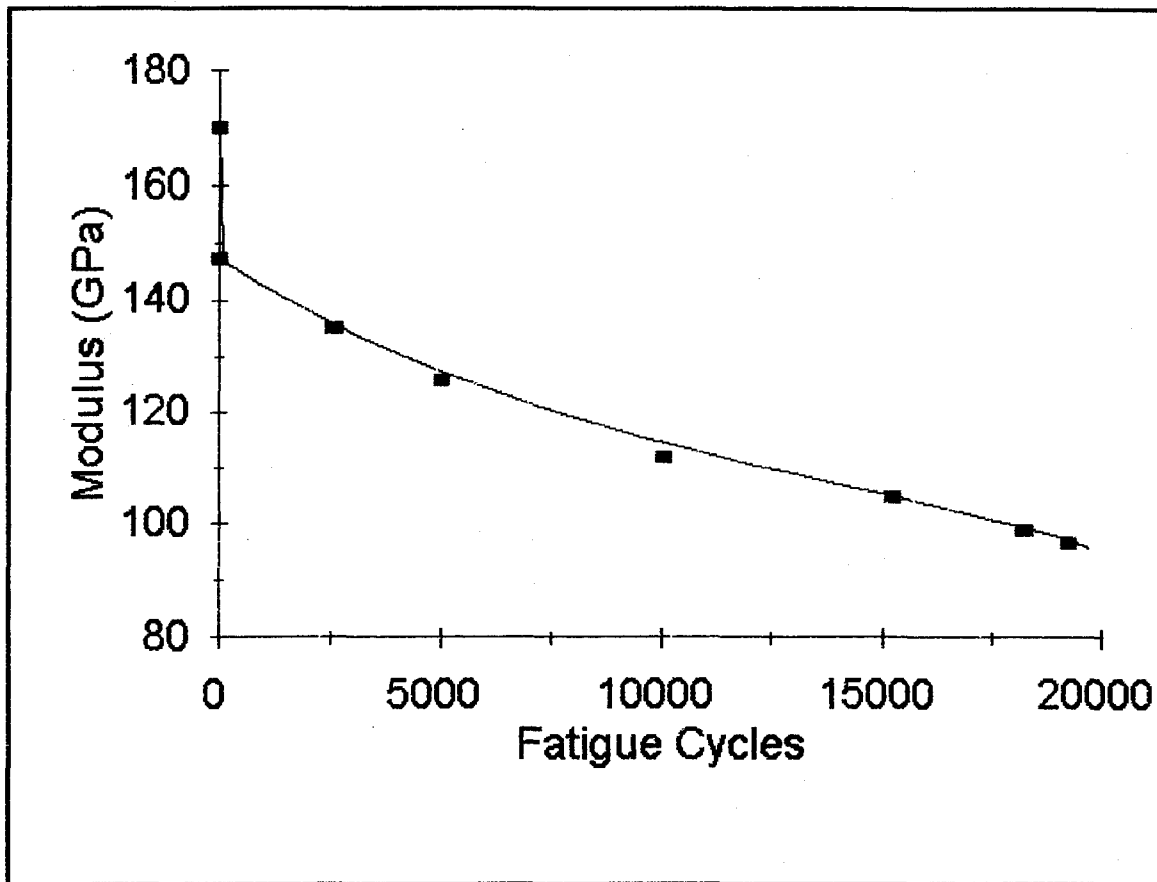
Figure 4-32   125 MPa Notched Stiffness Reduction

taking place during the test.   Initial stiffness reduction of

14% is observed from 170 GPa in the somewhat linear portion of

the loading curve of the first cycle to the 147 GPa first cycle

unloading stiffness.   After the first cycle, the stiffness

diminished at a fairly constant rate of 2 GPa per 1000 cycles

until the specimen failed.   The failure occurred at a stiffness

of about 100 GPa.

The next stress of notched fatigue test was the 110 MPa

test.   It cycled 24,802 times before failure.   A magnified view

of the fractured specimen is shown in Figure 4-33.   The 110 MPa

4.34
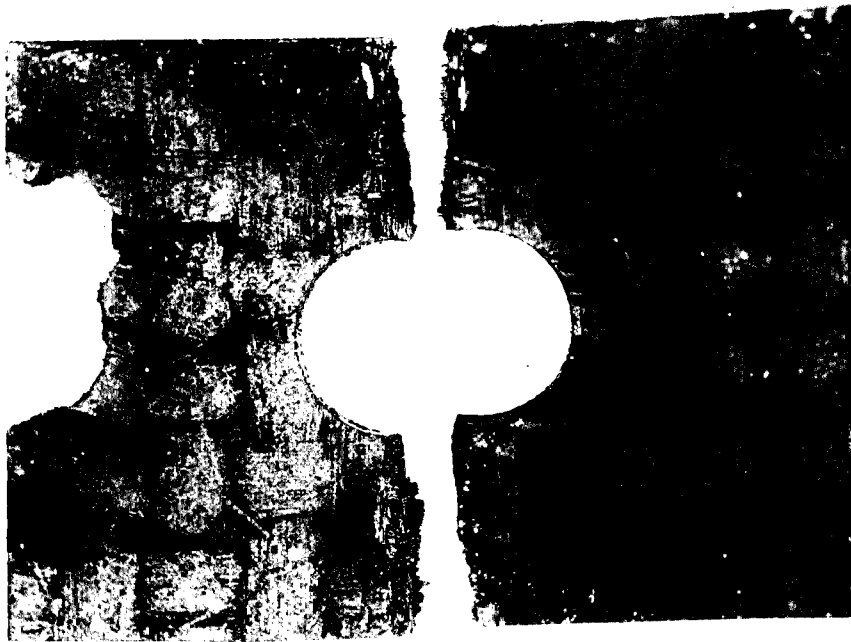
Figure 4-33   110 MPa Notched Fracture Surface, 8X Mag.

test stress-strain curves at four specific cycles are plotted

in Figure 4-34.   These curves showed a slight nonlinearity.

Residual strain accumulation exists indicating permanent

deformation as a result of fatigue.   Note increased hysteresis

over the life of the test indicating microstructural damage

accumulation.   The SEM photomicrographic view of the fractured

surface in Figure 4-35 displays a somewhat different character

than the notched monotonic tensile test surface (Figure 4-4)and

the 190 MPa fatigue test surface (Figure 4-24).   The surface of

the 110 MPa notched specimen exhibits shorter 0° fiber pullout.
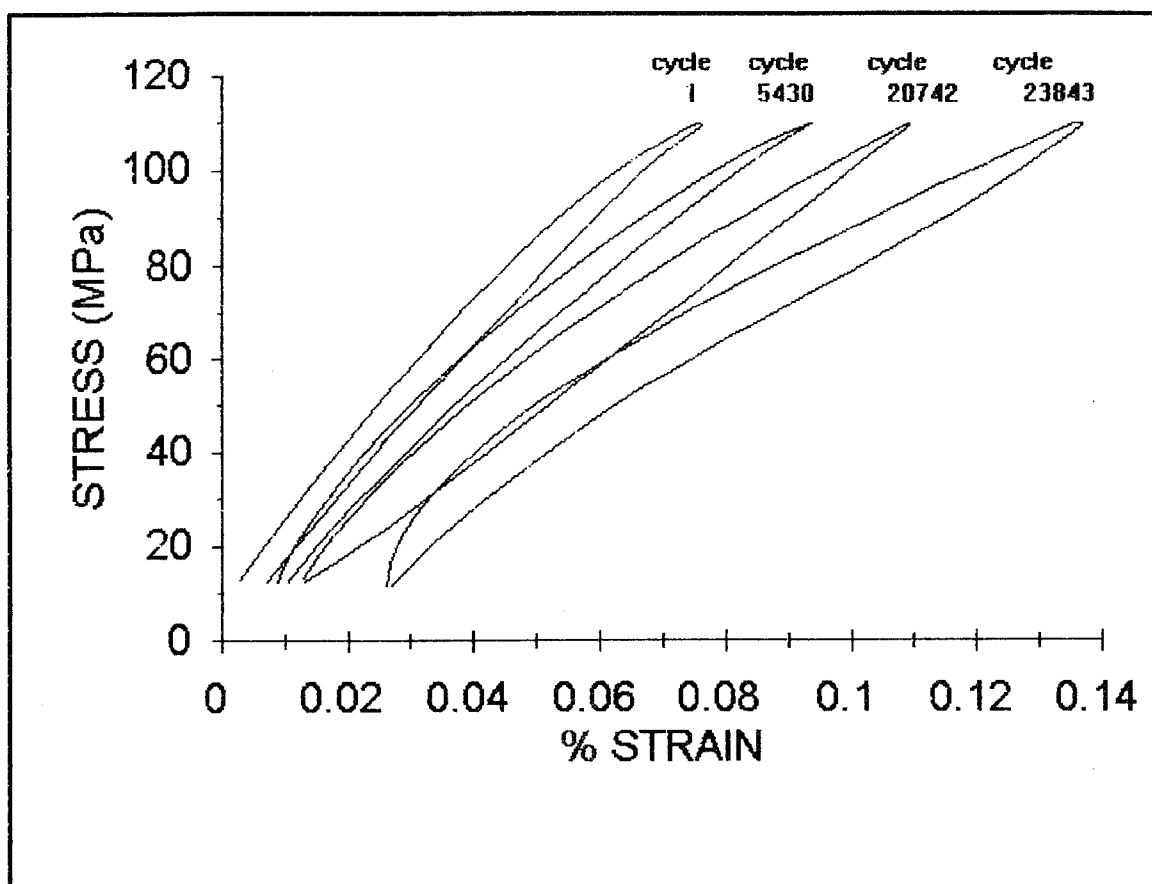
Figure 4-34   110 MPa Stress-strain Curves
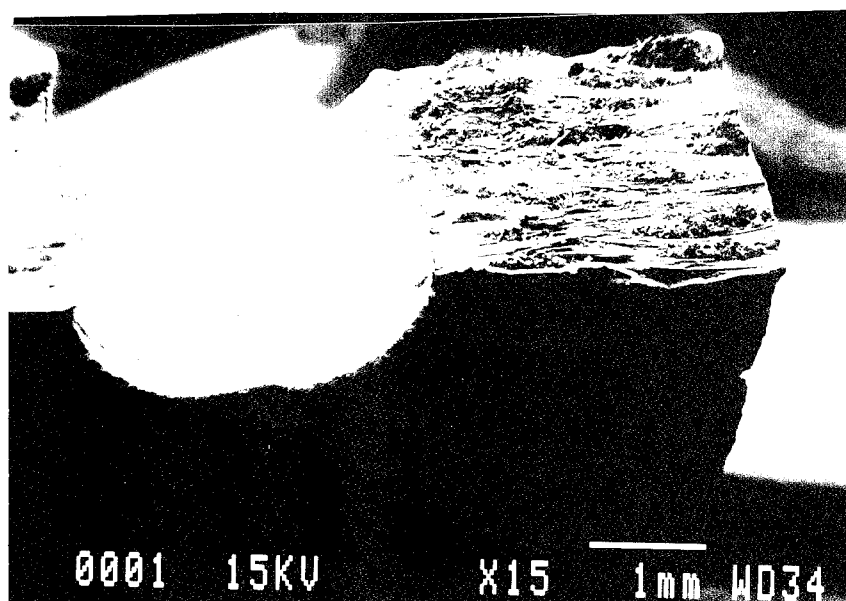
Figure 4-35   110 MPa Notched Test Micrograph of Fracture Surface, 45° Angle, 15X

Figure 4-36 shows the stiffness reduction over the life of the test. This is evidence of the microstructural damage taking place during the test. Initial stiffness reduction of 12% is observed from 170 GPa in the somewhat linear portion of the loading curve of the first cycle to the 150 GPa first cycle unloading stiffness. After the first cycle, the stiffness diminished at an increasing rate until the specimen failed at a stiffness of 76 GPa.
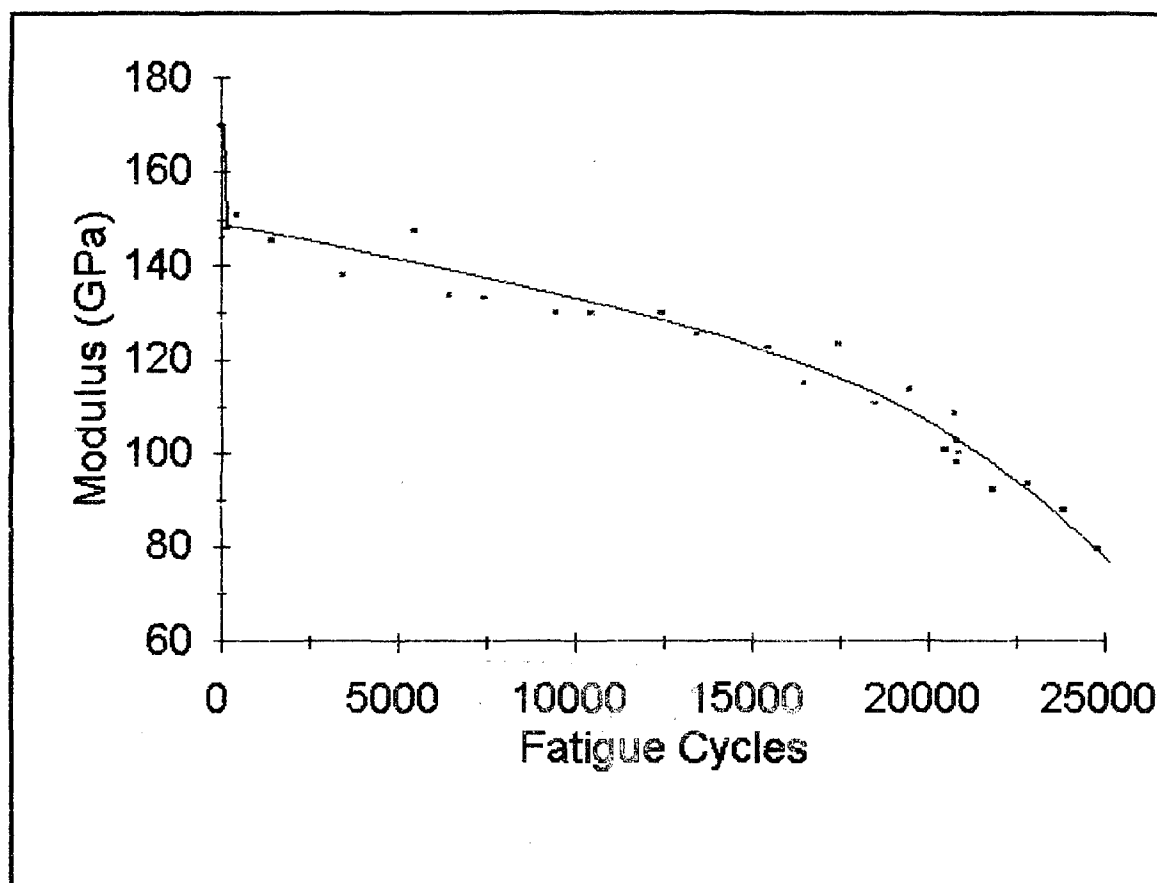
Figure 4-36   110 MPa Stiffness Reduction

The next stress level of notched fatigue test was 100 MPa. It cycled 100,000 times with no failure before the test was stopped. After several other tests (approximately a one month time period), this test was restarted but it only cycled 489 times before failure. A magnified view of the fractured specimen is shown in Figure 4-37. Figure 4-38 shows the stiffness behavior over the life of the test. Initial stiffness reduction is negligible, however a slight downward trend in stiffness is evident by the end of the test. Environmental factors probably influenced the failure. Fibers, exposed by fatigue cracking, could have oxidized during the aforementioned test pause allowing them to fail prematurely.

Figure 4-37 Fracture Surface, 100 MPa Notched Test, 8X
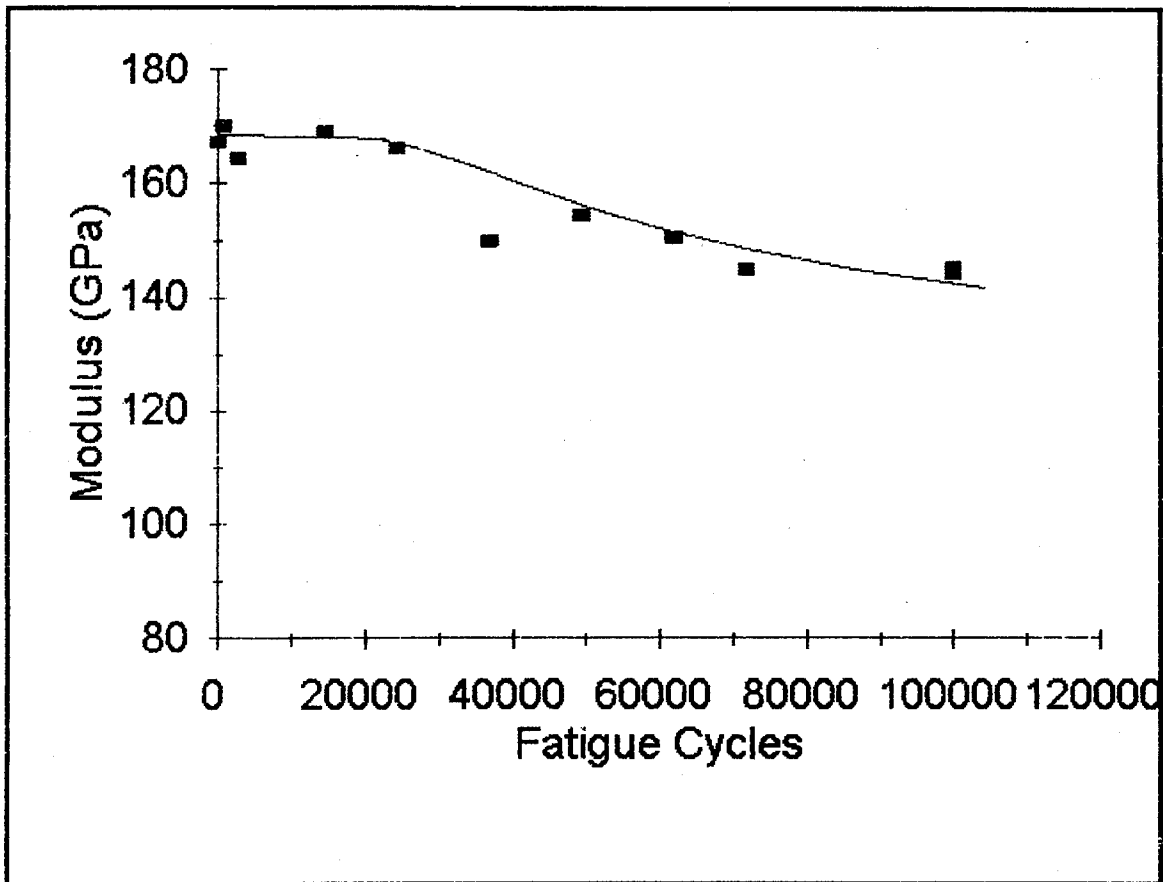
Figure 4-38   100 MPa Notched Stiffness Reduction

Due to the unusual failure of the 100 MPa specimen, another high cycle test was conducted at 95 MPa. The intention of this test was to establish the low stress portion of the S-N curve. The 95 MPa notched specimen endured 440,036 cycles without failure. Figure 4-39 shows the stiffness behavior over the life of the test. Note the negligible initial modulus degradation and little further degradation over the life of the test. This behavior implies 95 MPa provides the lower bound of the fatigue life of the notched case, i.e. the endurance limit.

4.39
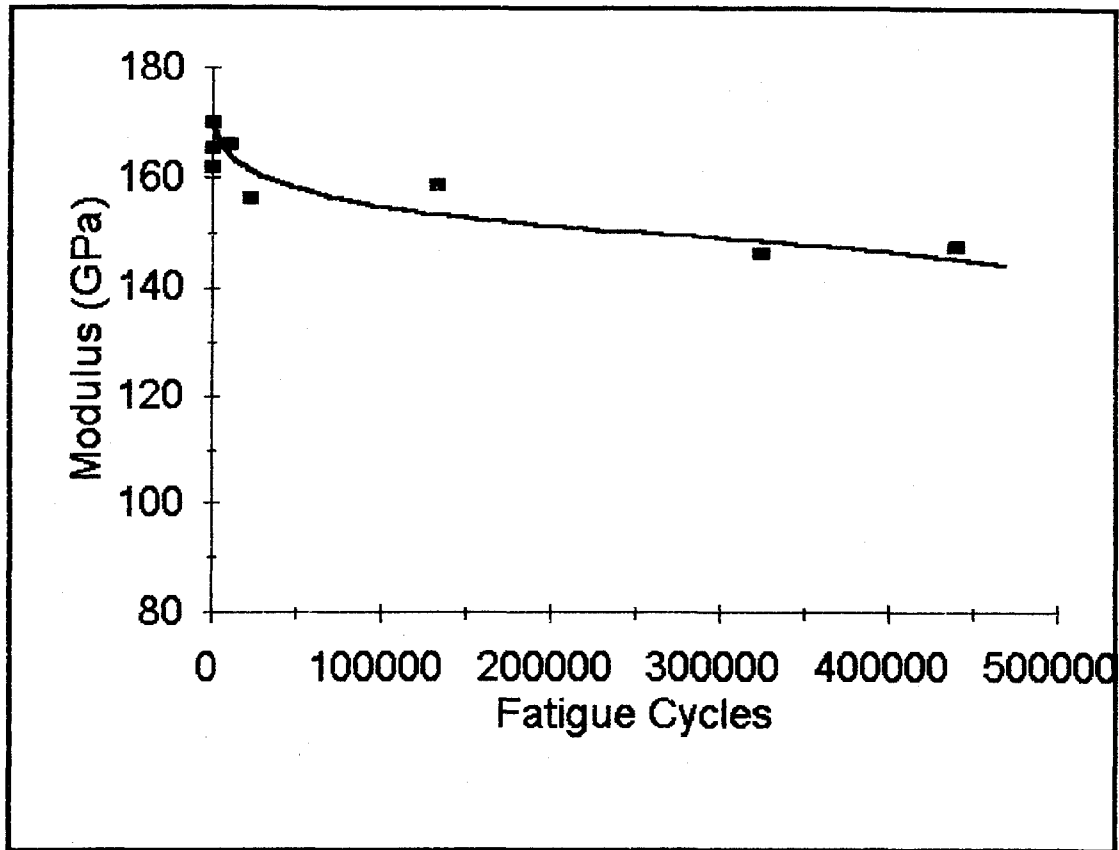
Figure 4-39   95 MPa Notched Stiffness Behavior

It is important to note that all notched specimens of the present study failed in a manner consistent with opening and closing, mode I (crack propagation normal to load plane) with no progression to rubbing mode II (crack progression parallel to load plane) as reported by Tsangarakis and Moschelle for unidirectional metal matrix and ceramic matrix composites [20, 26].

D.   S-N Curves

This section presents and discusses the S-N curves which were developed from the tests whose results are given in section IV A, B, and C.   All fatigue tests were conducted in the tension-tension mode at 1100°C.   The load was applied as a 1.0 Hz triangular wave.   The minimum to maximum load ratio in all cases was 0.1.   The tests are referenced by maximum applied stress level where the stress is defined as the applied tensile load per unit area.   The area used in determining the stress level is the cross sectional area at the gauge length and in the case of the notched specimens is reduced by the area of the hole as described in section III D.   The notched specimens had a centrally located circular hole and a notch diameter to specimen width ratio (D/W) of 0.331 ± 0.003.

Figure 4-40 shows the S-N curves of the notched and unnotched fatigue tests, using a logarithmic scale on the x axis (fatigue cycles).   This graph also includes the monotonic tensile strength as a data point corresponding to the first cycle of failure.   Table 1 in the appendix shows the stress levels and fatigue lives of the various notched specimens, while Table 2 provides the maximum stress levels and fatigue lives of the unnotched specimens.   The fatigue life diagrams of Figure 4-40 clearly illustrate the dependence of fatigue life

4.41
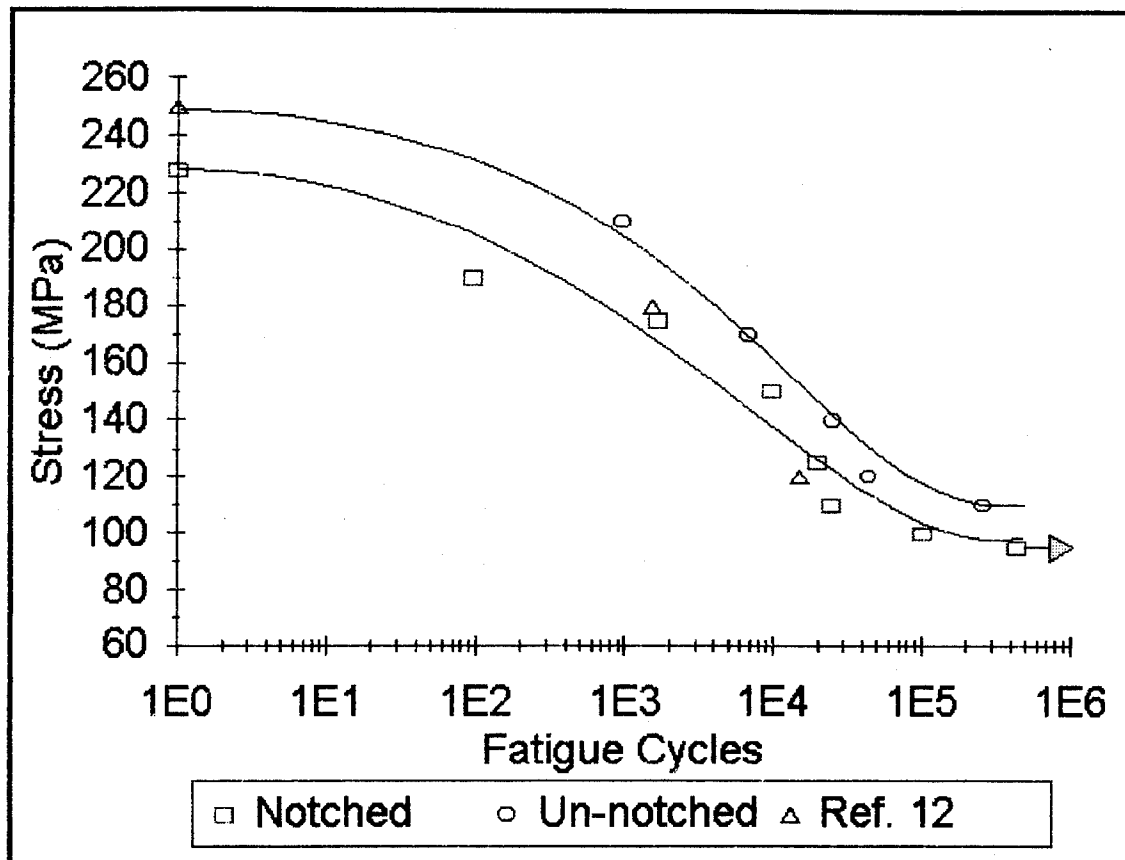
Figure 4-40   Fatigue Life Diagrams Including Monotonic Tensile Test Data Points

on maximum applied stress level.   The monotonic tensile and fatigue data provided by DuPont are also included, although these fatigue life data points were obtained at a frequency of 0.5 Hz[12].

Fatigue life is clearly a function of stress level, but only a slight geometry dependence is apparent from these curves.   The notched S-N curve is placed slightly above the 95 MPa and 100 MPa test data points.   This is done because of the suspected environmental degradation of the 100 MPa specimen and

the lack of failure in the 95 MPa specimen as described previously in the results section. If the monotonic tension data are excluded a fatigue life diagram may be drawn as presented in Figure 4-41.
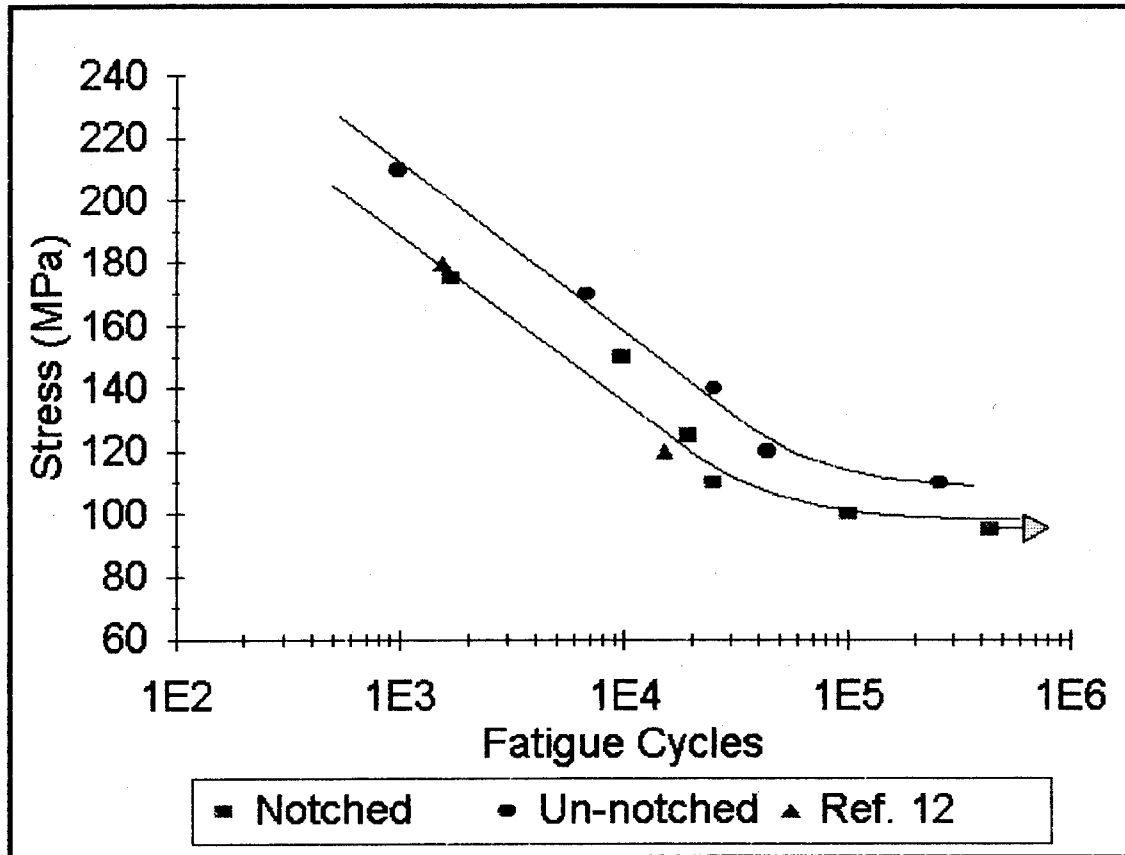
Figure 4-41   S-N Curves

In Figure 4-41 a clear difference between the fatigue behavior of notched and unnotched specimens is evident. The fatigue life of the unnotched specimens is longer by about a factor of four than that of the notched specimens until stress levels approach the fatigue limit values. Due to the difference in applied stress levels at a given fatigue life of

4.43

the notched and unnotched specimens, a more appropriate comparison is fatigue strength (applied stress level) between these two. For this purpose, the fatigue notch factor (β) is defined as the ratio of the fatigue strength of the notched specimen (σ_n) to that of the unnotched specimen (σ_{un}) at a given fatigue life[10].

$$\beta = \frac{\sigma_n}{\sigma_{un}} \qquad (5)$$

The fatigue notch factor for the present study remains fairly constant between 0.85 and 0.9 for the test range of this study. This fatigue notch sensitivity is considered insignificant.

In order to quantify the fatigue notch factor, the following observation is noted. Assume the first fatigue cycle on the notched specimen destroys a small zone adjacent to the notch and perpendicular to the loading axis. This assumption is validated by the difference in first cycle stress-strain behavior near the proportional limit (Figures 4-1 and 4-2) and scanning electron microphotographs presented previously (e.g. Figure 4-35). If this damage zone extends 0.4 mm into the specimen and the remaining undamaged area of the specimen is used to calculate the fatigue stress level, the adjusted notched fatigue life values fit well within the S-N scatter band of the unnotched specimens as shown in Figure 4-42.
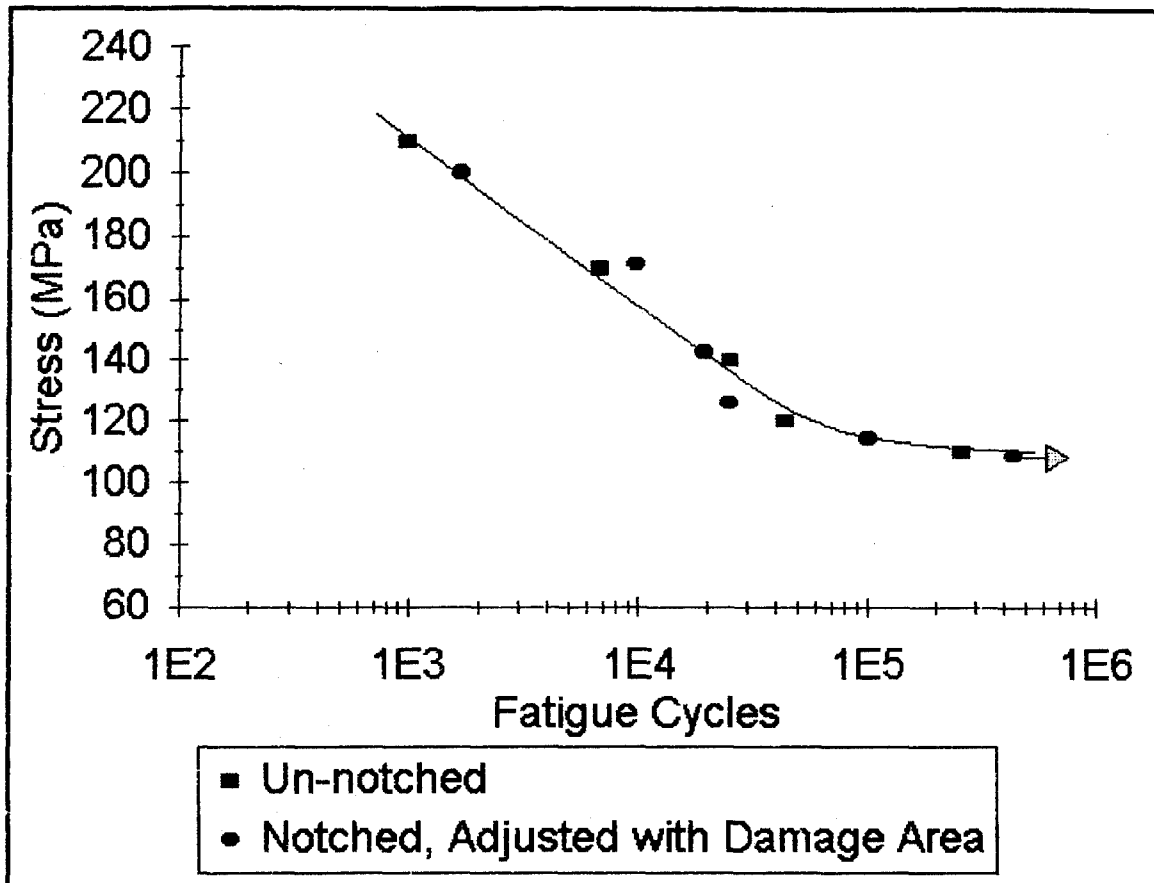
Figure 4-42   S-N Curves for Unnotched and Notched Adjusted
With Damage Area

E.   *Fatigue Modulus Behavior Comparison*

This section compares and contrasts the modulus behavior

of the enhanced SiC/SiC material for the unnotched and notched

specimens at various maximum stress levels. All fatigue tests

were conducted in the tension-tension mode at 1100°C. The load

was applied as a one hertz triangular wave. The minimum to

maximum load ratio in all cases was 0.1.   The tests are

4.45

referenced by maximum applied stress level where the stress is defined as the applied tensile load per unit area. The area used in determining the stress level is the cross sectional area at the gauge length and in the case of the notched specimens is reduced by the area of the hole as described in section III D. The notched specimens had a centrally located circular hole and a notch diameter to specimen width ratio (D/W) of 0.331 ± 0.003.

Significant insight may be gained by investigating the stiffness degradation, thus a comparison is presented for unnotched and notched specimens. First cycle modulus is the slope of the initial linear region (below the proportional limit) of the monotonic tensile stress-strain curve. The fatigue cycle modulus of the unnotched tests is the value generated by the Mate test software. Mate uses the maximum and minimum values of stress and strain to calculate the modulus.

The notched stiffness is found in much the same way; however, the reduced cross-sectional area at the hole is used to set the tensile load for the chosen stress values. Since the stress in the unnotched portion of the gage length is substantially less than the stress adjacent to the hole, the true average stress value in the gage length is less than that used to calculate the stiffness. Therefore, stiffness is a specimen property rather than a material property.

First, the modulus behavior of the unnotched specimens is presented in Figure 4-43 followed by stiffness behavior of the
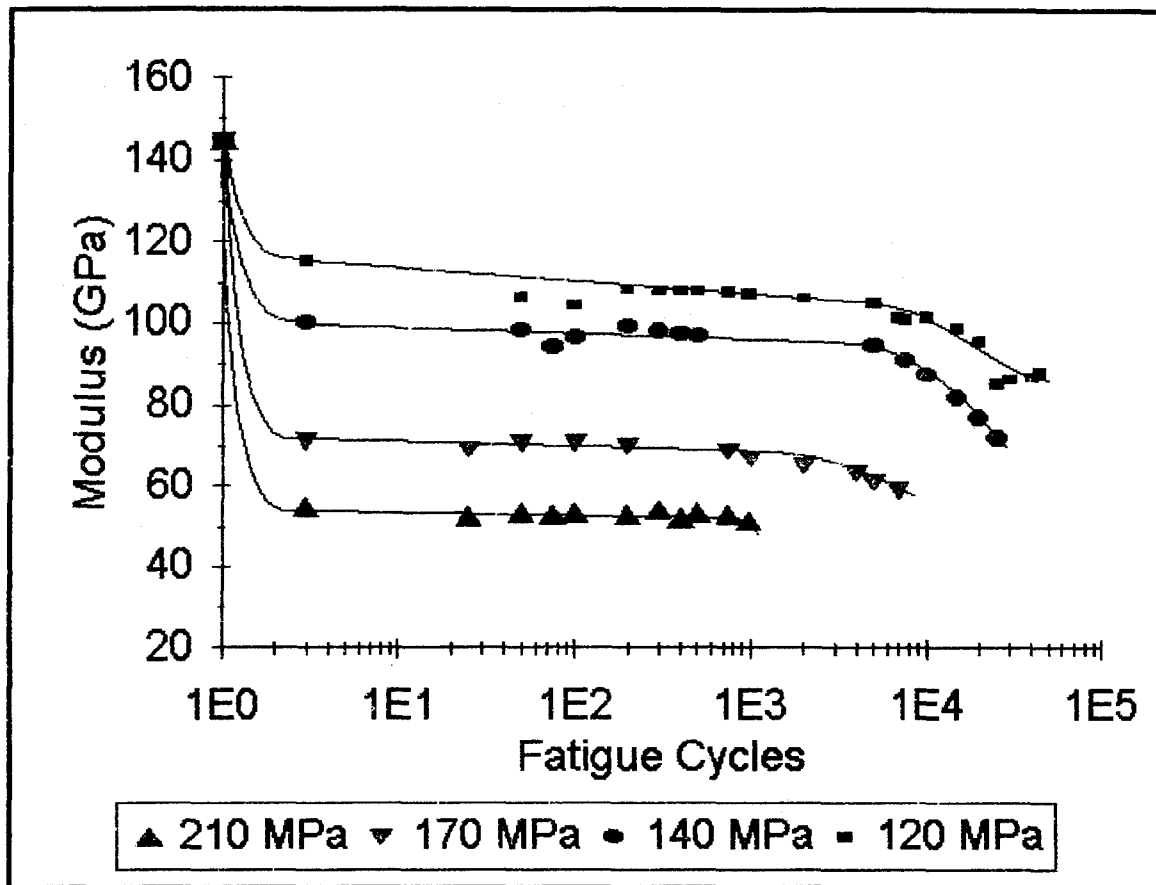
Figure 4-43   Modulus Reduction of Unnotched Specimens

notched specimens in Figure 4-44.   Four unnotched fatigue modulus reduction curves are presented in Figure 4-43.   The stiffness reduction comparison of five notched specimen tests is shown in Figure 4-44.   The curves are referenced by stress level.   Modulus reduction in CMCs often quantifies on a macroscopic level the damage taking place in the specimen during cycling.   As previously discussed, first cycle damage
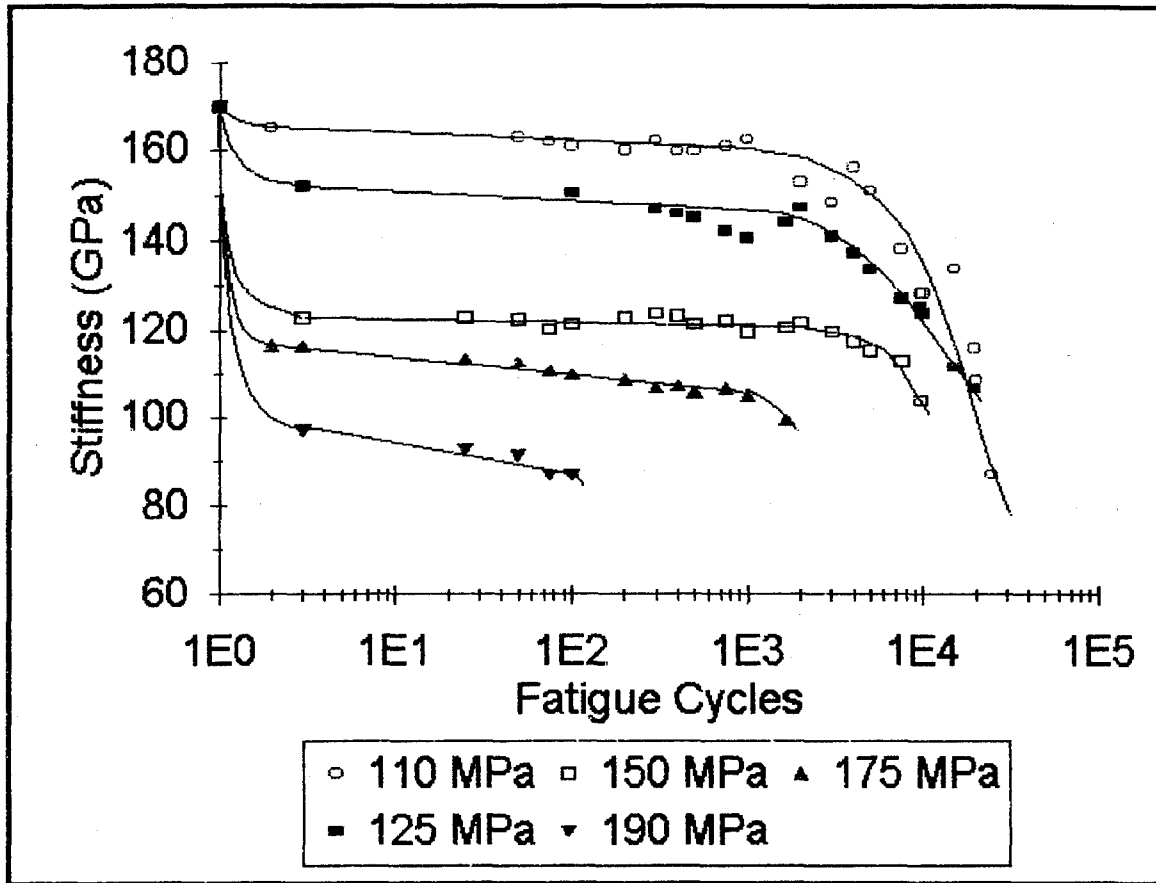
Figure 4-44   Stiffness Reduction, Notched Comparison

produces severe modulus degradation especially at the higher

stress levels.   In comparing these figures for notched and

unnotched modulus behavior, a similarity is evident between the

210 MPa unnotched and the 190 MPa notched tests.

The lower stress levels exhibit stiffness degradation over

the fatigue life while higher stress levels sustain most

stiffness degradation in the first cycle with little additional

degradation before failure.   Likewise the low stress tests in

both the notched and unnotched cases exhibit a similarity of

behavior.   In an attempt to examine further this comparison,

modulus and stiffness are normalized with respect to first cycle values.

Figure 4-45 presents the unnotched modulus comparison as in the previous graphs except modulus has been normalized in the form of E_i/E_1 where E_1 is the first cycle modulus in the
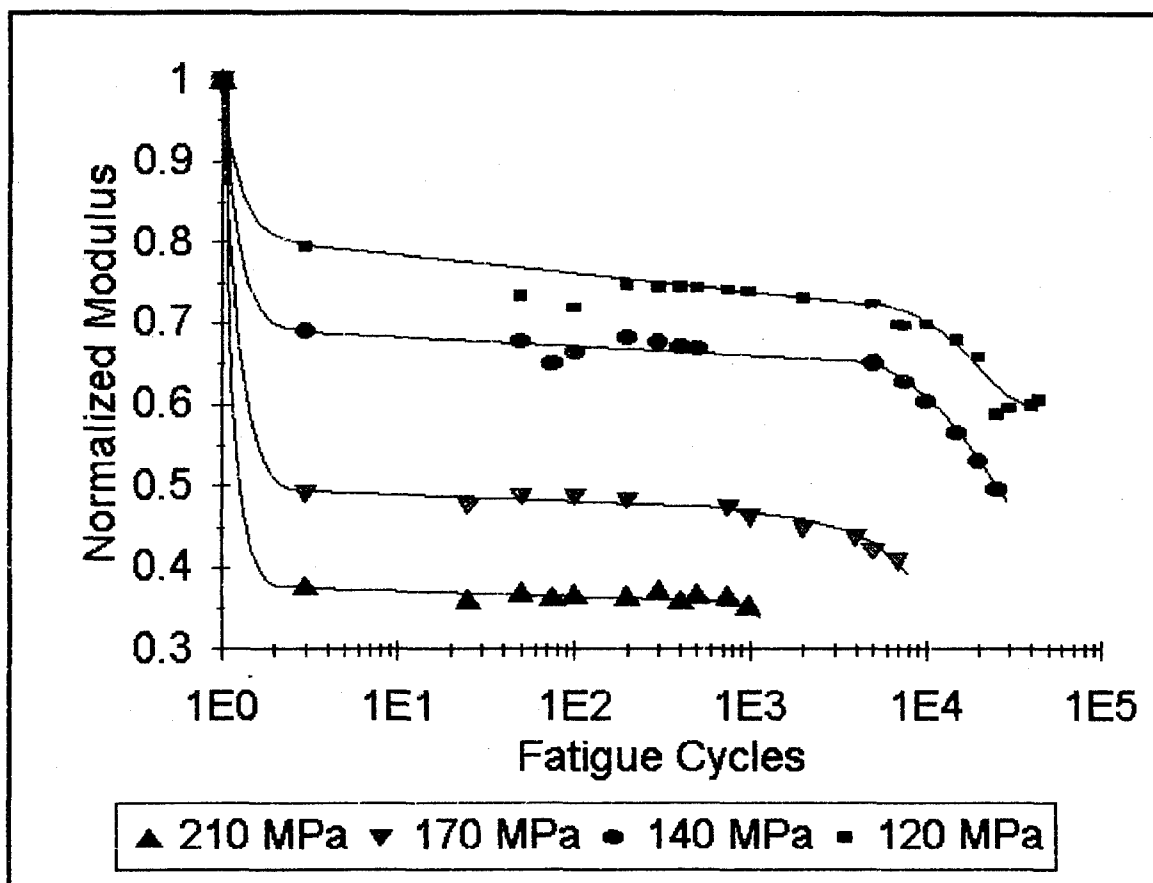
Figure 4-45 Normalized Modulus Reduction, Unnotched Fatigue Test Comparison

initial linear region of the stress strain curve. Figure 4-46 presents the corresponding normalized stiffness values for the notched case. In comparing notched and unnotched modulus

behavior, a similarity is evident between the 210 MPa unnotched and the 190 MPa notched tests. Both specimens suffer a large initial stiffness degradation with little further loss before failure. This implies a similarity in damage mechanisms
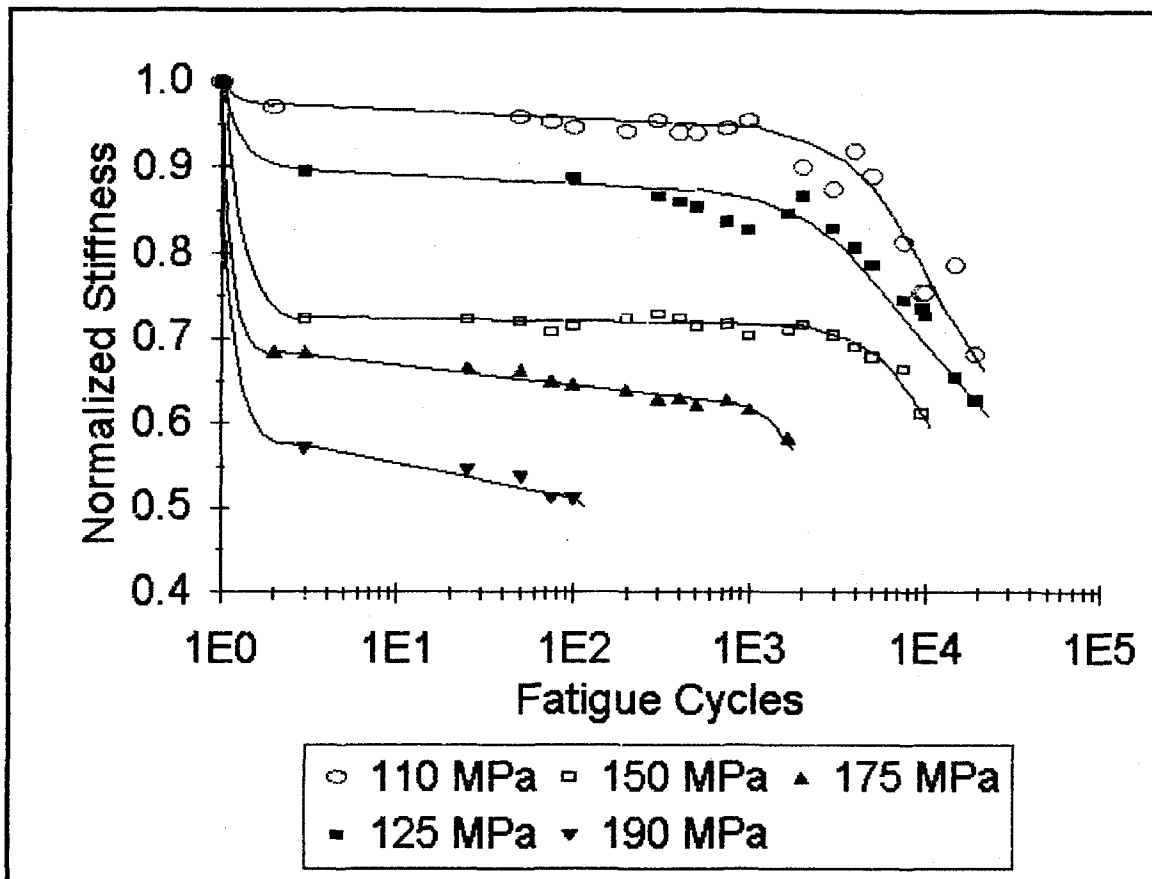
Figure 4-46 Normalized Stiffness Reduction, Notched Fatigue Test Comparison

at high stress levels in the notched and unnotched cases. At the 120 MPa stress level, normalized modulus for the unnotched specimen suffers first cycle modulus degradation and decreases gradually from that point until it reaches a value of about 0.6 before final specimen failure. In contrast, the modulus for

the notched specimens tested at or below 150 MPa remains
independent of fatigue until 3000 cycles. Beyond this, value
modulus decreases rapidly until specimen failure at a
normalized modulus value of 0.6.
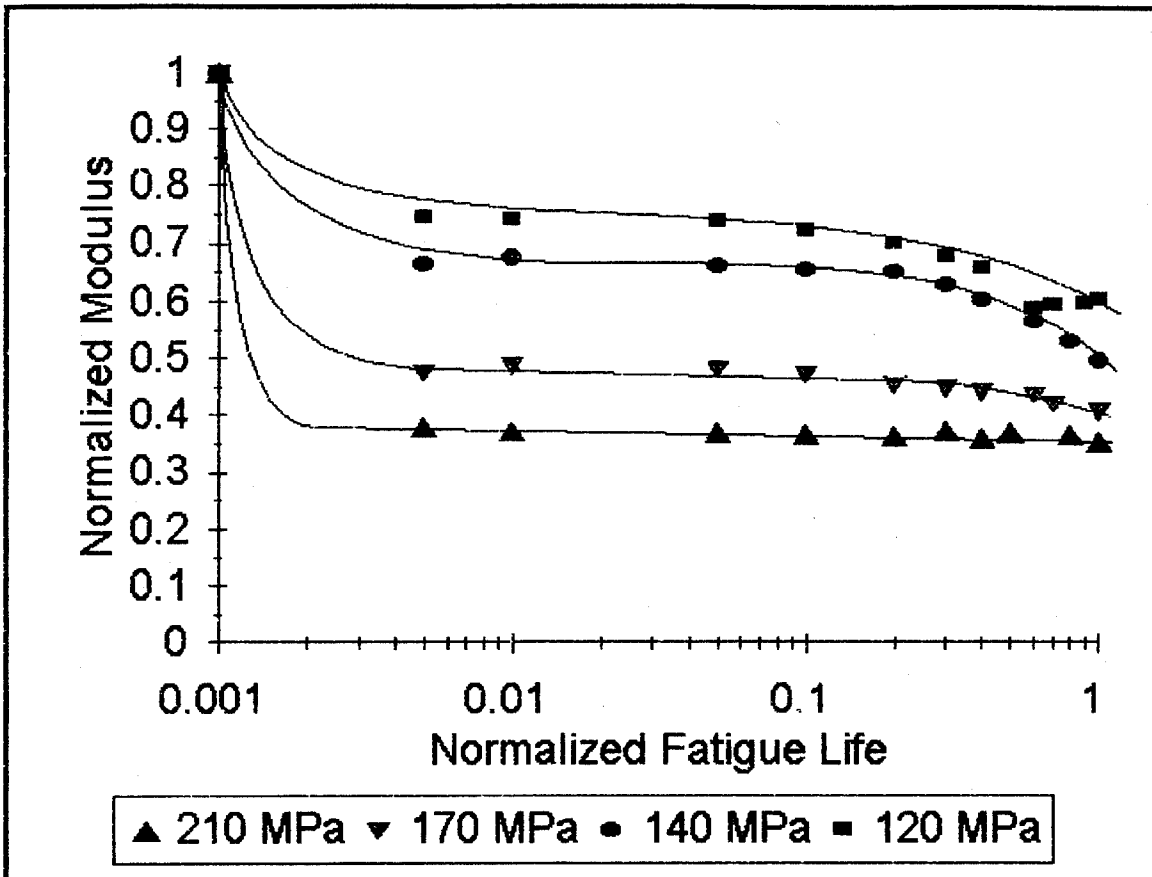
Figure 4-47 Normalized Unnotched Modulus Reduction Vs.
Normalized Cycles to Failure, Log Scale

Figure 4-47 presents the modulus reduction of the
unnotched tests normalized with respect to initial modulus on
the y axis and the normalized cycles to failure on the x axis.
The normalized cycles to failure is N_i/N_f where N_i is the number
of the cycle at any instant and N_f is the number of cycles to

failure of the specimen at the given maximum stress level. Figure 4-48 presents the notched stiffness behavior in the same format. Other than first cycle behavior, these curves have
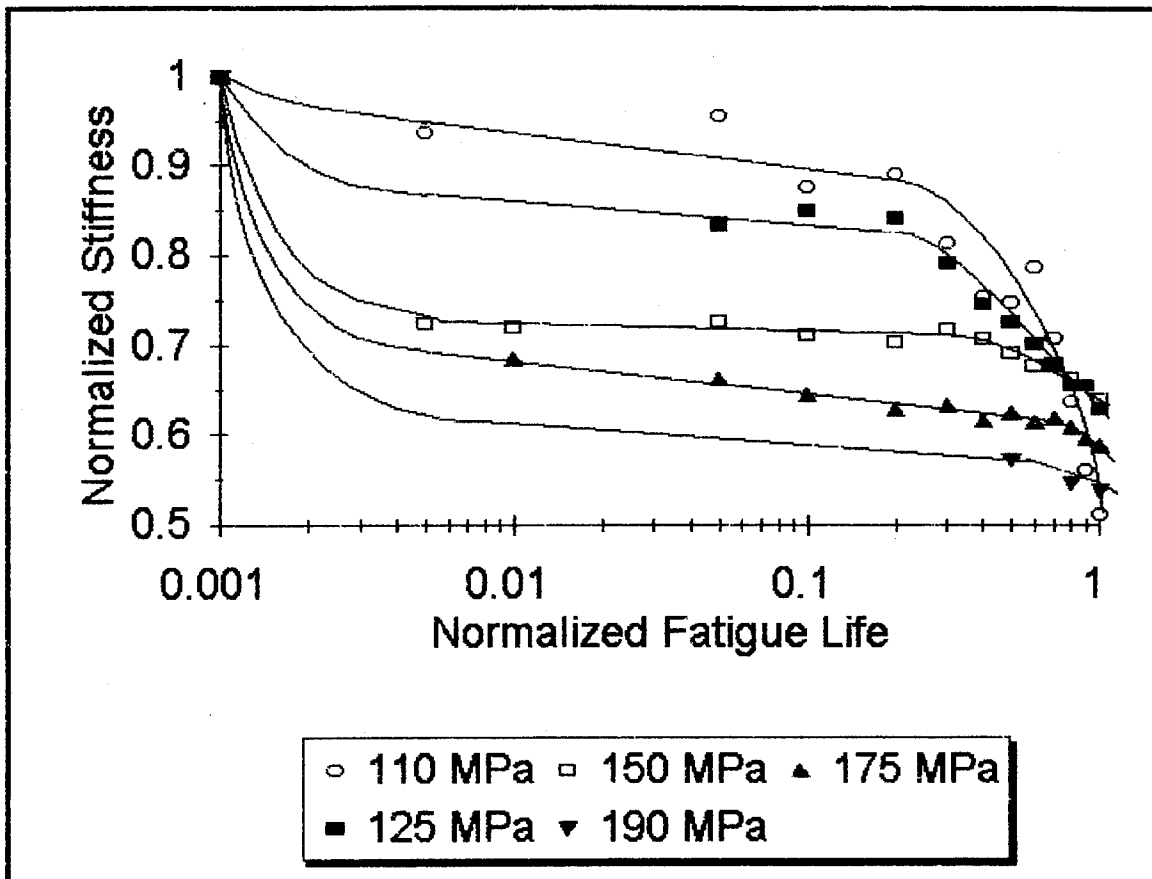
Figure 4-48 Normalized Notched Stiffness Reduction Vs. Normalized Cycles to Failure, Log Scale

collapsed to a very consistent shape. The modulus in all unnotched cases seems to stabilize after first cycle degradation, then decrease gradually to failure. The notched specimens, on the other hand, seem to exhibit a relatively constant degradation of stiffness over the life of the specimens.

Figure 4-49 presents the previous unnotched, normalized

modulus behavior using a standard scale on the x axis. Figure
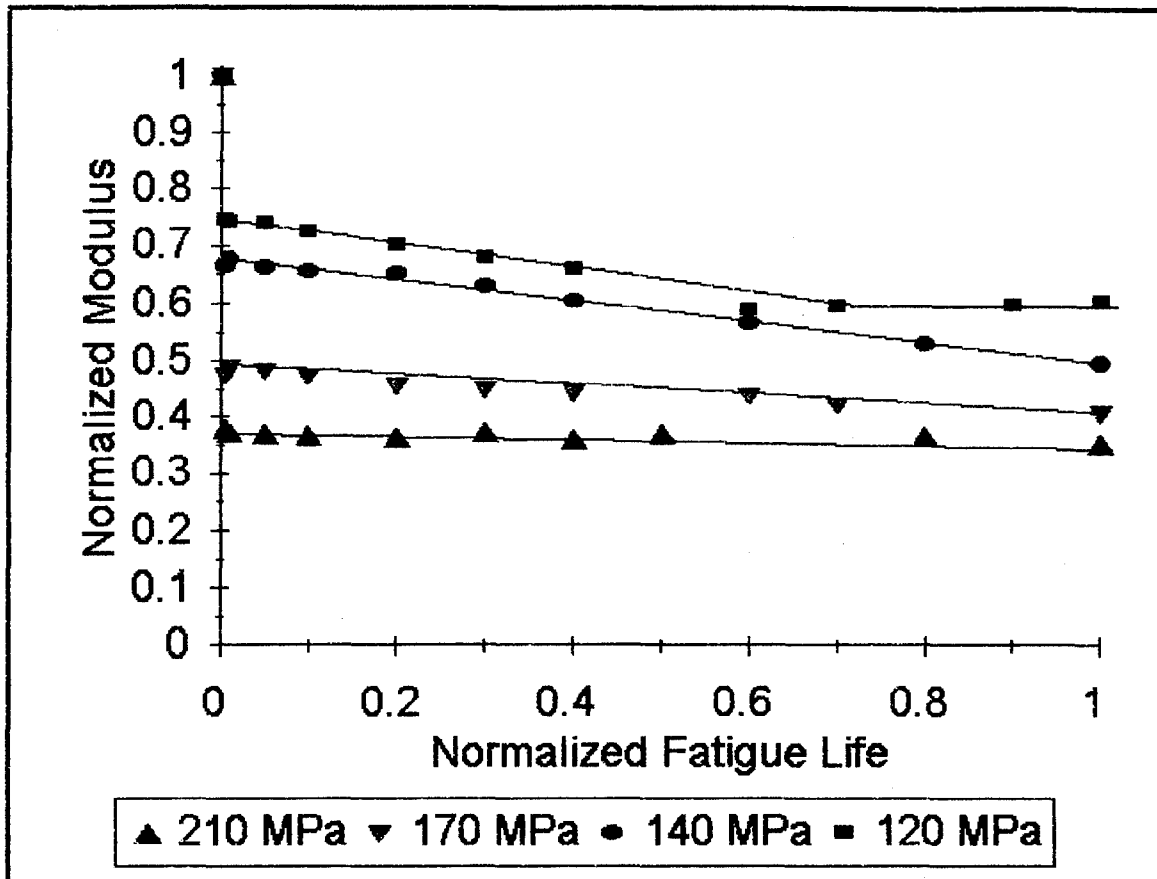
Figure 4-49   Normalized Unnotched Modulus Reduction on a Non
Log Scale

4-50 presents the similar representation of notched modulus

behavior.   On this normal scale the unnotched behavior seems

extremely linear after first cycle modulus degradation.   Two

aspects of the stiffness behavior of notched specimens are

worth noting.   First, the stiffness suffers a linear loss over

the life of the specimen in a similar manner as in the case of

4.53

the unnotched specimens. Second, the stiffness, in all cases, fell to 0.6 ± 0.1 of the first cycle value before failure.
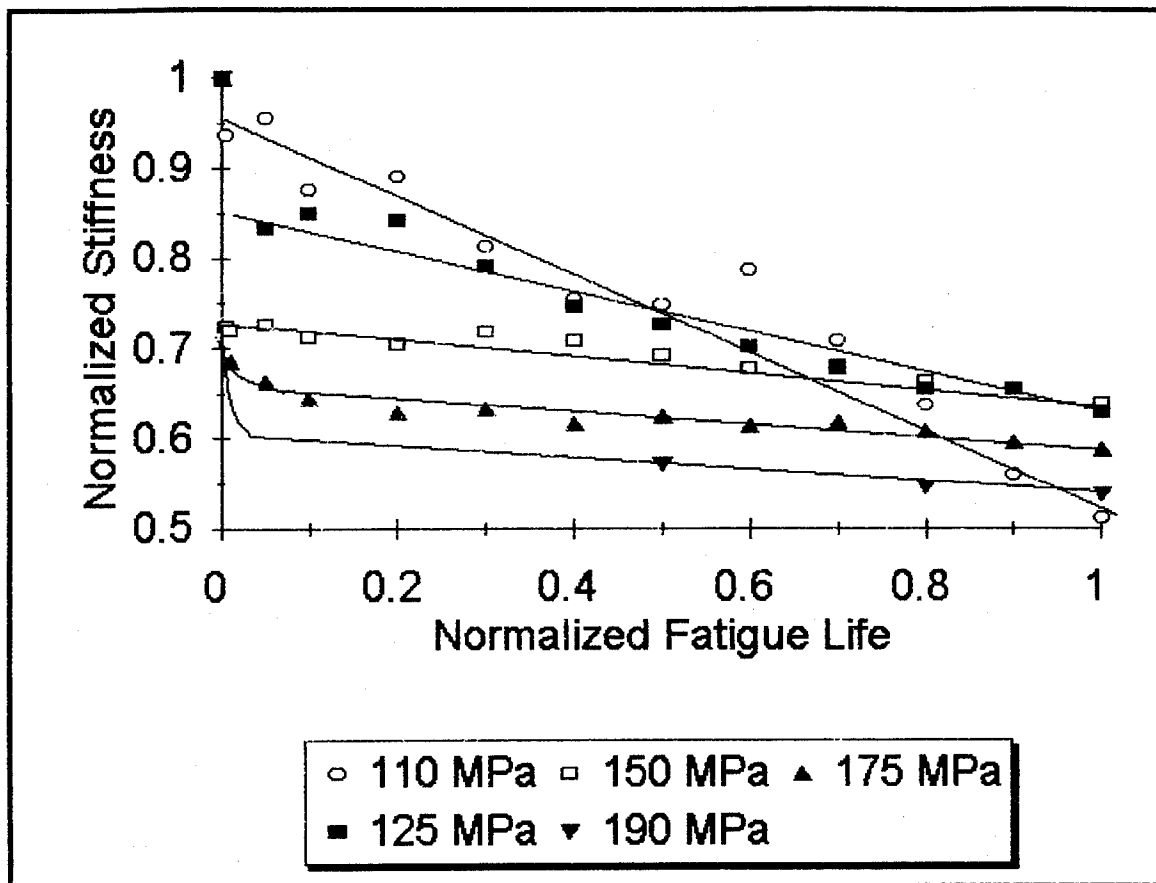
Figure 4-50 Normalized Notched Stiffness Reduction Vs. Normalized Cycles to Failure, Non-Log Scale

The low cycle/high stress behavior of both the notched and unnotched cases bears a marked similarity and indicates the presence of microstructural fatigue damage mechanisms in the form of multiple matrix micro-cracking, and fiber pull-out which predominantly take place in the first cycle. The higher stress level brings about catastrophic failure with very little warning, since most of the damage took place in the first

4.54

cycle. The high cycle/low stress modulus behavior in the notched and unnotched cases implies that specimens develop similar fatigue damage mechanisms over the life of the test. Since these tests are all above the endurance limit, either path leads to imminent failure. Because stiffness degradation is derived from the strain behavior, these stiffness degradation characteristics should very closely reflect the strain characteristics as discussed in the next section.

F.   Variation of Strain During Cycling

This section presents the variation of strain behavior over the fatigue life of the specimens. All fatigue tests were conducted in the tension-tension mode at 1100°C. The load was applied as a 1.0 Hz triangular wave. The minimum to maximum load ratio in all cases was 0.1. The tests are referenced by maximum applied stress level. First, the strain behavior of unnotched specimens is presented, followed by the strain behavior of the notched specimens.

The strain curves are compared and contrasted for high maximum fatigue stress versus low maximum fatigue stress in both the notched and unnotched cases. It should be noted that all strain discussed in this section is the mechanical strain only. Thermal strain has been removed by subtracting it from

4.55

total strain to give mechanical strain, ($\varepsilon - \varepsilon_{TH} = \varepsilon_M$) which is the quantity of interest.

Figure 4-51 shows the strain behavior of the 140 MPa unnotched specimen over its test life. This behavior is typical of the mid-stress region, exhibiting characteristics of both creep and modulus degradation. The variation in differential strain ($\varepsilon_{max}-\varepsilon_{min}$, where ε_{max} and ε_{min} are the strains corresponding to the maximum and minimum stress levels) over the fatigue life of the 140 MPa specimen should correspond to
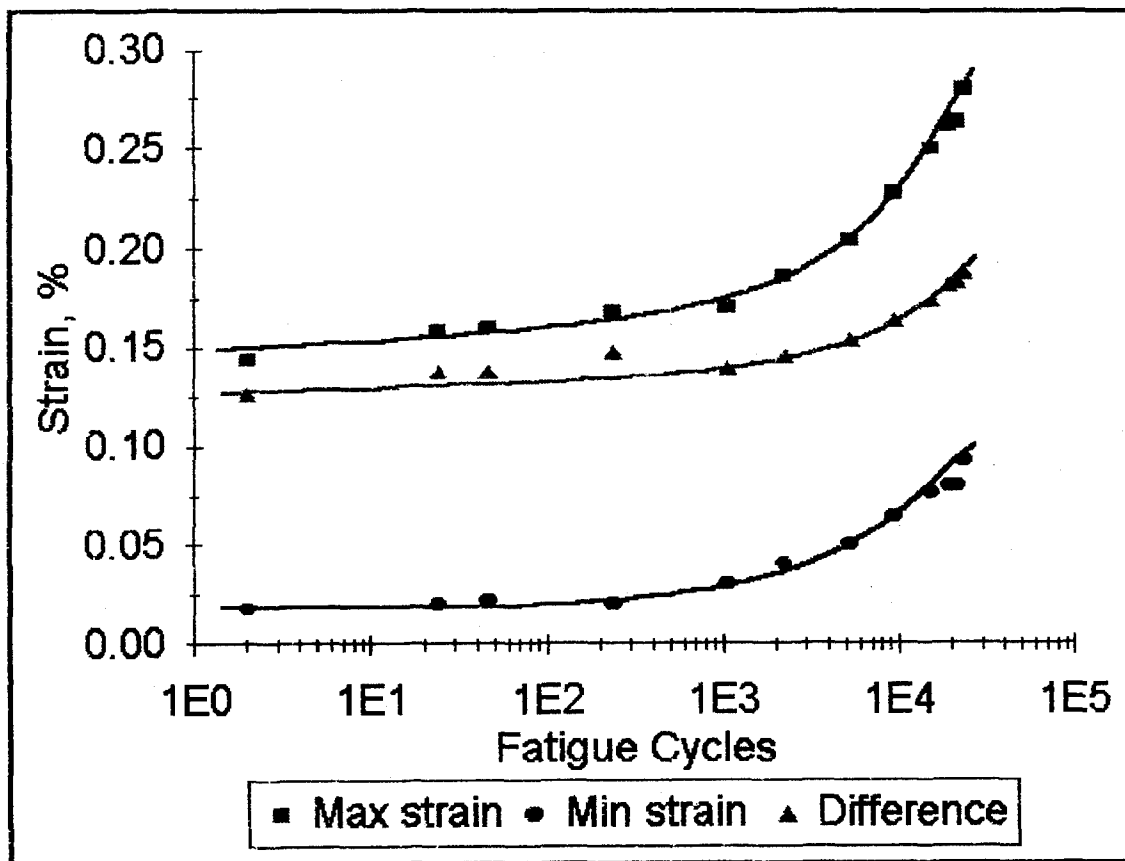
Figure 4-51 Strain Behavior of Unnotched Specimens at a Maximum Stress of 140 MPa

modulus degradation. If the differential strain were to remain at the same level over the life of the test, while maximum and minimum strain increased, the damage would be predominantly from creep. Notice this increased strain corresponds to the modulus reduction shown in Figure 4-45.

Figure 4-52 presents data on strain accumulated during the unnotched tests at (a) the maximum stress level, (b) the minimum stress level, and (c) the differential strain. These data correspond to tests carried out on the unnotched specimens
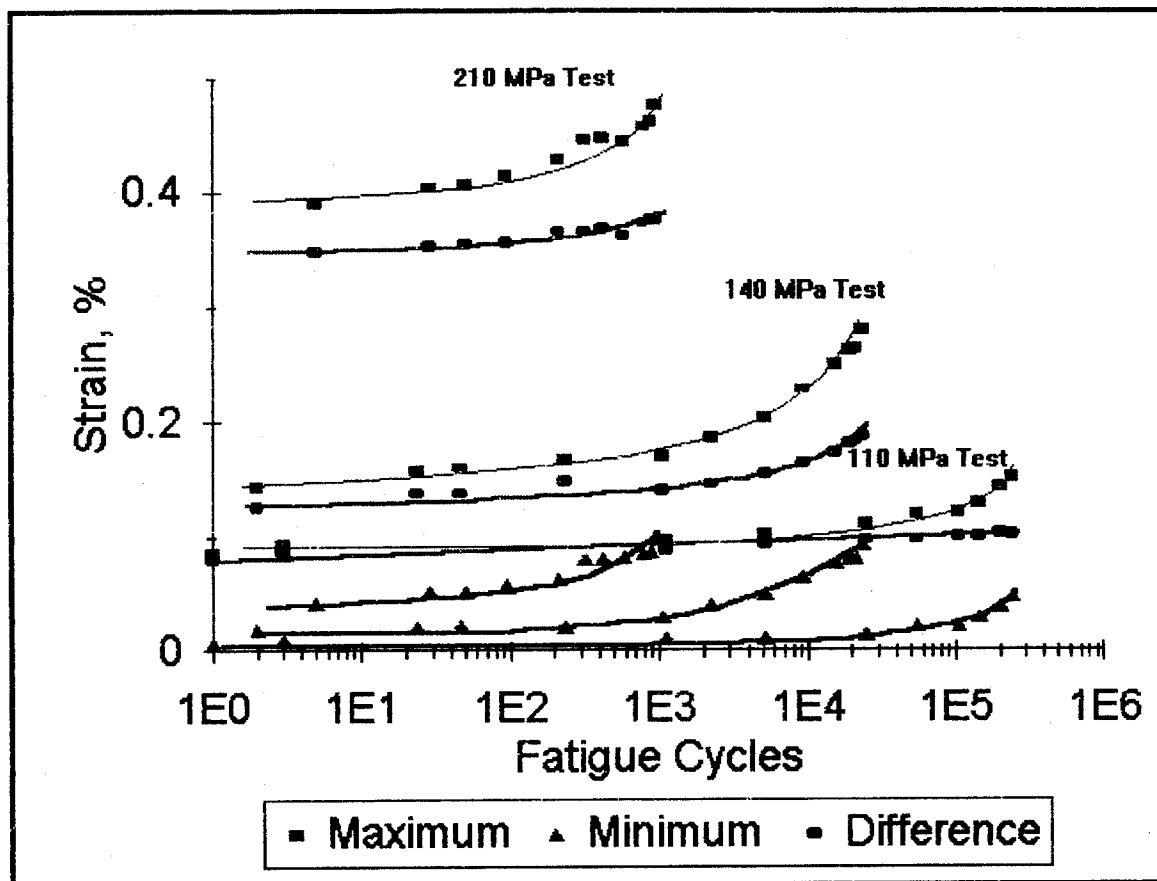
Figure 4-52   Strain Behavior of Unnotched Specimens at Three Load Levels

at fatigue stress levels of 210, 140, and 110 MPa. It is evident that the differential strain increases at a slower rate than the maximum and mimimum strain. This observation is consistent with the notion that creep plays a significant role during high temperature fatigue at a moderately high frequency (1.0 Hz).

Figure 4-53 presents data on strain accumulated during the notched tests at (a) the maximum stress level, (b) the minimum stress level, and (c) the differential strain. The 190 MPa specimen is the high stress case, 150 MPa is the mid stress
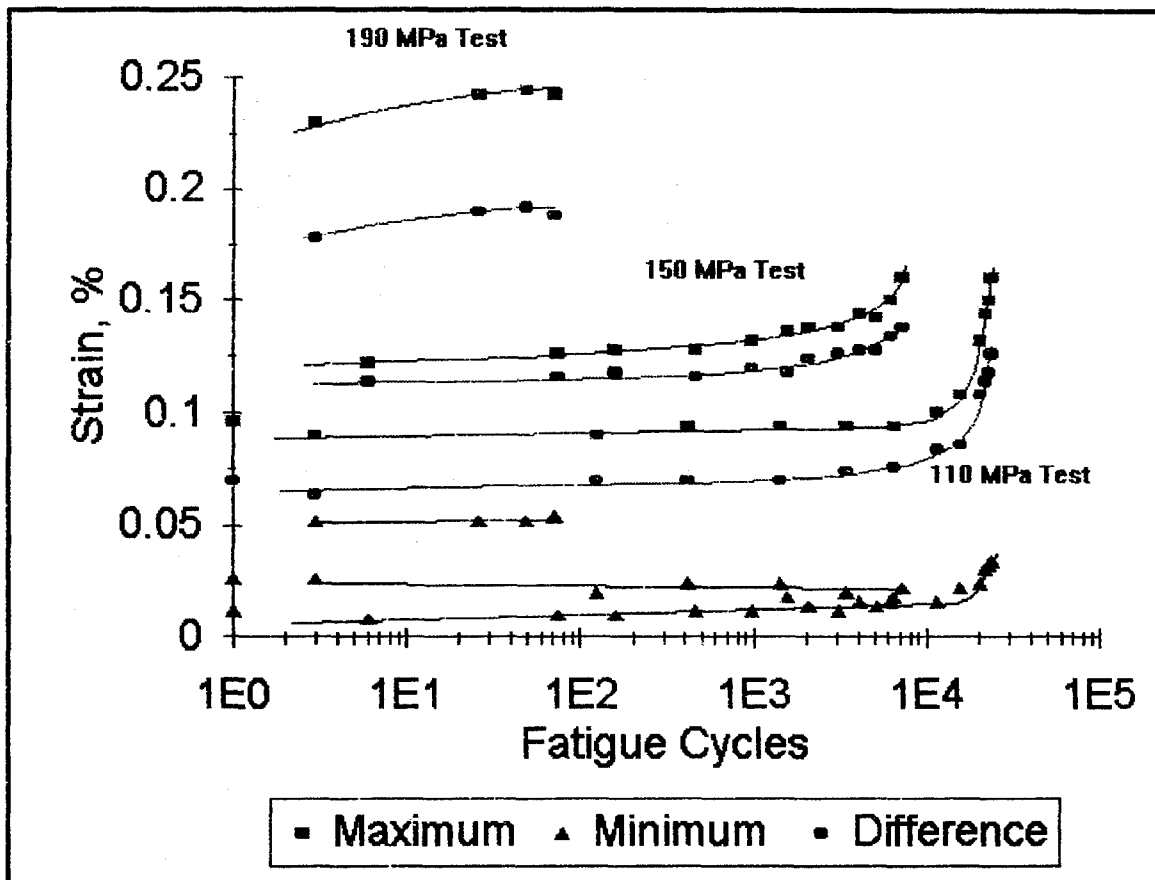
Figure 4-53   Strain Behavior of Notched Specimens at Three Load Levels

level and 110 MPa is the lowest stress level shown. These differential strain curves display some dependence on fatigue cycles; however, the maximum strain rate still increases more than the differential strain rate. This indicates creep plays a less significant role in notched fatigue behavior than it did in unnotched fatigue.

G.   *Damage Mechanisms*

This section discusses the damage mechanisms in the low stress (high cycle fatigue) vs. high stress (low cycle fatigue) tests for both notched and unnotched specimens. First, the test results for unnotched and notched specimens are compared in order to bring out similarities in their deformation behavior and fracture surface topography. Second, low cycle tests are contrasted with high cycle tests to elucidate the difference between the two regimes. Third, low cycle tests are compared to monotonic tensile tests to illustrate the similarity in their damage characteristics. Fourth, a brief description of the damage mechanisms applicable to monotonic tensile tests as well as high stress fatigue tests is offered. This is followed by a discussion of damage mechanisms pertaining to high cycle (low stress) fatigue tests.

As a first step in the discussion of damage mechanisms, a comparison is made between the notched and unnotched specimens. The S-N curve of section IV D has already established the similarity of notched vs. unnotched fatigue behavior on a macroscopic level. Similarities in the macroscopic deformation behavior of the notched and unnotched specimens was also reflected in their monotonic tensile strength and tensile stress-strain curves. Figures 4-54 and 4-55 present the 120 MPa unnotched fracture surface and the 110 MPa notched fracture surface respectively both at a magnification of 50X. Both scanning electron microscope (SEM) photographs are at approximately a 45° angular perspective to illustrate the length of yarn and fiber pullout. Note the equal fraction of fiber breakage to fiber pullout in both fracture surfaces. One may also observe the similarity in the height of protruding fibers.

Further microscopic evidence is presented in Figures 4-56 and 4-57 at a higher magnification. Figure 4-56 presents a scanning electron microphotograph of the 110 MPa notched specimen near the edge of the hole. Figure 4-57 shows the 110 MPa unnotched specimen near the edge of the fracture surface. These microphotographs confirm the microscopic similarity of the notched and unnotched specimens. These macroscopic and microscopic similarities between notched and unnotched tests

Figure 4-54   Unnotched Fracture Surface, 120 MPa Test, 50X
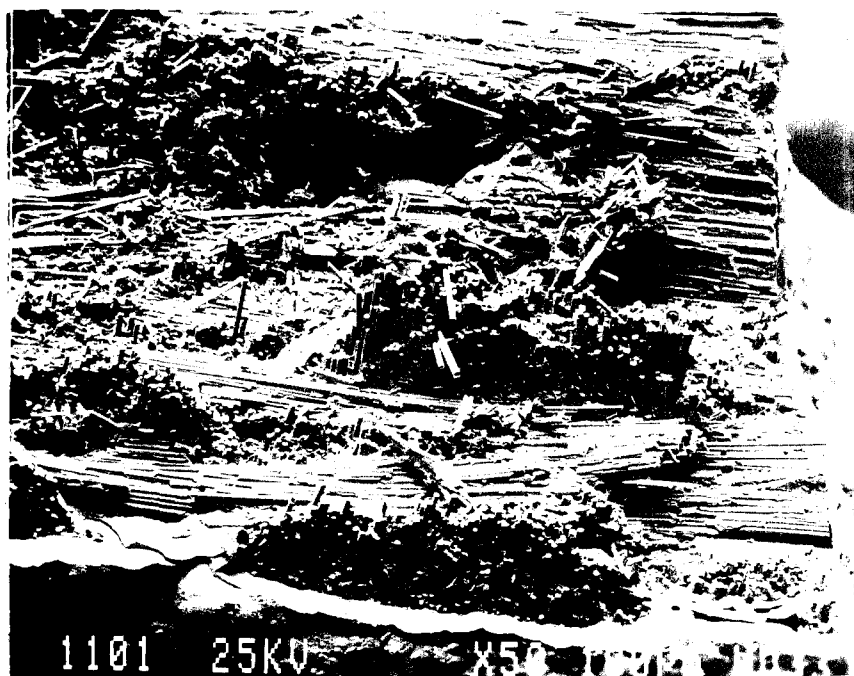
Figure 4-55   Notched Fracture Surface, 110 MPa Test, 50X

4.61

Figure 4-56   110 MPa Notched Specimen, Micrograph of
Fracture Near Hole, 250X

Figure 4-57   110 MPa Unnotched Specimen, Micrograph of
Fracture Near Edge, 200X

substantiate the claim that notched and unnotched specimens had essentially the same type of damage.

A noticeable difference exists between low cycle and high cycle fatigue fracture surfaces. The low stress fatigue fracture surface contained the more reflective areas than the high stress fatigue fracture surface. Comparative micrographs of the notched and unnotched fracture surfaces failed at low cycles and high cycles, obtained from optical microscopy are shown in Figures 4-58 and 4-59. For a closer inspection of this phenomenon the author chose to investigate these surfaces with scanning electron microscopy.
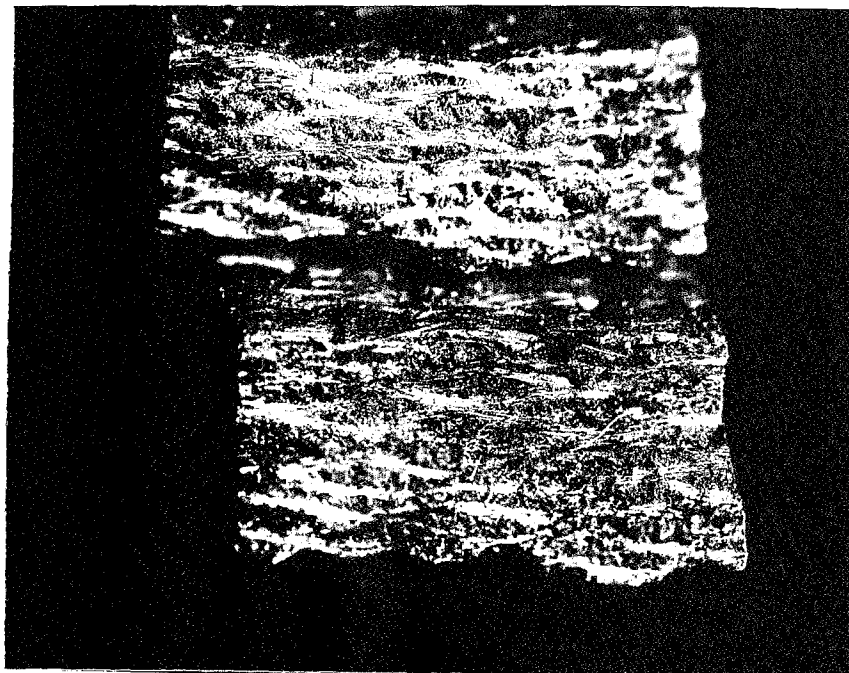
Figure 4-58 Micrograph Comparison, Unnotched Specimen Fracture, 8X, 210 MPa (top) 120 MPa (bottom)
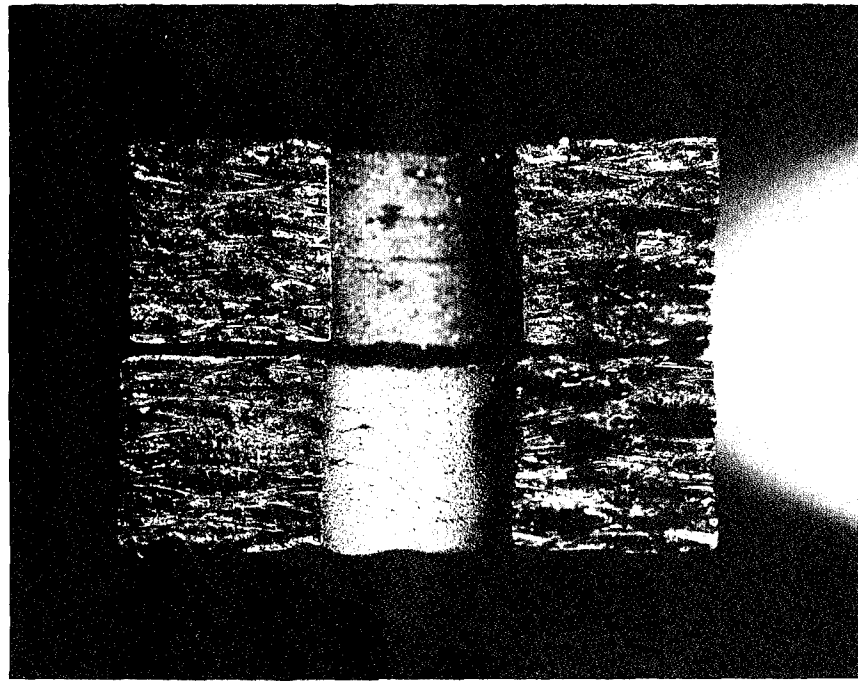
Figure 4-59   Micrograph Comparison, Notched Specimen
Fracture, 8X, 110 MPa (top)   190 MPa (bottom)

Figure 4-60 presents a scanning electron micrograph of the

210 MPa unnotched fracture surface, while Figure 4-61 presents

the 110 MPa unnotched fracture surface.   Both surfaces are

magnified 50 times and both are tilted at an angle of 45°.The

210 MPa test results in a fracture characterized by fibrous

surface due to fiber pullout of the 0° yarns.   Long clusters of

fibers (some with 0.7 mm peaks) are visible where 0° yarns have

pulled free of the opposing fracture surface.   At the lower

stress levels the failure surface exhibits far less fiber or

yarn pullout.   A small number of fibers are observed, some as

much as 0.14 mm in height;   however, the majority of the 0°

Figure 4-60   Unnotched Fracture Surface, 210 MPa Test, 50X Mag.
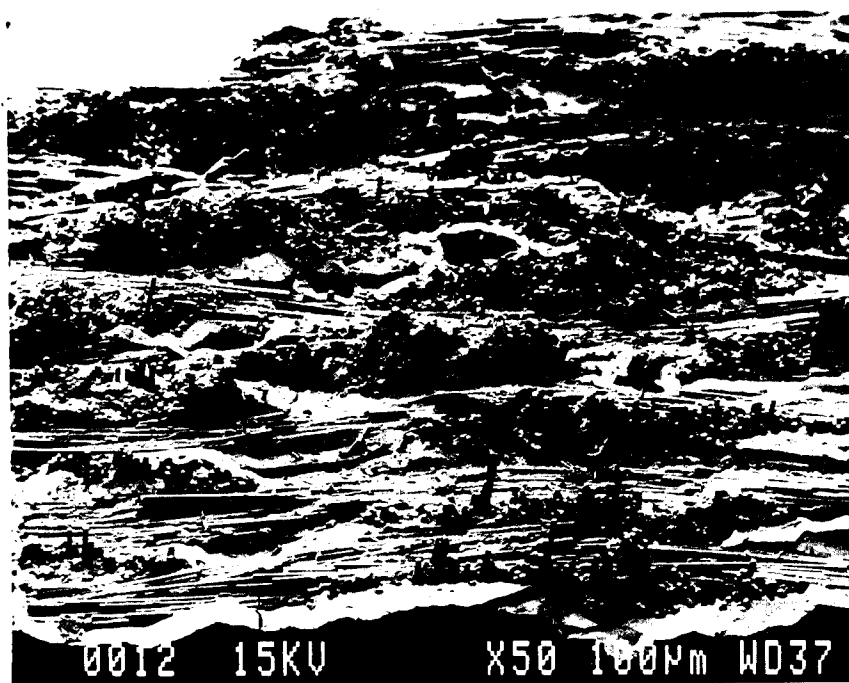
Figure 4-61   Unnotched Fracture Surface, 110 MPa Test, 50X Mag.

yarns are broken cleanly. The strain and modulus behavior during cycling of the 110 MPa specimen also suggests that a different fatigue damage mechanism operates at low stress levels. Low stress fatigue behavior is, therefore, substantially different from that of the high stress fatigue behavior.

Next, a comparison of high stress/low cycle fatigue with monotonic tensile test behavior demonstrates their similarity. Figure 4-62 presents a scanning electron microphotograph of the notched monotonic tensile test specimen. Comparing this surface to that of the 210 MPa unnotched fatigue test (Figure 4-60) shows the similar fracture surface character. Both
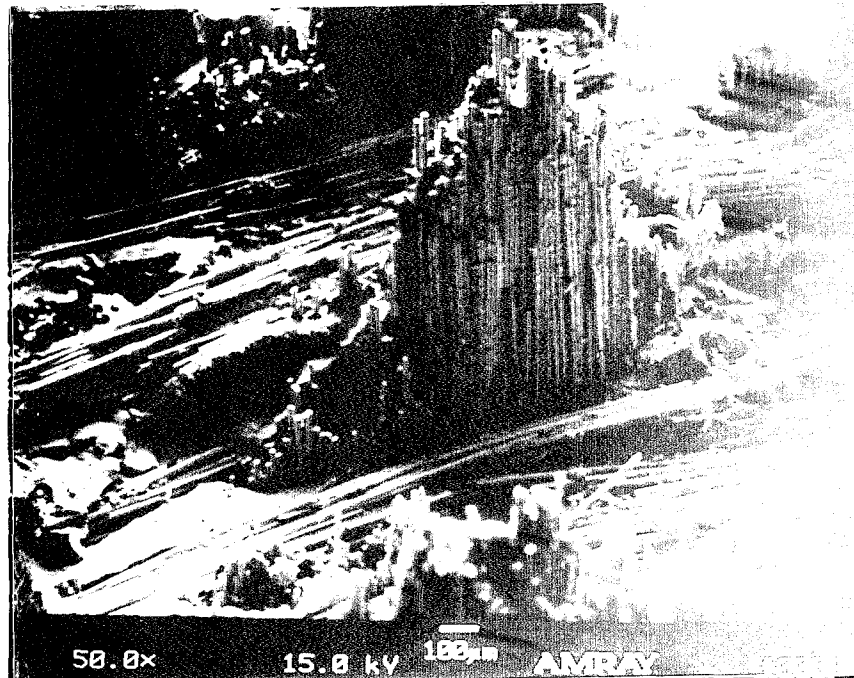
Figure 4-62 Fracture Surface, Notched Monotonic Tensile Test, 50X Mag.

surfaces exhibit a long fiber pullout (~1.0 mm) and a small percentage of surface fracture of the 0° yarn fibers. As illustrated in section 4 A, (Figures 4-1 and 4-2) the first cycle of both the 190 MPa notched and 210 MPa unnotched tests extended well into the nonlinear region of the monotonic stress-strain curve (80% of σ_{ult}). This also indicates that first cycle stress, during high stress/low cycle fatigue, activates the same damage mechanisms as the monotonic tensile tests. Stress-strain behavior and microscopic examination both confirm that high stress/low cycle fatigue damage is essentially the same as monotonic tensile damage.

Monotonic tensile damage mechanisms at elevated temperature were described by Chen [4] and substantiated by the monotonic tensile tests of section 4 A of the present work. First, at relatively low stress levels (about 85 MPa), inter-yarn cracking takes place in the porous regions between the 90° yarns and is illustrated schematically in Figure 2-4. Second, at relatively high stress levels (about 150 MPa) 90° yarn matrix cracking occurs. Chen describes the 90° matrix cracking as "the dominant damage mechanism for failure of the composite at the high temperature conditions and a major contributing factor in the non-linear deformation". Fiber/matrix interface debonding also takes place at these higher stress levels and

4.67

subsequently 0° yarn fracture precipitates final failure of the specimen. 0° yarn fracture involves matrix cracking within the yarns, fiber breakage, and yarn splitting. Evidence of these damage mechanisms is presented in Figures 4-60 and 4-62. The long 0° yarn fiber bunch in the center of Figure 4-62, for instance, displays yarn splitting and fiber pullout (as evidence of matrix cracking, interface debonding, and fiber breakage).

The above damage mechanisms are closely related to the toughening mechanisms of multiple matrix micro-cracking, fiber pullout, and crack deflection[4]. Multiple matrix cracking produces multiple parallel cracks in the matrix of the 90° fibers as the matrix fails and the fibers have not yet reached their critical stress level. This type of fracture is referred to as a multiple fracture system. The most important multiple fracture effect is that the energy absorbed by producing the extra cracks adds to the overall fracture strength of the material.

Fiber pullout is a crack arrest mechanism occurring in the 0° yarn. During fiber pullout, the broken fibers resist further matrix cracking by frictional sliding which occurs as the broken ends of the fibers pull out of the fractured matrix. Energy is dissipated through the creation of new surfaces associated with the pullout of the fibers. Maximum axial

stress in the fiber occurs at the matrix crack plane. This fiber pullout requires an appropriate level of interfacial shear stress to permit load carrying by the fiber without causing it to break at the crack front (see figure 2-1).

Matrix crack deflection occurs in the lateral yarn region of the composite. Crack bowing originates from the second phase particles in the path of a propagating crack[9]. The crack tends to bow between the second phase particles until the fracture toughness of the particles is reached. This bowing causes the stress intensity along the deflected crack to decrease thus increasing fracture toughness. The matrix cracks are deflected and sometimes completely arrested as they approach and bypass fiber strands which are equivalent to second phase particles in this system. The clearly defined shape of the fibers in the 90° yarns in Figure 4-60 and 4-62 is evidence of this crack deflection.

During low-stress fatigue tests inter-yarn cracking takes place as previously described. Multiple matrix micro-cracking also takes place in a manner similar to that previously described. However, in low stress fatigue testing, stress levels fail to reach that required for interface debonding. Without interface debond, cracks may prematurely propagate through the interface, into the fibers. Figure 4-63 presents a scanning electron micrograph of the 110 MPa unnotched fatigue

test. This photograph shows the lack of fiber pullout. Closer inspection of Figure 4-63 reveals that fiber/matrix interface debonding did indeed take place adjacent to the 90° yarn. Fibers located inside the 0° yarn, however show no indication of interface debond, indicating the fracture propagated through the yarn with little regard to fiber/matrix interface. Figure

Limited
Interface
Debond
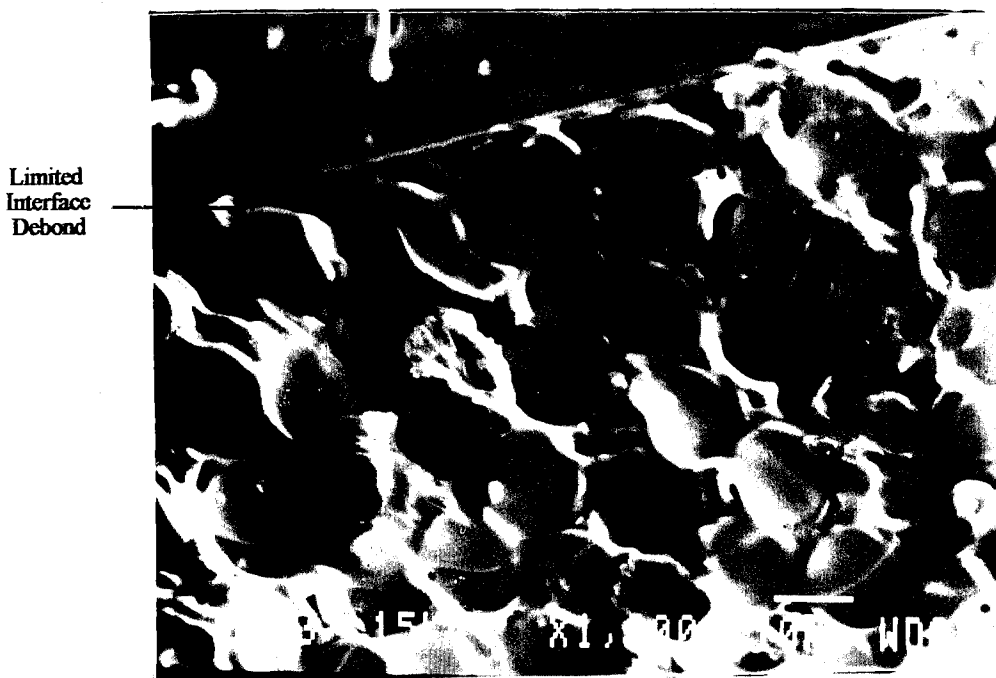
Figure 4-63 Micrograph of 0° Fiber Breakage, 110 MPa Unnotched Test, 1000X

4-60 and 4-62 also illustrate this contrast in behavior between low stress and high stress fatigue damage. This damage progression is consistent with the strain behavior of the 110 MPa unnotched test. Low stress/high cycle fatigue damage

mechanisms, then, seem to have reverted to the undesirable CMC failure mode discussed in section II. This mode is the failure resulting from relatively weak fibers and relatively strong interfacial bonds allowing the matrix crack to penetrate through the fibers.

V. CONCLUSIONS

The objective of this study was to investigate the high temperature deformation behavior of a ceramic matrix composite (CMC) under monotonic and fatigue loading conditions. The CMC used in this work was an enhanced SiC/SiC formed by chemical vapor infiltration (CVI) employing a plain weave fabric reinforcement. The laminate consisted of 11 plies. Static and fatigue tensile tests were performed at an elevated temperature (1100°C) on eight notched specimens and six unnotched specimens. All notched specimens had a hole, with a diameter to width ratio (D/W) of 0.33. Monotonic tests were performed on one each of the notched and unnotched specimens, while the remaining 12 specimens were fatigue tested. All fatigue tests were conducted in a load controlled mode and employed a triangular load wave with a load ratio of 0.1 and a frequency of 1.0 Hz.

The stress-strain curve for the unnotched specimen in monotonic tension was characterized by a linear response up to 60 MPa, regarded as the proportional limit. The failure stress level was found to be 230 MPa. Since this specimen failed outside the gage length, the actual ultimate tensile strength is expected to be slightly higher than this value. In contrast, the notched specimen showed no clearly defined

proportional limit. However, the failure strength of the notched specimen (228 MPa) was approximately equal to that of the unnotched specimen. Except for the initial nonlinearity of the notched stress strain curve, the notched and unnotched specimens exhibited similar deformation behavior under monotonic loading.

Fatigue tests were conducted using maximum stress levels varying from 95 to 210 MPa. Fatigue life was of course a function of applied stress and the fatigue limit was above the proportional limit of the material. The S-N curves for the notched and unnotched tests were compared to evaluate the fatigue notch sensitivity due to the hole. Fatigue tests of unnotched specimens indicated a fatigue limit of 105 MPa. Fatigue tests of the notched specimens had a run-out of about one half a million cycles at 95 MPa indicating this is as a fatigue limit. Fatigue strength of the notched specimens was, in general, 10 to 15% below the unnotched fatigue strength. Furthermore, the S-N curves for the notched and unnotched specimens were quite similar. Thus it may be concluded that the presence of a notch has little effect on fatigue life of the tested CMC.

Stiffness degradation was evaluated for all tests. In both notched and unnotched specimens, first cycle degradation established the new stiffness, characteristic of the given

stress level. Subsequent stiffness, in most cases, decreased steadily until final fracture occurred. At low stress levels, the stress-strain curves showed increasing hysteresis and decreasing slope over the life of the test. At the lowest stress level (110 MPa), the unnotched test showed very little change during the course of the fatigue test i.e. less progressive modulus degradation before failure. Strain behavior showed inverse correlation with stiffness behavior as would be expected due to microstructural damage taking place during fatigue. Stress-strain behavior over the life of the notched specimens was qualitatively similar to the behavior of the unnotched specimens; except the aforementioned 110 MPa unnotched behavior.

After testing, the specimens were sectioned and examined. Characterization of the fracture surface indicated that in all cases, the failure of the notched specimens initiated adjacent to the hole while failure of the unnotched specimens initiated at the edges and inherent pores. The failure mode in monotonic and high stress fatigue tests was inter-yarn cracking between the 0° and 90° yarns followed by transverse matrix cracking of the 90° yarns, and finally by matrix cracking, fiber pullout, and yarn cracking of the 0° yarns. The above damage progression was characteristic of both notched and unnotched specimens.

In the low stress/high cycle fatigue regime, on the other hand, scanning electron micrographs of fracture surfaces in both the notched and unnotched tests showed smooth regions and lack of fiber pullout in the region of damage initiation. This type of surface revealed that the crack penetrated with no deflection along the fiber/matrix interface regions. Fatigue at low stresses, therefore, did not activate the desired crack arrest mechanisms such as fiber pullout.

VI. RECOMMENDATIONS

The temperature should be perturbed for tension-tension fatigue cycling to investigate the effect of temperature variations on fatigue life and strength of the material. Thermo-mechanical fatigue cycling should also be performed as well as tension-compression cycling.

Strain behavior of this enhanced SiC/SiC material, as discussed in section IV F, made it evident that creep tests are in order. The apparent degradation of fatigue life, using a loading spectrum of 0.5 Hz, reported by DuPont[12], further substantiates this assertion. Load frequency and hold times should be perturbed in a series of tests to develop S-N curves characterizing the effects of these two parameters.

Bibliography

1. Aveston, J., G.A. Cooper, and A. Kelley. "Single and Multiple Fracture," The Properties of Fiber Composites, Conference on Proceedings, National Physical Laboratory. 15-16. Surrey, England: Guildford IPC Science and Technology Press, 1971.

2. Brennan, J. J. and K. M. Prewo. "Silicon Carbide Fibre Reinforced Ceramic Matrix Composites Exhibiting High Strength and Toughness," *Journal of Materials Science, 10*: 2371-2383 (August 1982).

3. Bullock, Daniel E. *Failure Characterization of a Fiber Reinforced Ceramic Matrix Composite with Circular Holes.* MS thesis, AFIT/GAE/ENY/91D-19. School of Engineering, Air Force Institute of Technology (AU), Wright-Patterson AFB OH, December 91

4. Chen, Winnei Y. *Characterization of the Tensile Behavior of Ceramic Woven Fiber Composites.* PhD Dissertation. University of Delaware, Newark Delaware, Spring 1993

5. Davidson, D.L. *Fracture Mechanics of Continuous Fiber and Textile Reinforced Metal and Ceramic Matrix Composites: Interim Technical Report, February 1994.* Contract N000014-93-C-0040. Arlington VA: Office of Naval Research, February 1994 (AD-A277343).

6. Delale, Feridun and Been M. Liaw. *Microcracking and Toughness of Ceramic-Fiber/Ceramic-Matrix Composites Under High Temperature: Final Report, 1 Aug 1987-30 September 1989.* Contract AF-AFOSR-0288-87. New York: City College of the City University of New York, December 1989 (AD-A218516).

7. Evans, A.G. "The Mechanical Performance of Fiber-Reinforced Ceramic Matrix Composites." *Materials Science and Engineering, A107*: 227-239 1989

8. Evans, A.G. "Ceramic Matrix Composites: Challenges and Opportunities," Presented at work held by AGARD Structures and Materials Panel. 2.5-2.13. Antalya Turkey. April 1993 (AD-A276 040)

9. Faber, K. T. and Evans, A. G. "Crack Deflection Processes-I Theory," *Acta Metallurgica et Materialia, 31*: 565-576 (1983)

10. Fujii, Toru, Toru Shiina, and Kazuya Okubo. "Fatigue Notch Sensitivity of Glass Woven Fabric Composites Having a Circular Hole under Tension/Torsion Biaxial Loading," *Journal of Composite Materials, 28*: 234-251 (March 1994).

11. Geoghegan, Phillip J. "Chemical Vapor Infiltrated Composites," in *Flight Vehicle Materials, Structures, and Dynamics Vol 3.* Ed. Levine, R.S. and others. New York: American Society of Mechanical Engineers, 1992.

12. Headinger, M.H. Preliminary Engineering Data, 7 May 94, Pencader Plant, P.O. Box 6100, Newark, Delaware 19714-6100

13. Holmes, John W. *Mechanics of Elevated Temperature Fatigue Damage in Fiber-Reinforced Ceramics, 1 Dec 1990-30 Nov 1992.* Contract AF-AFOSR-0106-91. Ann Arbor MI: University of Michigan, January 1993 (AD-A262403).

14. John, Reji and Noel E. Ashbaugh. "Fatigue Crack Growth in Ceramics and Ceramic Matrix Composites," *Symposium on Cyclic Deformation, Fracture, and Nondestructive Evaluation of Advanced Materials.* 28-51. Philadelphia PA: ASTM, 1992.

15. Mall, S., W.R. Moschelle, and J.J. Pernot, "Fatigue Behavior of a Fiber-Reinforced Ceramic-Matrix Composite with a Circular Hole" *Composites Science and Technology, 49*: 173-182 1993.

16. Mallick, P.K. *Fiber-reinforced Composites: Materials, Manufacturing, and Design -2nd ed.* New York: Marcel Dekker, Inc., 1993, pages 525-529

17. Marshall, D.B. and A.G. Evans. "Failure Mechanisms in Ceramic Fiber/Ceramic Matrix Composites," *Journal of the American Ceramic Society, 68*: 225-231 (May 1985).

18. Mol, John H. *Fracture Toughness Testing of a Ceramic Matrix Composite at Elevated Temperatures.* MS thesis, AFIT/GAE/AA/88D-26. School of Engineering, Air Force Institute of Technology (AU), Wright Patterson AFB, OH, December 1988 (AD-A202738).

19. Mehran, Elahi and others. "Elevated Temperature Cyclic Fatigue of Silicon Carbide Fiber Reinforced Silicon Carbide Matrix Composites," *18th Annual Conference on Composites and Advanced Ceramics Materials.* 3-12. Cocoa Beach FL: Jan 1994

20. Moschelle, William R. *Fatigue Behavior and Failure Mechanisms of Centrally Notched [0] and [(0/90)] Silicon Carbide Reinforced Aluminosilicate Glass.* MS Thesis, AFIT/GAE/ENY/91D-19. School of Engineer ng, Air Force Institute of Technology (AU), Wright-Pat erson AFB OH, December 1991.

21. Naik, Niranjan K. *Woven Fabric Composites.* Lancaster PA: Technomic Publishing Co. Inc., 1994.

22. Pagano, Nicholas J. "Micromechanical Failure Modes in Brittle Matrix Composites." Presented at work held by AGARD Structures and Materials Panel. 4.1-4.10. Antalya Turkey. April 1993 (AD-A276 040)

23. Pluvinage, P. and J.M. Quenisset "Numerical Simulation of the Tensile Behavior of 2D-SiC/SiC Cross-Ply Laminates," *Journal of Composite Materials, 27*: 152-174 (1993).

24. Prewo, K. M. "Fatigue and Stress Rupture of Silicon Carbide Fiber-Reinforced Glass-Ceramics," *Journal of Materials Science, 22*: 2695-2701 (1987).

25. Rouby, D. and P. Reynaud "Role of Interfaces on the Cyclic Fatigue Behaviour of Ceramic Matrix Composites." Presented at work held by AGARD Structures and Materials Panel. 6.1-6.10. Antalya Turkey. April 1993 (AD-A276 040)

26. Tsangarakis, Nikos, John M. Slepetz, and John Nunes "Static and fatigue Notch Strength Prediction in Alumina Fiber Reinforced Aluminum Plates with a Circular Hole," *Journal of Composite Materials, 22*: 386-393 (April 1988).

27. Yajima, S. et al. "Synthesis of a Polytitanocarbosilane and its Conversion into Inorganic Compounds," *Journal of Materials Science, 16*:1349-1355 (1981).

APPENDIX A

Test Results

Table A-1 Notched Tests

Reduced Width (mm)	Thickness (mm)	Cycle 1 Stiffness (GPa)	Fatigue Stiffness (GPa)	Maximum Stress (MPa)	Number of Cycles to Failure
6.472	3.345	170		225	static
6.421	3.358	180	97	190	95
6.510	3.317	155	112	175	1676
6.325	3.353		122	150	9687
6.457	3.327	170	125	125	19554
6.490	3.325	150	150	110	24802
6.393	3.345		180	100	100489
6.462	3.307	170	170	95	440036+

+ This specimen did not fail

Table A-2 Unnotched Tests

Width (mm)	Thickness (mm)	Cycle 1 Modulus (GPa)	Fatigue Modulus (GPa)	Maximum Stress (MPa)	Number of Cycles to Failure
8.156	3.317	145		230+	Static
8.085	3.327	115	54	210	977
8.034	3.358	117	72	170	6780
8.113	3.261		100	140	25343
8.199	3.360		115	120	44041
8.052	3.343	130	119	110	259249

+ This value is lower than would have been achieved
had the specimen broken in the gage length

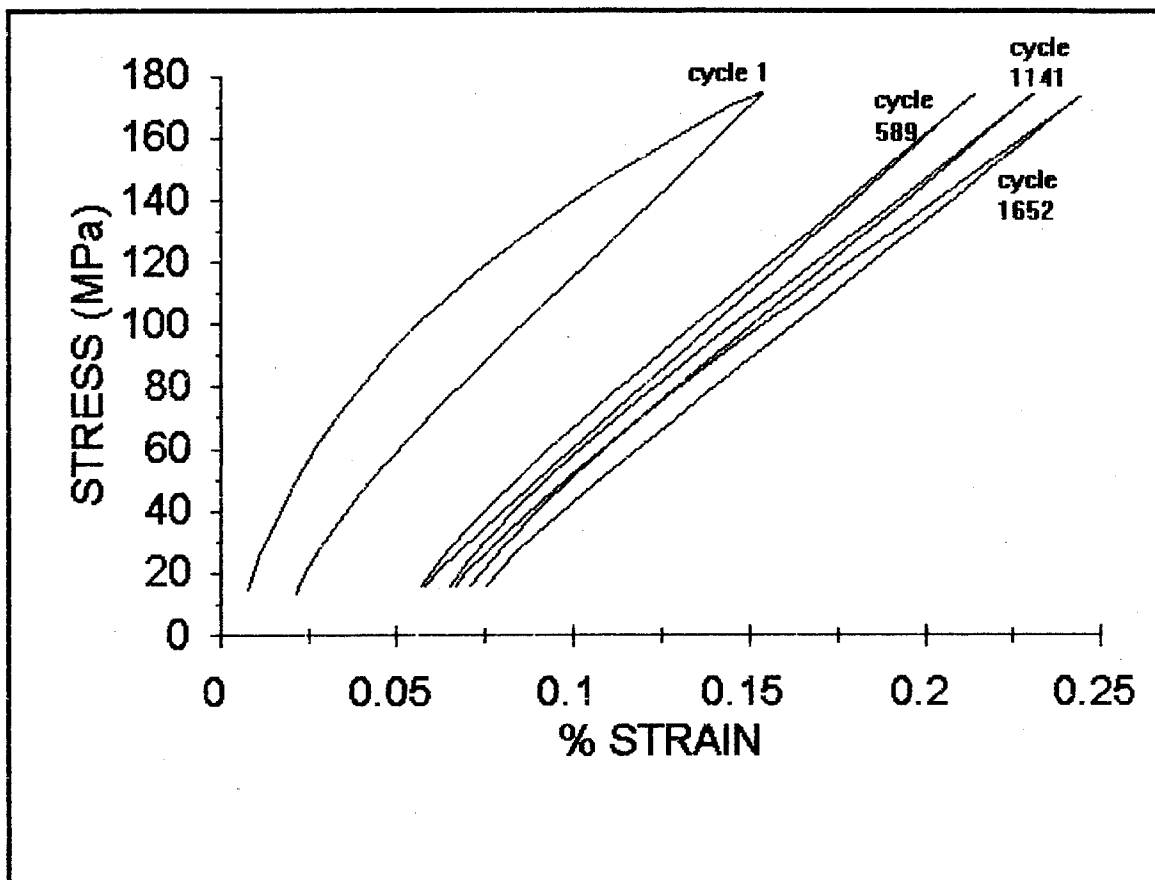*Notched Test Stress-strain Curves*
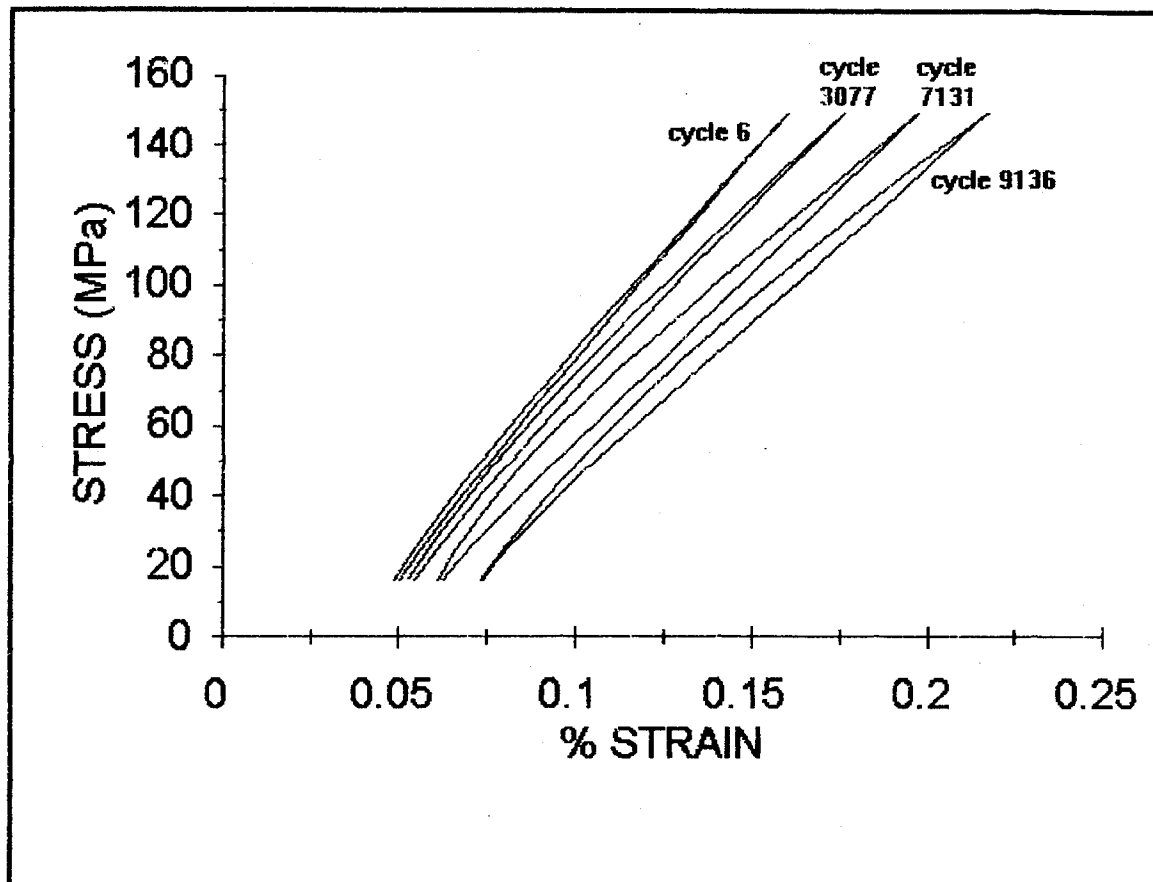

Figure B-1 Stress-strain, 175 MPa Notched Test
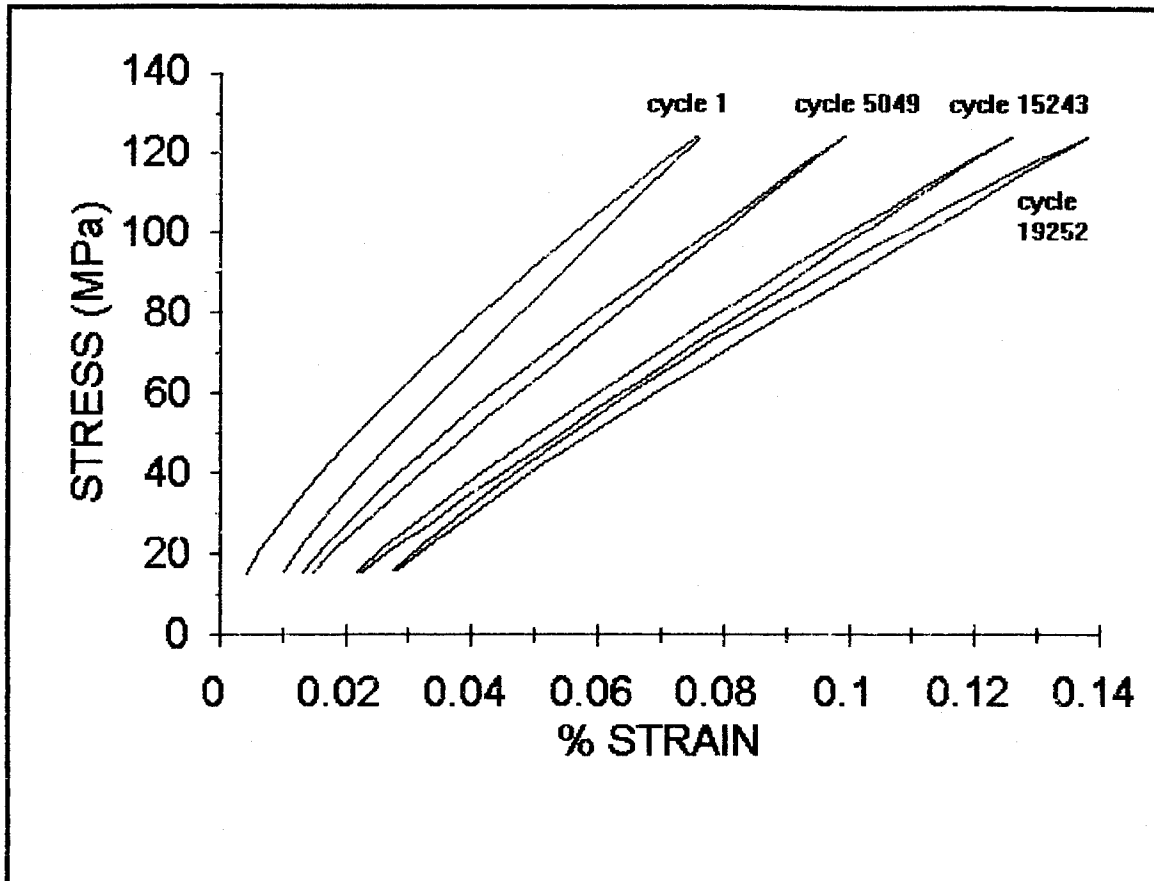
Figure B-2 Stress-strain, 150 MPa Notched Test

Figure B-3 Stress-strain, 125 MPa Notched Test
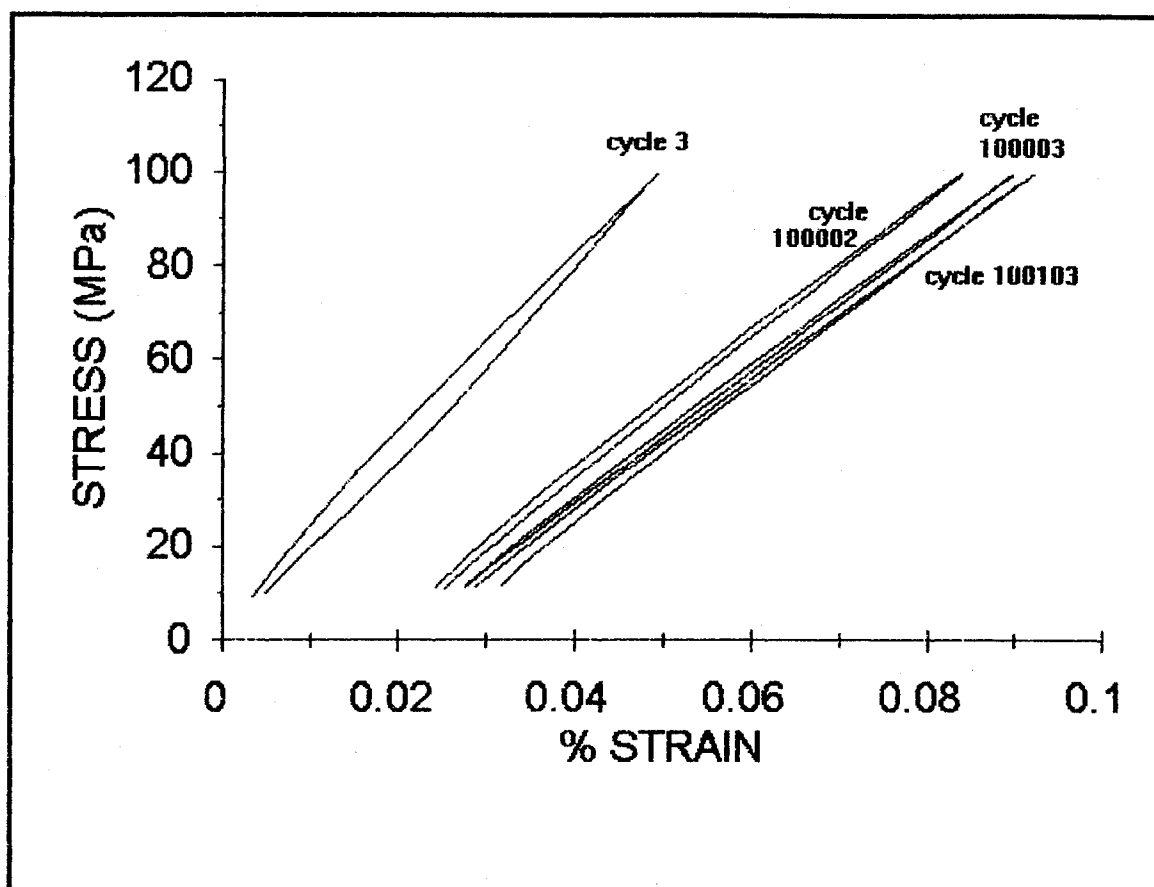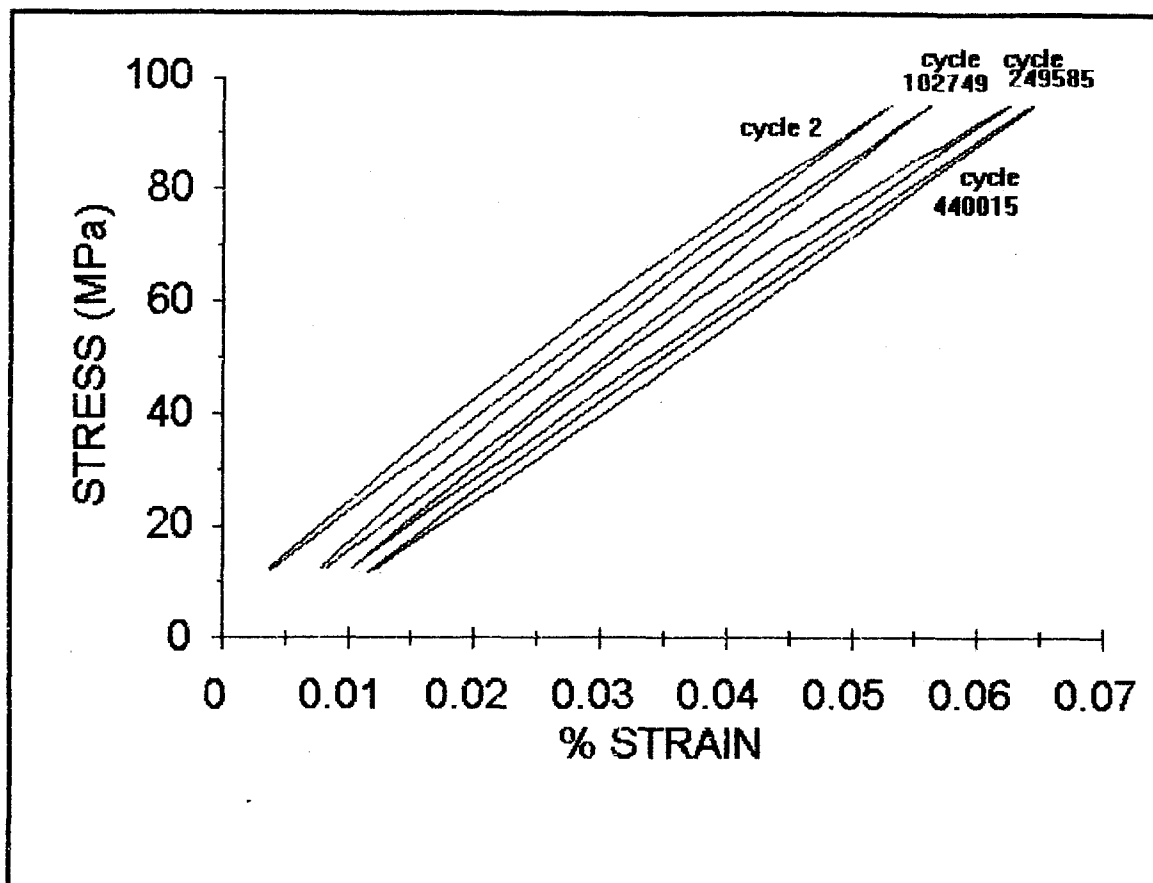
Figure B-4 Stress-strain, 100 MPa Notched Test

Figure B-5 Stress-strain, 95 MPa Notched Test

VITA

Captain Daniel J. Groner was born 8 October 1958 in Clarion, Pennsylvania. He graduated from Allegheny Clarion Valley High School in 1977. He entered the Air Force in August of that year to be trained as an Electronic Warfare Systems(EWS) technician. After initial training at Keesler AFB, MS; he served as an apprentice and journeyman technician at 4th Component Repair Squadron, Seymour-Johnson AFB, NC. He then served as a technician and supervisor in the 43 Avionics Maintenance Squadron EWS shop at Andersen AFB, Guam. After a break in service he was assigned to England AFB, LA where he served as a technician, and supervisor in the 23rd Component Repair Squadron EWS shop, and an instructor in the 309th Field Training Detachment. While serving as an instructor, Technical Sergeant Groner was selected for the Airman Education and Commissioning Program(AECP). He completed the formal education portion of his AECP when he graduated from the University of Florida in December 1989. After commissioning in April 1990 he was assigned to the 6595 Test and Evaluation Group where he served as a Test Controller and Propulsion Systems Engineer on the Rail Garrison, Reentry System Launch, and Small Missile Programs. He entered the School of Engineering, Air Force Institute of Technology in May 1993.

REPORT DOCUMENTATION PAGE

Public reporting burden for this collection of information is estimated to average 1 hour per response, including the time for reviewing instructions, searching existing data sources, gathering and maintaining the data needed, and completing and reviewing the collection of information. Send comments regarding this burden estimate or any other aspect of this collection of information, including suggestions for reducing this burden, to Washington Headquarters Services, Directorate for Information Operations and Reports, 1215 Jefferson Davis Highway, Suite 1204, Arlington, VA 22202-4302, and to the Office of Management and Budget, Paperwork Reduction Project (0704-0188), Washington, DC 20503.

1. AGENCY USE ONLY (Leave blank)	2. REPORT DATE	3. REPORT TYPE AND DATES COVERED
	December 1994	Master's Thesis (Final)

4. TITLE AND SUBTITLE	5. FUNDING NUMBERS
Characterization of Fatigue Behavior of 2-D Woven Fabric Reinforced Ceramic Matrix Composite at Elevated Temperature	

6. AUTHOR(S)

Daniel J. Groner, Captain, USAF

7. PERFORMING ORGANIZATION NAME(S) AND ADDRESS(ES)	8. PERFORMING ORGANIZATION REPORT NUMBER
Air Force Institute of Technology WPAFB OH 45433-6583	AFIT/GAE/ENY/94D-15

9. SPONSORING/MONITORING AGENCY NAME(S) AND ADDRESS(ES)	10. SPONSORING/MONITORING AGENCY REPORT NUMBER
W. R. Moschelle, Captain WL/POTC WPAFB, OH 45433-6583	

11. SUPPLEMENTARY NOTES

12a. DISTRIBUTION/AVAILABILITY STATEMENT	12b. DISTRIBUTION CODE
Approved for public release; Distribution unlimited	

13. ABSTRACT (Maximum 200 words)

This study investigated the fatigue behavior and associated damage mechanisms in notched and unnotched enhanced SiC/SiC ceramic matrix composite specimens at 1100°C. Stiffness degradation, strain variation, and hysteresis were evaluated to characterize material behavior. Microscopic examination was performed to characterize damage mechanisms. During high cycle/low stress fatigue tests, far less fiber/matrix interface debond was evident than in low cycle/high stress fatigue tests. Notched specimens exhibited minimal stress concentration during monotonic tensile testing and minimal notch sensitivity during fatigue testing. Damage mechanisms were also similar to unnotched.

14. SUBJECT TERMS	15. NUMBER OF PAGES
Ceramic Matrix Composites, Fatigue, Notched specimen, High Temperature, Ceramics	126
	16. PRICE CODE

17. SECURITY CLASSIFICATION OF REPORT	18. SECURITY CLASSIFICATION OF THIS PAGE	19. SECURITY CLASSIFICATION OF ABSTRACT	20. LIMITATION OF ABSTRACT
Unclassified	Unclassified	Unclassified	UL